DOE/ID/12655-2
(DE90015283)

Energy CONSERVATION

LONG-TERM TESTING OF IN-SITU CERIUM OXIDE COATED ANODES FOR ALUMINUM ELECTROWINNING

Phase II

Final Report for the Period December 1, 1987—April 30, 1989

By
H. L. King

October 1989

Work Performed Under Contract No. AC07-86ID12655

For
U.S. Department of Energy
Office of Industrial Technologies
Washington, D.C.

By
ELTECH Research Corporation
Fairport Harbor, Ohio

DISCLAIMER

This report was prepared as an account of work sponsored by an agency of the United States Government. Neither the United States Government nor any agency thereof, nor any of their employees, makes any warranty, express or implied, or assumes any legal liability or responsibility for the accuracy, completeness, or usefulness of any information, apparatus, product, or process disclosed, or represents that its use would not infringe privately owned rights. Reference herein to any specific commercial product, process, or service by trade name, trademark, manufacturer, or otherwise does not necessarily constitute or imply its endorsement, recommendation, or favoring by the United States Government or any agency thereof. The views and opinions of authors expressed herein do not necessarily state or reflect those of the United States Government or any agency thereof.

DISCLAIMER

Portions of this document may be illegible in electronic image products. Images are produced from the best available original document.

DISCLAIMER

This report was prepared as an account of work sponsored by an agency of the United States Government. Neither the United States Government nor any agency thereof, nor any of their employees, makes any warranty, express or implied, or assumes any legal liability or responsibility for the accuracy, completeness, or usefulness of any information, apparatus, product, or process disclosed, or represents that its use would not infringe privately owned rights. Reference herein to any specific commercial product, process, or service by trade name, trademark, manufacturer, or otherwise does not necessarily constitute or imply its endorsement, recommendation, or favoring by the United States Government or any agency thereof. The views and opinions of authors expressed herein do not necessarily state or reflect those of the United States Government or any agency thereof.

This report has been reproduced directly from the best available copy.

Available to DOE and DOE contractors from the Office of Scientific and Technical Information, P.O. Box 62, Oak Ridge, TN 37831; prices available from (615)576-8401, FTS 626-8401.

Available to the public from the National Technical Information Service, U. S. Department of Commerce, 5285 Port Royal Rd., Springfield, VA 22161.

Price: Printed Copy A07
Microfiche A01

Printed in the United States of America, Office of Scientific and Technical Information, Oak Ridge , Tennessee

DOE/ID/12655--2

DE90 015283

LONG-TERM TESTING OF IN-SITU CERIUM OXIDE COATED ANODES FOR ALUMINUM ELECTROWINNING

Phase II - Final Report
December 1, 1987 - April 30, 1989

October 1989

By
H. L. King

Work Performed Under Contract DE-AC07-86ID12655

Prepared for
U. S. Department of Energy
Idaho Operations Office, Idaho Falls, ID
Sponsored by the Office of the Assistant Secretary
for Conservation and Renewable Energy
Office of Industrial Technologies
Washington D.C.

Prepared by
ELTECH Research Corporation
625 East Street
Fairport Harbor, Ohio 44077

Summary

The ELTECH Anode Phase II Project (Contract Number DE-AC07-86ID12655), as supported by the Department of Energy (DOE) from December 1988 through April 1989, focused on long-term testing of in-situ anodically deposited cerium oxide (CEROX) coatings on nickel ferrite/Cu cermets. The specific objective of this research was to determine the effectiveness of the CEROX coating in reducing the transfer of cermet components to the produced aluminum.

A dosing regimen was first established for the minimum addition of cerium to the cell necessary to produce targeted CEROX coatings on the cermet anode and the periodic additions necessary to maintain coating thicknesses. The effects of the addition of CeF_3 on CEROX coating formation was evaluated for targeted coating thicknesses at three different current densities.

Analytical procedures were identified for determining alumina concentrations and the cryolite bath ratio for quasi-commercial baths.

Four short-term tests (nominal 10 h) were performed to compare the Standard Bath to three quasi-commercial baths at 1.0 A/cm^2 and the preferred CEROX coating (1.0mm thick) at alumina saturation. The Standard Bath consists of commercial-grade cryolite with 5% CaF_2 at a bath ratio (BR) of 1.35 and saturated with alumina at 980°C. The purpose of the tests were to identify the effects of bath additives on the CEROX coating and to identify shifts in the cerium partition coefficient in acidic baths, that may require adjustment of the addition of cerium for the long term tests in acidic baths.

Four tests (50 h) using vertical TiB_2 cathodes were performed at 1 A/cm^2 using the Standard Bath (BR 1.35) and an acidic bath (BR 1.15) to determine the effects of flowing aluminum on the cerium partition coefficients and metal impurities. Both electrolytes were evaluated in a static and a stirred bath containing 1 wt% CeF_3 and saturated with alumina.

Long-term testing (nominal 100 h) was performed using the preferred CEROX coating (1.0mm) in a Standard Bath at current densities of 0.6, 1.0 and 1.4 A/cm^2. The long term Standard Bath tests were compared to long term tests run under the same conditions for bath ratios of 1.2 and 1.6.

Long-term testing of in-situ CEROX coating on nickel ferrite/Cu cermet anodes shows favorable protection of the cermet from cryolite corrosion. As little as 0.15 wt% total metallic impurities in the Al was present under the most favorable conditions. With the expected use of this technology with suitable inert anode substrates, an economic

analysis was made for the recovery of cerium from aluminum metal produced in cells equipped with in-situ CEROX coated anodes. The economic analysis is a paper study based on a literature search of patents and standard sources of survey information of aluminum production and plant capacities for the aluminum smelting process.

Conclusions

Long-term testing of in-situ anodically-deposited CEROX coatings on nickel ferrite/Cu cermet anodes proved that the CEROX coatings provided significant protection to the anodes from the cryolite bath. When compared to a anode tested in a cerium-free bath under the same conditions, the CEROX coating reduced the Fe contamination in the metal by >97% for the 1.0 A/cm^2 current density.

1. The best protection of the cermet anode by the in-situ deposited CEROX coating was demonstrated in the non-acidic bath (BR 1.6) at alumina saturation at a current density of 1.4 A/cm^2. The Fe contamination of the aluminum was 0.04 wt% while total metal impurities (Fe, Cu, and Ni) were 0.15 wt%.

2. Severe anode corrosion was observed for all tests performed at a current density of 0.6 A/cm^2 because of cermet delamination within the cermet near the cermet-CEROX coating interface.

3. Sufficient concentration of cerium must be present in the cell at the beginning and during electrolysis for full protection.

4. Cerium must be added within 5 min if cerium is not previously added.

5. Cerium can be recovered from aluminum metal as CeF_3 and $CeCO_3$ at a calculated cost of $7.82/ton ($8.62/metric tonne) of aluminum produced based on manufacturing costs.

Recommendations

Although the anodically-deposited CEROX coatings were proved to provide corrosion protection to the cermet substrates, oxygen generated during electrolysis reacted with the Cu in the cermets. This reaction was enhanced by the fact that the anodes had; (a) an interconnecting Cu phase, (b) a significant porosity (7%) and (c) anode geometry that allows oxygen to interfere with the CEROX coating deposition. Based on the fact that the most protective CEROX coatings (i.e uniform with low porosity) were obtained with a cryolite BR of 1.6 at a current density of 1.4 A/cm^2, the following studies are recommended:

1. Develop cermet anodes for further testing that have low porosity and non-interconnected metal phases with a bullet shape to prevent oxygen entrapment.

2. Evaluate the CEROX coatings in alumina saturated cryolite at BRs between 1.4 to 1.6 and current densities approaching 2.0 A/cm^2. This would address the issue: capital investment cost versus production volume.

3. New tall carbon crucibles should operate with a carbon anode until sodium absorption subsides, in order to avoid wide swings in the BR.

Contents

Summary i

1. Introduction 1

1.1 Background 1
1.2 Objective 3
1.3. Scope 3
1.4. Technical Accomplishments 3

2. Background 4

3. Previous Work On Inert Anodes 5

3.1 Metal Anodes 5
3.2 Boride, Carbide, and Nitride Anodes 6
3.3 Metal Oxide Anodes 6
3.4 Cermet Anodes 7

4. In-Situ CEROX Coatings 8

4.1 Thermodynamics of Ce in a Hall Cell Environment 8

4.1.1 Electrochemical Deposition of CEROX 8
4.1.2 Chemical Deposition of CEROX 12
4.1.3 Cerium Partitioning 12

4.2 Materials and Methods 15

4.2.1 Materials 15
4.2.2 Cermet Anodes Fabricated by ELTECH 15
4.2.3 ELTECH Ni ferrite/Cu Cermet Characterization 15
4.2.4 Test Cell Design and Operating Protocol 32
4.2.5 Background Corrosion 37
4.2.6 Analytical Protocol 39
4.2.7 Alumina/CeF_3 Feeder 43

4.3 Short Term Tests 43

4.3.1 CEROX Dosing Regimen 45
4.3.2 Quasi-Commercial Electrolytes 48
4.3.3 Half-Saturated Alumina Tests 60

4.4 Long Term Saturated Alumina Tests 63

4.4.1 Outline of Experiments 63
4.4.2 Results and Discussion 63
4.4.3 Summary and Conclusions 98

4.5 Vertical Cathode Effects 101

5. Utilization and Recovery of Cerium 104

5.1 Conceptual Plant Desighn For Cerium Recovery 104
5.2 Estimated Quantity of Cerium Retained in the System 105
5.3 Estimated Losses of Cerium in the System 108
5.4 Cost Estimates of Each Step in Utilizing and Recycling Cerium 108

6. References 111

Appendix 1: Normalization Example 111

FIGURES

1. AlF_3 Activity at 1000°C 10

2. Predominance Diagram for Oxidation of CeF_3. 11

3. Predominance Diagram for Oxidation of CeF_3, AlF_3 Activity = 10-5 13

4. Predominance Diagram for Oxidation of CeF_3, AlF_3 Activity = 5 X 10-4 14

5. Resistivity Versus Temperature, ELTECH Cu Cermet. . .17

6. Resistivity Versus Temperature, PNL Cu Cermet 18

7. Specific Heat 21

8. Thermal Diffusivity 23

9. Thermal Conductivity. 24

10. Thermal Expansion 26

11. Coefficient of Expansion. 27

12. Typical Microstructure of PNL $NiFe_2O_4$/Cu Cermet . . .29

13. High Magnification of PNL $NiFe_2O_4$/Cu Cermet 29

14. Typical Microstructure of ELTECH $NiFe_2O_4$/Cu Cermet. .31

15. High Magnification of ELTECH $NiFe_2O_4$/Cu Cermet. . . .31

16. Short Term Test Cell. 34

17. Short Term Test 35

18. Long Term Test Cell 36

19. Long Term Test. 38

20. Bath Ratio as a Function of Wt% AlF_3. 41

21. Alumina Feeder. 44

22a. 100% CeF_3 Initially, 1.4 A/cm^2, 1.5% CeF_3 47

22b. 100% CeF_3 Initially, 0.6 A/cm^2, 1.5% CeF_3 47

23. 0% CeF_3 Initially, 1.4 A/cm^2, 0.5% CeF_3 47

24. 8 H Tests, CEROX Coating Resistance 50

25a. Microscopy, 8 h test, Standard Bath 53

25b. Microscopy, 8 h test, Bath 1. 53

25c. Microscopy, 8 h test, Bath 2. 53

25d. Microscopy, 8 h test, Bath 3. 53

26. Microscopy, 8 h test, Interior of Tested Samples, Standard Bath. 56

27. Microscopy, 8 h test, Edge of Cermet Next to CEROX coating, Bath 2 57

28. Microscopy, 8 h test, Cu Depleted Zone, Standard Bath 58

29. The CeF_3 and CuO Layer Developed Between the CEROX Coating and Ni-ferrite Substrate, Bath 3. 59

30. Fe Contamination Versus Bath Ratio for Standard Bath and DOE baths. 61

31. Cell Voltage versus h, BR = 1.35 and 1.6, 1.0 and 1.4 A/cm^2 66

32. Cell Voltage versus hours, BR = 1.2 67

33. Cell Voltage versus hours, 0.6 A/cm^2. 68

34. Microscopy, 100 h test, BR=1.2, 0.6 A/cm^2 71

35a. Microscopy, 100 h test, BR=1.35, 0.6 A/cm^2. 72

35b. Microscopy, 100 h test, BR=1.35, 0.6 A/cm^2 Area 1. 73

35c. Microscopy, 100 h test, BR=1.35, 0.6 A/cm^2 Area 2. 73

36. Microscopy, 100 h test, BR=1.6, 0.6 A/cm^2 74

37. Microscopy, 100 h test, BR=1.6, 0.6 A/cm^2, 40X. . . .76

38a. Microscopy, 100 h test, BR=1.6, 0.6 A/cm2 77

38b. Microscopy, 100 h test, BR=1.6, 0.6 A/cm^2, Cu Map . .77

38c. Microscopy, 100 h test, BR=1.6, 0.6 A/cm^2, Fe Map . .78

38d. Microscopy, 100 h test, BR=1.6, 0.6 A/cm2, Ni Map . .78

39. Microscopy, 100 h test, BR=1.2, 1.0 A/cm^2 79

40. Microscopy, 100 h test, BR=1.35, 1.0 A/cm^2. 81

41. Microscopy, 100 h test, BR=1.6, 1.0 A/cm^2 82

42. Microscopy, 100 h test, BR=1.2, 1.4 A/cm^2 83

43a. Microscopy, 100 h test, BR=1.2, 1.4 A/cm^2 83

43b. Microscopy, 100 h test, BR=1.2, 1.4 A/cm^2,
Fe Map. 84

43c. Microscopy, 100 h test, BR=1.2, 1.4 A/cm^2
Ni Map. 84

43d. Microscopy, 100 h test, BR=1.2, 1.4 A/cm^2
Cu Map. 84

44. Microscopy, 100 h test, BR=1.35, 1.4 A/cm^2. 85

45a. Microscopy, 100 h test, BR=1.35, 1.4 A/cm^2. 86

45b. Microscopy, 100 h test, BR=1.35, 1.4 A/cm^2,
Fe X-ray Map. 86

45c. Microscopy, 100 h test, BR=1.35, 1.4 A/cm^2,
Ni X-ray Map. 86

45d. Microscopy, 100 h test, BR=1.35, 1.4 A/cm^2,
Cu X-ray Map. 86

46a. Microscopy, 100 h test, BR=1.35, 1.4 A/cm^2,
Area 2, Fe X-ray Map. 87

46b. Microscopy, 100 h test, BR=1.35, 1.4 A/cm^2,
Area 2, Ni X-ray Map. 87

46c. Microscopy, 100 h test, BR=1.35, 1.4 A/cm^2,
Area 2, Cu X-ray Map. 87

46d. Microscopy, 100 h test, BR=1.35, 1.4 A/cm^2,
Area 2, BEI 87

47. Microscopy, 100 h test, BR=1.6, 1.4 A/cm^2 88

48a. Microscopy, 100 h test, BR=1.6, 1.4 A/cm^2,
CEROX coating, Bottom 89

48b. Microscopy, 100 h test, BR=1.6, 1.4 A/cm^2,
CEROX coating, Corner 89

49. Normalized Metal Purity, 100 h tests, BR=1.35 92

50. Normalized Metal Purity, 100 h tests, BR=1.2. 94

51. Normalized Metal Purity, 100 h tests, BR=1.6. 96

52. Normalized Metal Purity, 100 h tests, 1.0 A/cm^2 . . .97

53. Wear Rates, 100 h tests 99

54. Comparison of an Untested TiB_2 Cathode and a Tested Cathode With Meltline Corrosion 102

55. Photograph of a Tested Cathode and Anode from a Stirred Experiment. 102

56. Flowsheet for the Recovery of Cerium. 106

57. Cerium Metal Inventory. 107

58. Cost of Utilization & Recovery of Cerium. 109

59. Estimated Investments and Manufacturing Costs For Cerium Recovery 110

TABLES

1. Specific Heat Results 20

2. Thermal Diffusivity Results 22

3. Thermal Conductivity Calculations 22

4. Thermal Expansion Results 25

5. Typical Phase Composition Based on Semiquantitative EDS Analysis. 30

6. CEROX Coating Resistance. 49

7. Comparison of Anodes from DOE Baths and Standard Bath. 52

8. Cerium Partitioning 55

9. Long Term Tests 64

10. Cell Voltage Data 65

11. Long Term Test Results. 70

12. Cermet Components in Recovered Metal and Bath, BR=1.35 91

13. Cermet Components in Recovered Metal and Bath, BR=1.2. 93

14. Cermet Components in Recovered Metal and Bath, BR=1.6. 95

LONG TERM TESTING OF IN-SITU CERIUM OXIDE COATED ANODES FOR ALUMINUM ELECTROWINNING

1. INTRODUCTION

The ELTECH Phase II Anode Project focused on long-term testing of in-situ anodically deposited cerium oxide (CEROX) coatings on nickel ferrite/Cu cermets. The specific objective of the research was to determine the effectiveness of the CEROX coating in reducing the transfer of cermet components to the produced aluminum.

1.1 BACKGROUND

In the conventional Hall-Heroult process, anode carbon is consumed according to the reaction

$$Al_2O_3 + 3/2\ C = 2\ Al + 3/2\ CO_2 \qquad (1)$$

with the side reaction of

$$Al_2O_3 + 3C = 2\ Al + 3\ CO. \qquad (2)$$

Although, according to the reaction in Equation (1), 0.33 kg of carbon is theoretically required for each kilogram of aluminum, the actual consumption is nearly 0.5 kilograms. The exit gas from a Hall-Heroult cell contains 10 to 50% CO.[1] Loss of carbon is also caused by selective oxidation, cracking and arcing. Because of metal purity considerations, a relatively pure coke with low ash content must be used as anode carbon. Further, non-uniform wear of the carbon anode imposes an energy penalty because a uniform inter-electrode gap cannot be maintained.

Because of the cost of building and maintaining a carbon anode plant and the energy penalty associated with the use of carbon anodes, the use of inert anodes has long been proposed.[2,3]

With and inert anode, the net cell reaction is

$$Al_2O_3 = 2\ Al + 3/2\ O_2. \qquad (3)$$

The reversible potential for this reaction at 1000°C is 2.2 V compared to 1.15 V for the conventional process. Despite this, a net energy savings is expected with the use of inert anodes.[4] The major savings would be in petroleum coke and its energy content. It has been estimated that U.S. consumption of petroleum coke for anode carbon is 2.27 M ton/y.[5]

A major savings associated with the use of an inert anode is expected from improvements in cell design and operation.

Alcoa has estimated that if the anode-cathode gap could be lowered from the present 4.4 to 1.9 cm, a 23% decrease in the energy requirement would be achieved.[5] Additional energy savings may also result from reduced pollution control costs and decreased voltage drop in external cell components.

The material requirements of an inert anode in an aluminum reduction cell include: (a) low solubility in the molten cryolite bath, (b) oxidation resistance, (c) thermal shock resistance, (d) high electrical conductance compared to carbon, (e) low oxygen overpotential, and (f) adequate mechanical strength.[2,3] In addition to these requirements, the material must be low cost and easily fabricated into large shapes.

Early work on inert anodes concentrated on metals and ceramic oxides. Metals generally have high electrical conductivity, but with the exception of some of the precious metals, were subjected to massive oxidation. Some of the oxide ceramics have been found to have very low solubility in cryolite melts, but characteristically have low conductivities. It is generally acknowledged that no metal oxide has been found to meet the requirements of an inert anode.

In recent years, various cermet anodes, developed by Alcoa,[5] have received considerable attention. By including a metallic phase in the ceramic matrix, high electrical conductivity cermets have been obtained while maintaining the corrosion-resistance properties of the ceramic. The most promising results were obtained with a material containing a nickel ferrite matrix and 17% Cu. Targeted dissolution rates were obtained in laboratory tests with this cermet. However, these dissolution rates have not been proven in pilot-scale tests.

In the past several years, ELTECH Systems Corporation has demonstrated the anodic deposition of a cerium oxyfluoride (CEROX) from conventional Hall-Heroult cryolite melts.[6] This led to the proposed use of CEROX as a self-forming anode coating, deposited <u>in-situ.</u> The significance of this concept is that it provides a mechanism for the protection of an anode substrate against corrosive attack.

The DOE sponsored Anode Project Phase II for 1988 was a continuation of work performed in Phase I, where the in-situ Cerox coating was evaluated for protection of the cermet anode from the cryolite bath in short-term testing (nominal 10 h). The study in Phase I concluded that no detectable attack on the substrate was evident under the best case conditions. The recommendation was for long term testing to establish the preferred Cerox coating thickness and operating conditions to ensure steady state cell operations and to quantify wear rates.

1.2 OBJECTIVE

The Phase II research was performed to establish a technical data base on the chemical, physical, and performance properties of substrates and deposited coatings for use as electrodes in Hall-Heroult cells. The tasks were directed towards in-situ deposition and analysis of cerium oxide (CEROX) coatings on copper/nickel ferrite cermets.

1.3 SCOPE

The primary scope of this research was long-term testing (100 h) of in-situ deposited CEROX coatings on cermet substrates to determine the effectiveness of CEROX in reducing the transfer of cermet anode components to the produced aluminum and bath and to identify the preferred coating and operating conditions for optimal anode protection.

Corrosion resistance of the coated structures was evaluated by microstructural analysis and by chemical analysis of the electrolyte and the aluminum metal. Cerium mass balances were also performed to determine the effect of experimental variables on the cerium concentration in the aluminum. The electrical resistance of the coatings were assessed by monitoring the change in the iR component of the anode potential for the nominal 10 h tests.

1.4 TECHNICAL ACCOMPLISHMENTS

For the long-term testing program, at alumina saturation, it was proven that in-situ CEROX coating provided by 1.0 wt% CeF_3 reduced the Fe contamination in the metal by >97% when compared to cerium-free bath for a current density of 1.0 A/cm^2 and a BR of 1.35. However, the optimum cermet protection that resulted in the best metal purity (Fe 0.05 wt% and total metal impurities for Fe, Ni, and Cu of 0.15 wt%), was achieved by an in-situ CEROX coating (CeF_3 1.0 wt%) on the cermet substrate at a BR of 1.6 and a current density of 1.4 A/cm^2.

Further, it was proven that in long-term testing of in-situ CEROX coatings on cermet anodes under quasi-commercial bath ratios, the CEROX coating stability is sensitive to the AlF_3 activity. This evidence supports the FACT analysis, which shows that lower AlF_3 activity (higher BR) favors the formation of CeO_2.

All anode evaluations at the low current density of 0.6 A/cm^2 underwent a cermet to cermet separation near the CEROX coating interface for all of the simulated commercial electrolyte conditions.

An economic study was performed on the "Utilization and Recovery of Cerium in Aluminum Smelter Operations." The economic analysis included in this final report is a study based on a literature search of patents and standard sources of survey information of commercial aluminum production and plant capacities for the aluminum smeltering process. It was estimated that the cost of cerium recovery from the aluminum metal will be $7.82/ton ($8.62/metric tonne).

2. BACKGROUND

The use of dimensionally stable anodes for aluminum electrowinning has been considered since the time of Hall's original work and has been the subject of considerable research.[2,3] Inert anodes offer the promise of operating cost savings by elimination of consumable carbon anodes and lower cell voltages, achieved by reduction of the anode-cathode distance and reduction of anode polarization. The energy requirement for the conventional Hall-Heroult cell is summarized below.[7]

Energy Requirement for Hall-Heroult Process

Cell	Cell Voltage (V)
Thermodynamic potential	1.2
iR loss in bath	1.9
Anode polarization	0.5
iR loss in electrode and current collectors	0.9
TOTAL CELL VOLTAGE	4.5

Although the reversible potential for a dimensionally stable oxygen anode is approximately one volt greater than that of a carbon anode, this increased voltage can be more than offset by lower overvoltage and ohmic losses. The polarization requirement for an inert anode has been reported to be 0.2 V less than that of a carbon electrode.[2] In addition, the electrical conductivity of cermet anodes may become three times that of carbon[8] and would greatly reduce ohmic losses in the anode. The use of an inert anode, in combination with a wettable cathode, also offers the potential of reducing the interelectrode distance, thus greatly lowering the ohmic drop in the electrolyte. The development of a more compact cell design may also result from this technology. The energy requirement for a Hall-Heroult cell using inert anodes is summarized below. It is assumed that the anode-cathode gap is half that used in the conventional process and the anode

polarization is 0.2 V less than that in the carbon electrodes.

Energy Requirement for Hall-Heroult Cell with Inert Anode

Cell	Cell Voltage (V)
Thermodynamic potential	2.2
iR loss in bath	1.0
Anode polarization	0.3
iR loss in electrodes and current collectors	0.9
TOTAL CELL VOLTAGE	4.4

The material properties required of an inert anode in an aluminum reduction cell include[2]:

1. Insolubility in the molten fluoride melt
2. Oxidation resistance
3. Thermal shock resistance
4. Electrical resistivity less than or comparable to carbon
5. Low oxygen overpotential

In addition, adequate mechanical strength and resistance to the dissolved aluminum found in the electrolyte have been noted as other requirements.[9]

3. PREVIOUS WORK ON INERT ANODES

The use of inert anodes in aluminum reduction cells has been proposed since the time of Hall's initial invention. Indeed, Hall himself devoted a great deal of effort in the pursuit of an oxygen anode. Unfortunately, the problems initially encountered, i.e., metal contamination, anode life, conductivity, and cost persist to this day. Past efforts to develop an inert anode have been reviewed by Billehaug and Oye.[2] More recent efforts have largely concentrated on cermet materials in work carried out at Alcoa. A summary of previous work is presented below.

3.1 METAL ANODES

Although platinum group metals may meet these criteria[2], the prohibitive cost would preclude their use. Less noble metals

are generally not suitable as inert anodes. Belyaev and Studentsov[10,11] found that copper, nickel, chromium, and silver were not resistant to oxygen. The oxide layers which formed spalled off, exposing fresh metal surfaces to be attacked. Kronenberg[12] also found copper and nickel to be severely attacked under anodic polarization. Copper anodes, which were originally suggested by Hall, have been tested on an industrial scale with no success.[13]

3.2 BORIDE, CARBIDE, AND NITRIDE ANODES

Refractory metal borides, carbides, and nitrides have been proposed as anodes. However, studies with these materials have shown that in all cases, they have corroded greatly during electrolysis.[14]

3.3 METAL OXIDE ANODES

Because of their stability in the presence of oxygen, oxide ceramics have been studied as inert anodes for aluminum electrowinning by the Hall-Heroult process. However, all candidate materials examined to date have exhibited a finite solubility in the cryolite melt, which leads to unacceptably high metal contamination levels in the electrowon aluminum. Moreover, the least soluble oxides are thermodynamically unstable with respect to the aluminum that is dissolved in the electrolyte. These problems have presented the major obstacle in the development of the dimensionally stable anode technology.

Early investigations by Belyaev and Studentsov[10] identified Fe_3O_4, SnO_2, NiO, and ZnO as the oxides having the lowest solubility in molten cryolite and the highest stability in laboratory polarization tests. The rate of corrosion of a Fe_3O_4 anode was found to be independent of current density. The electrowon aluminum was also found to contain up to 1.5% iron.

In a subsequent study, Belyaev[15] found that ferrites such as $NiOFe_2O_3$ and $ZnFe_2O_4$ had higher electrical conductivity and better corrosion resistance than the pure oxides. Since then, a large number of patents have been issued describing the use of metal oxide and mixed metal oxides as inert anodes. However, in nearly all cases, the most serious problem continues to be the dissolution of the oxide into the cryolite[3] and in turn, the contamination of the electrowon aluminum.

Of the oxides considered, SnO_2 has received the most attention because of low solubility[2] and high electrical conductivity, achieved by doping. Unfortunately, unacceptably high levels of tin in the aluminum product have been repeatedly observed.[16] It has been proposed that the corrosion of the SnO_2 is through chemical attack by dissolved

aluminum, which is present at a level of several tenths of a percent.[17,18] Various engineering approaches have been attempted to reduce SnO_2 corrosion,[16,19,20] including oxygen protection. However, none of these approaches have been adopted commercially. It is generally acknowledged that a more rugged anode needs to be developed. SnO_2 does have a large data base on its performance and does provide a valuable control substrate that is readily available.

3.4 CERMET ANODES

In 1982, Alcoa[21] disclosed the development of a cermet anode composed of 70% $NiFe_2O_4$/NiO and 30% Ni metal. Both the ceramic phase and metal phase were continuous in this material. The $NiFe_2O_4$/NiO had low chemical solubility in cryolite. The Ni metal phase improved both the electrical conductivity of the material and improved its mechanical properties, such as thermal shock resistance.

Rapid development of this material led to the eventual testing in a 2500 A pilot cell.[8] Although failure of the test after 21 d of operation was attributed to degradation of the cermet/steel conductor connection, an autopsy of the tested anode revealed that microstructural changes in the cermet precluded extended operation of the cell. Later studies indicated that corrosion of the Ni phase by oxidation or electrolysis occurs during operation, causing cracking and bath penetration.

The leaching of the metal phase from the cermet led Tarcy[22] to screen various pure metals and commercially available alloys to find a material with a higher polarization requirement for anodic dissolution than Ni. Although none of the metals or alloys tested, other than platinum, were sufficiently resistant to serve as an inert anode alone, copper and Cu/Ni alloys were proposed to be promising candidates for a metal phase in the cermet. It was found that the passivating layer on Cu and Cu/Ni alloys tends to spall off the surface of a metal surface, but not when incorporated into the ceramic matrix.

Subsequently, Ray[23] developed a new cermet material in which the Ni-Fe alloy is replaced by Cu-Ni-Fe. It was reported that this material does not degrade with time and forms a passive layer that prevents loss of the metallic phase.

A series of cermet materials containing 83 to 95 wt% metal oxide and 5 to 17% Cu metal was examined in 30 h laboratory bench tests.[24] The aluminum produced contained impurities of 0.3 to 0.07% Ni, 0.26 to 0.34% Fe and 0.05 to 0.12% Cu. These levels fall just within the Alcoa target of total impurities of <0.5%.

Recently, the development of the copper containing nickel

ferrite has continued at Battelle's Pacific Northwest Laboratories (PNL). Processing of the cermet has been refined to minimize anode wear. In addition, the effect of various bath chemistries has been examined. Long-term testing on improved cermet material is planned to establish wear rates and projected lifetimes.

4. IN-SITU CEROX COATINGS

ELTECH Systems Corporation has been actively involved in research for inert anodes for aluminum electrowinning since the mid-1970s. The program initially involved screening of various oxide ceramics (including SnO_2) and cermets; several promising candidates were identified,[25,26] although unacceptable high corrosion rates would prevent commercial use.

The recent development of the CEROX coating technology can be traced back to late 1982, when it was accidently discovered that cerium dioxide could be anodically deposited from a molten cryolite electrolyte. When 1 wt% cerium oxide was added to a conventional Hall cell bath, it was noted that a 1 mm thick gray-blue coating was formed on the surface of a palladium anode. Subsequent x-ray diffraction of the coating confirmed the major phases to be cerium dioxide (CEROX), with cryolite detected as a minor phase. Mass balance calculations also proved that most of the cerium added to the system was deposited at the anode as cerium oxide. The deposition of the CEROX coating was later found to be quite reproducible and applicable to both metallic and ceramic substrates. The first patent describing the CEROX coating technology was recently issued.[27]

4.1 THERMODYNAMICS OF CE IN A HALL CELL ENVIRONMENT

In order to define the equilibria involved in the deposition of CEROX, the thermodynamics of the Ce-Al-Na-O-F system has been examined. The anodic deposition of CEROX can be effectively described as either an electrochemical or chemical process. Therefore, both cases are presented here.

4.1.1 Electrochemical Deposition of CEROX

The electrochemical deposition of CeO_2 can be expressed as two half reactions and is written

Anode: $2\ CeF_3 + 4/3\ Al_2O_3 = 2\ AlF_3 + 2\ CeO_2 + 2/3\ Al^{+3} + 2e^-$

Cathode: $2/3\ Al^{+3} + 2e^- = 2/3\ Al.$

The net reaction would be

$$2\ CeF_3 + 4/3\ Al_2O_3 = 2\ CeO_2 + 2\ AlF_3 + 2/3\ Al \qquad (4)$$

The delta G^o for this reaction at 1300 K is 141390 cal, which corresponds to an applied emf of 3.06 V. The anodic deposition of CeO_2 is of course, in competition with the oxygen evolution reaction, written as

$$Al_2O_3 = 2\ Al + 3/2\ O_2. \qquad (5)$$

Equation (5) has a free energy change of 301680 cal, corresponding to an applied emf of 2.18 V.

Based on standard free energy change only, it would appear that CeO_2 deposition would never occur. However, it must be noted that delta G^o for Equation (4) is influenced by the AlF_3 activity, which in pure cryolite has been estimated to be between 10^{-5} and 10^{-3}.[1] Yoshida and Dewing[18] estimated the AlF_3 activity in a cryolite bath with varying cryolite ratios (Figure 1).

In order to visualize the dependence of CeO_2 depositions on AlF_3 activity and applied potential, a predominance diagram (Figure 2) was constructed from FACT calculations. All species other than AlF_3 were assumed to be in their standard state. In addition to Equation (4), the equilibria

$$2\ CeF_3 + Al_2O_3 = Ce_2O_3 + 2\ AlF_3 \qquad (6)$$

$$1300\ K\ \text{delta}\ G^o = 86559\ cal$$

$$Ce_2O_3 + 1/3\ Al_2O_3 = 2\ CeO_2 + 2/3\ Al \qquad (7)$$

$$1300\ K\ \text{delta}\ G^o = 54830\ cal$$

$$Ce + AlF_3 = CeF_3 + Al \qquad (8)$$

$$1300\ K\ \text{delta}\ G^o = -65734\ cal$$

$$2\ Ce + Al_2O_3 = Ce_2O_3 + 2\ Al \qquad (9)$$

$$1300\ K\ \text{delta}\ G^o = -44918\ cal$$

were considered. As can be seen in Figure 2, at AlF_3 activities $<10^{-3}$, the deposition of CeO_2 becomes thermodynamically possible at normal O_2 evolving potentials in pure cryolite. The CeO_2 deposition is not possible at CO_2 evolving potentials at practical AlF_3 activities. It is also predicted that at very acidic conditions (high AlF_3 activity 10^{-2} or greater), CeO_2 deposition is not favored at O_2 evolving potentials.

In summary, CeO_2 deposition is possible, largely because of the low AlF_3 activity in cryolite melts. In normal acidic melts, deposition can occur at high O_2 overpotentials.

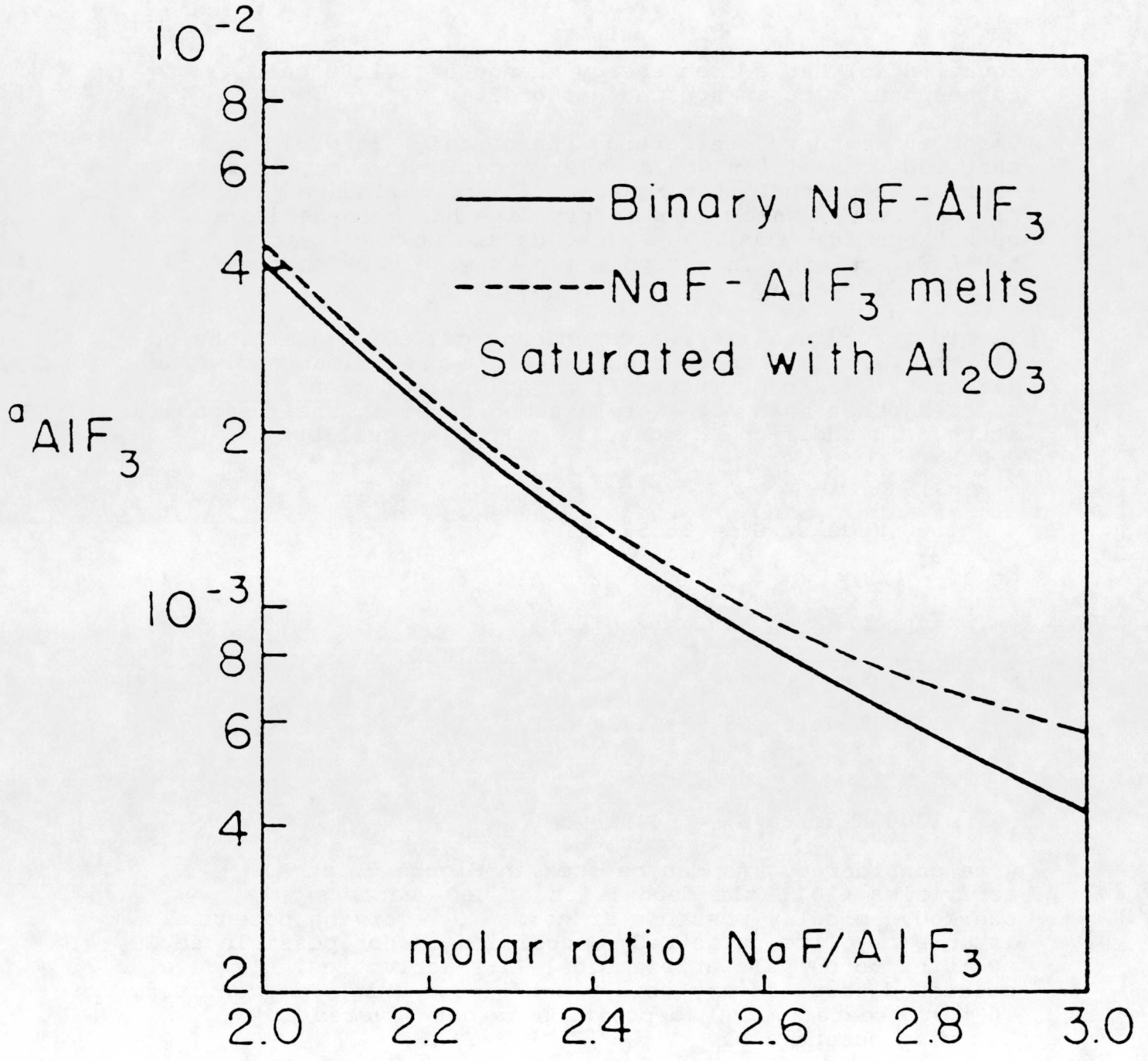

Figure 1 AlF_3 Activity at 1000°C
Yoshida and Dewing[18]

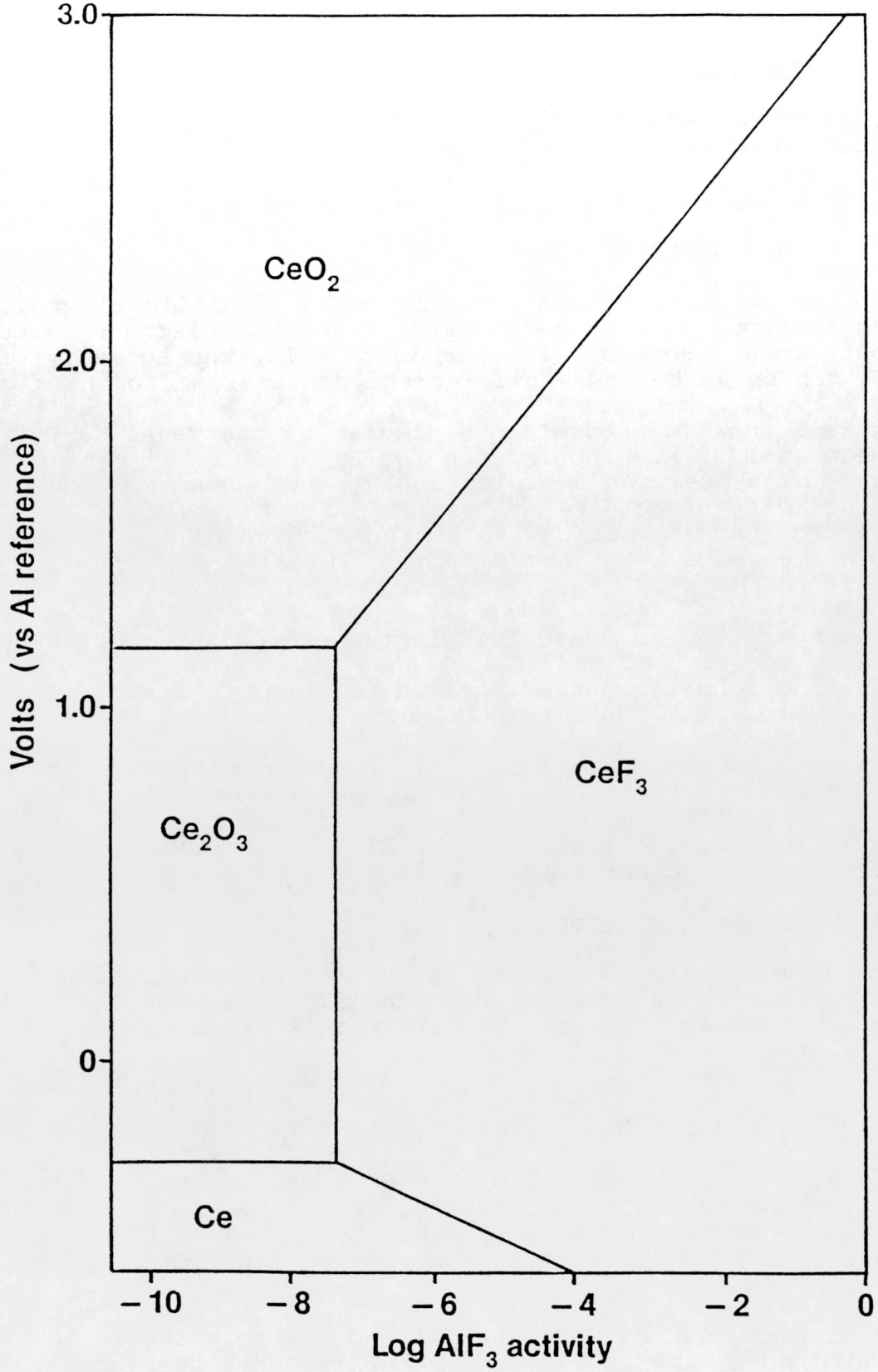

Figure 2 Predominance Diagram for Oxidation of CeF_3

4.1.2 Chemical Deposition of CEROX

Cerium oxide deposition could also occur by chemical oxidation of CeF_3 by the reaction

$$2\ CeF_3 + Al_2O_3 + 1/2\ O_2 = 2\ CeO_2 + 2\ AlF_3 \qquad (10)$$

1300 K delta G^o = 40892 cal.

From the large, positive value of delta G^o, it is clear that with all species in the standard state, the reaction is not spontaneous. However, in a cryolite melt, the activity of AlF_3 can be quite low, shifting the equilibrium to the right.

Figure 3 shows a predominance diagram of the Ce-Al-Na-O-F system at 1300 K, plotting the log Al_2O_3 activity versus the log O_2 pressure. An activity of 10^{-5} was assumed for AlF_3. The activity of Na_3AlF_6 was set at 0.3. As would be expected, CeO_2 formation is favored at high Al_2O_3 activity and O_2 pressure. At 1 atm O_2, the critical Al_2O_3 activitiy is 3×10^{-4}.

For comparison, an identical diagram was constructed assuming an AlF_3 activity of 5×10^{-4} (Figure 4). In this case, more oxidizing conditions are required to form CeO_2. At 1 atm O_2, the critical Al_2O_3 activity is ~0.3.

Just as with the electrochemical oxidation, the chemical oxidation of CeF_3 to CeO_2 is possible only because of the low activity of AlF_3 in cryolite. In acidic melts, CeO_2 deposition is less likely. High Al_2O_3 activity and O_2 pressure promote oxidation.

4.1.3 Cerium Partitioning

In a Hall-Heroult cell using CEROX coated anodes, an equilibrium is expected to be established between the Ce in the aluminum and CeF_3 in the melt and is given by

$$CeF_3 + Al = Ce + AlF_3 \qquad (11)$$

1300 K delta G^o = 66047 cal.

According to Equation 11, with the reactants and products in their standard state, Al will not reduce CeF_3. However the formation of intermetallics, e.g., $CeAl_4$ and $CeAl_2$ would lower the Ce activity in Al and promote the reduction of CeF_3.

The distribution of Ce in the Al and the melt should be determined by the equilibrium established by the above reaction. Therefore, we have

$$K_{eq} = a_{Ce} \times a_{AlF3} / a_{CeF3} \times a_{Al}. \qquad (12)$$

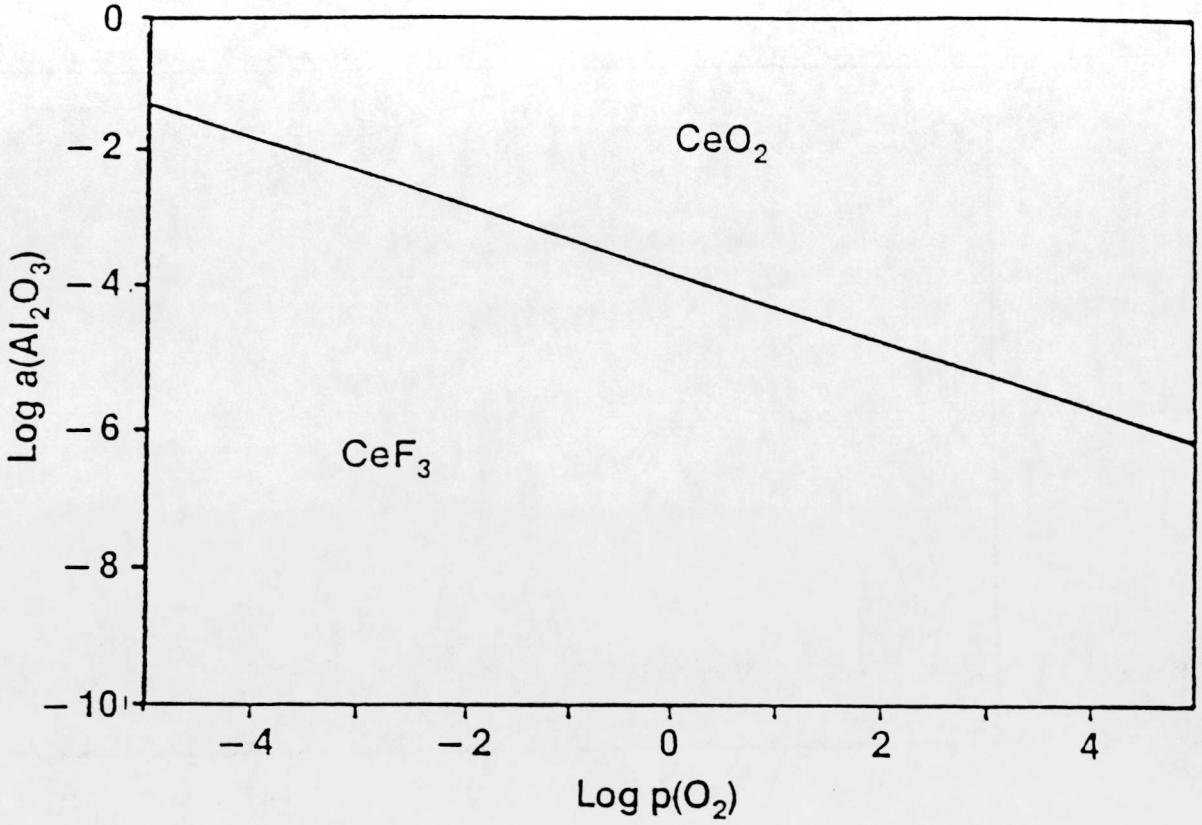

Figure 3 Predominance Diagram for Oxidation of CeF_3
AlF_3 Activity=10^{-5}, Na_3AlF_6 Activity=0.3

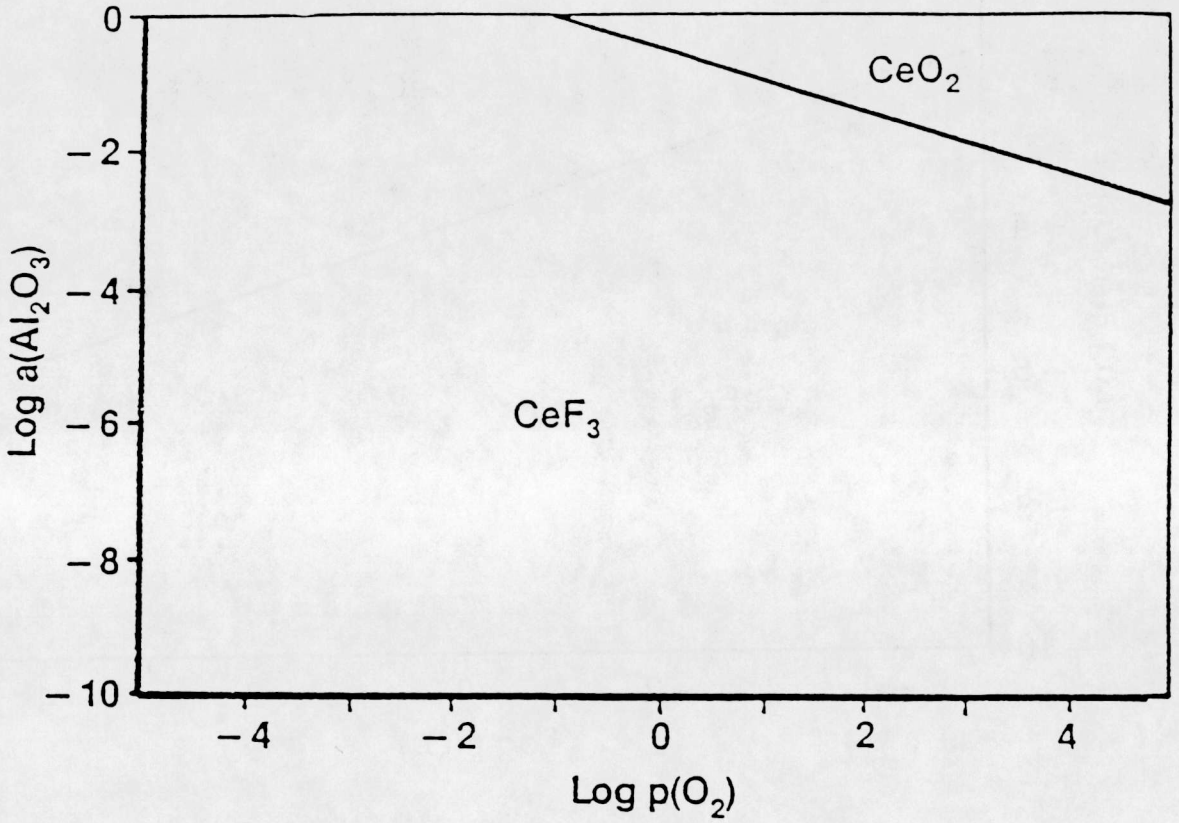

FIGURE 4
Predominance Diagram for Oxidation of CeF_3
AlF_3 Activity=5 X 10^{-4}, Na_3AlF_6 Activity=0.3

Assuming the activity of AlF_3 and Al should be constant we can therefore define a partition coefficient as the ratio of Ce in the Al and the Ce in the melt as

$$PC = \frac{Ce\ (Al)}{Ce\ (melt)} \quad . \qquad (13)$$

This should be nearly constant for conditions with low Ce concentration but will vary with AlF_3 activity.

4.2 MATERIALS AND METHODS

4.2.1 Materials

Synthetic cryolite from American Fluoride Co. contained 50 ppm Fe (Lot 1178 Fine Powder No. 1-680) and was used as received, in all experiments. Anhydrous aluminum oxide 99% purity (Certified Lot A-591) and calcium fluoride 99.9% purity (Lot C-89) were obtained from Fisher Scientific Co. Before use, these were dried at 700°C under vacuum (13.33 Pa) for 24 h. Cerium fluoride 99.9% purity (Lot C-28-H) was obtained from Morton Thiokol, Inc. Anhydrous aluminum fluoride (Lot A-1115) was obtained from Cerac Inc. with >99.9% purity. High purity aluminum ingot (99.999%, Lot H-25-F) was obtained from Morton Thiokol, Inc with 20 ppm of Fe.

4.2.2 Cermet Anodes Fabricated by ELTECH

A 1 kg batch of nickel ferrite powder (ALCOA specification) was prepared by reacting 483 g of iron oxide and 517 g of nickel oxide at 900°C in air. After firing, the material was passed through a 50 mesh screen to deagglomerate the powder, and was divided into two 500 g batches. The ferrite powder batches were then V-blended with 17 wt% Cu metal (2 μm Cerac). This was repeated for four batches of powder and then the lots of ferrite powder and Cu metal mixtures were blended into one master batch of over 4 kg.

Rubber molds of 1-in. diameter were filled with 105 g of the powder blend from the master batch and isopressed at 50 kpsi. The isopressed greenforms were sintered in a flowing argon atmosphere at 1350°C for 1 h. Each sintered greenform produced two 3/4-in. diameter anodes. The maximum density achieved was 5.76 g/cc.

4.2.3 ELTECH Cu Nickel Ferrite Cermet Characterization

The ELTECH produced Ni ferrite/Cu cermet was characterized and compared to the PNL cermet. Electrical, thermal, and chemical characteristics were measured and the microstructure characterized.

4.2.3.1 Electrical Resistivity

Electrical resistivity determinations were performed at the ELTECH Geneva Labs by the 4-probe technique on a programmed automatic apparatus from room temperature to 990°C in air. Both production ELTECH samples and PNL materials from the Phase I Anode Project were measured with measurements taken during both heating and cooling. Each sample was thermally cycled twice. The results from the second thermal cycle of each is compared below.

	Resistivity ohm-cm		Conductivity $ohm^{-1}cm^{-1}$
	30°C	990°C	990°C
PNL Cermet (13474-48-1)	3397 (85°C)	0.027	25
ELTECH Cermet	0.06	0.020	50

The first cycle of the ELTECH copper cermet showed a jump in the resistivity on cooling. The sample was cycled a second time for a comparison to the second cycle of the PNL cermet (Figures 5 and 6). Both samples indicated lack of hysteresis on cooling and heating for their second cycle.

Upon comparison to the PNL cermet, the ELTECH cermet showed a metal-like conductivity with little temperature dependance while the PNL cermet exhibited a semiconductor-like resistivity with thermal activation. This difference can be attributed to how the copper metal phase is dispersed in the ceramic matrix.

Optical microscopy shows the PNL cermet has large patches of copper metal with little interconnection in the ceramic matrix. The microstructure of the ELTECH cermet, on the other hand, contains small particles of copper metal more uniformly dispersed throughout the ceramic matrix as an interconnected network. Because of the greater dispersion of the Cu metal in the ELTECH cermet, there is more metallic interconnection that gives the metallic character to the electrical resistivity exhibited by the ELTECH cermet.

4.2.3.2 Thermal Properties

The thermal studies were performed at the Thermal-Physical Laboratory at Purdue University on production ELTECH cermets.

The specific heat, C_p, was measured using a standard Perkin-Elmer Model DSC-2 Differential Scanning Calorimeter (DSC) using sapphire as a reference material. Results are given in

FIGURE 5
Resistivity vs.Temperature
ELTECH Cu Cermet

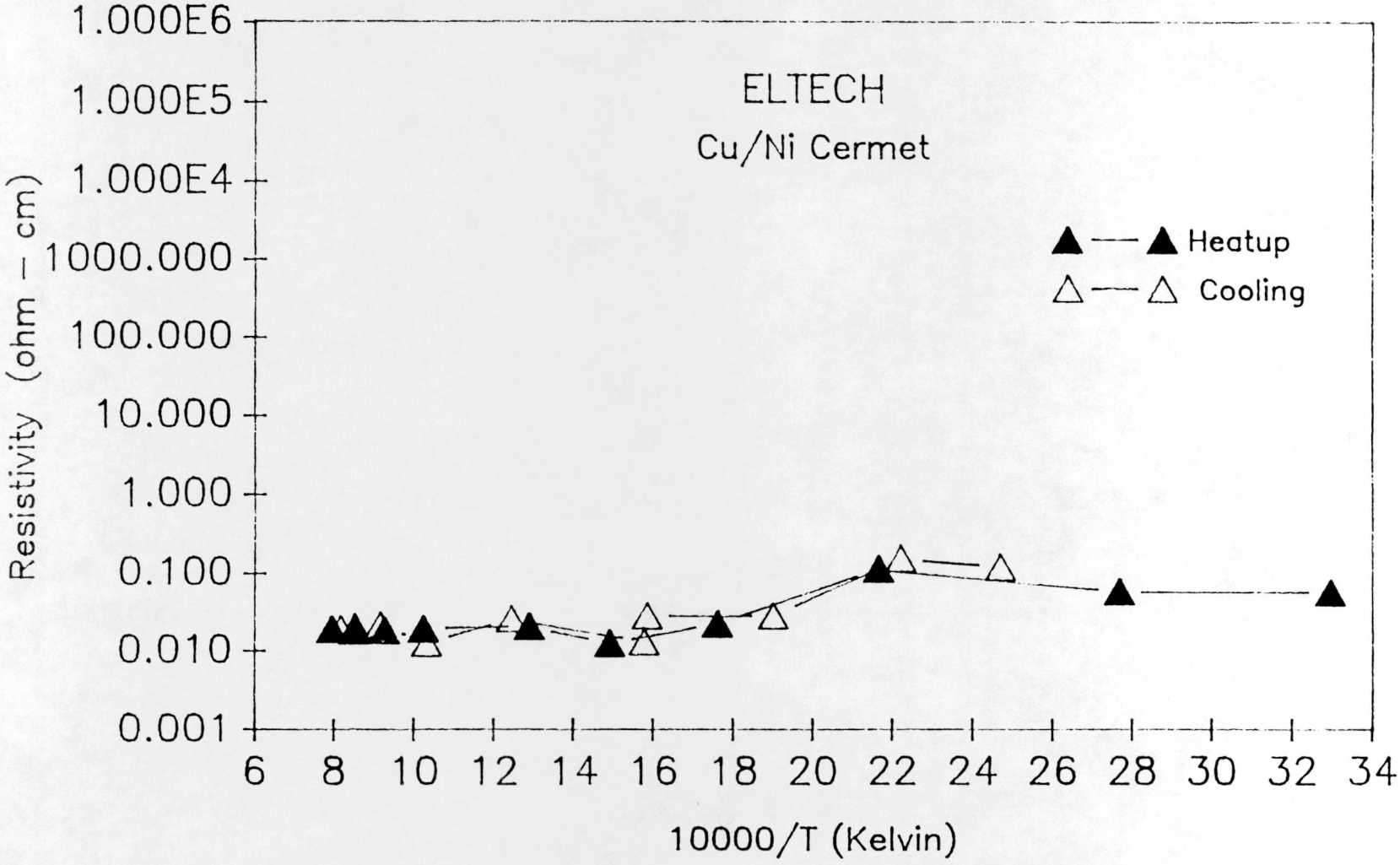

FIGURE 6
Resistivity vs Temperature
PNL Cu Cermet

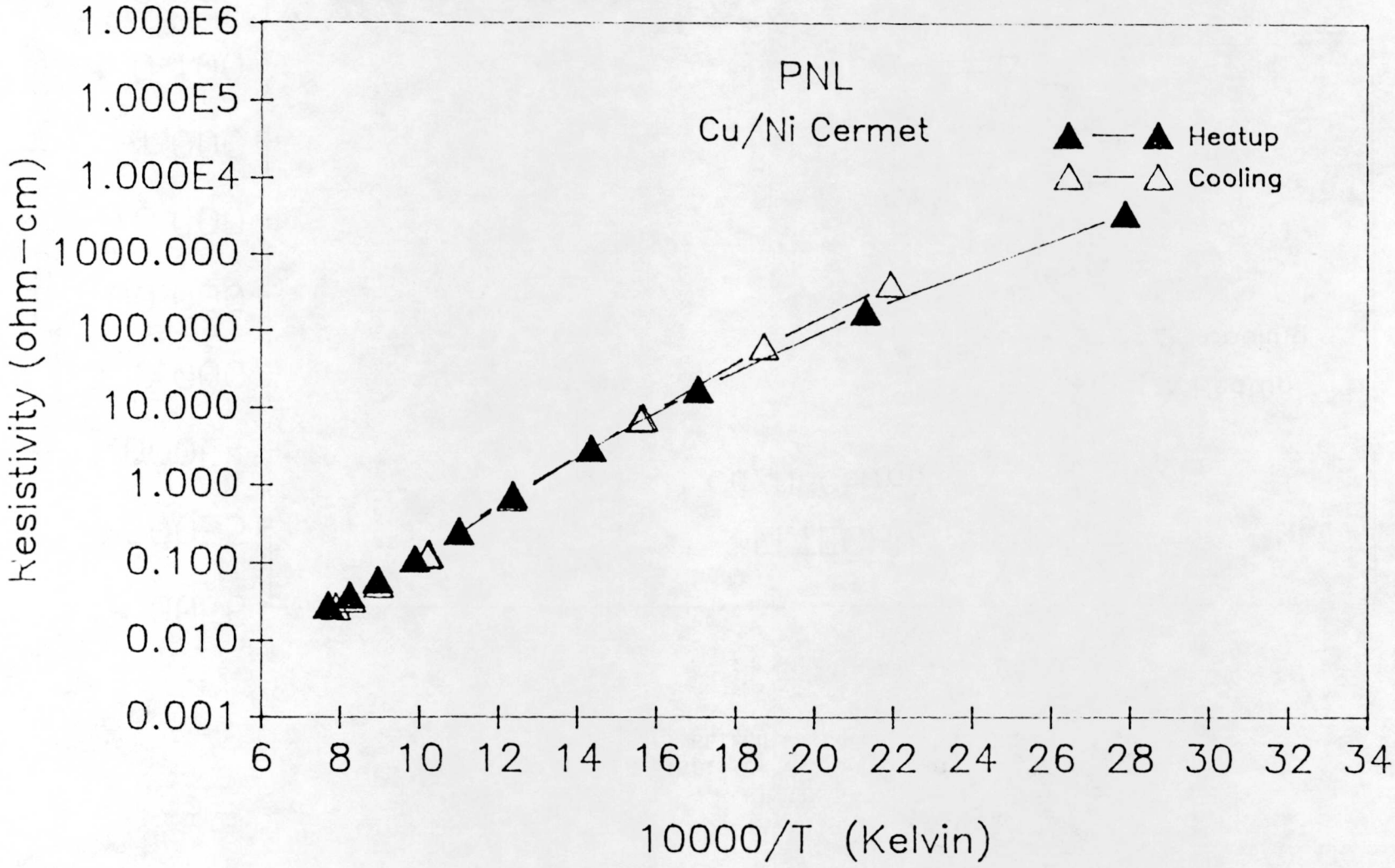

Table 1 and are plotted in Figure 7. There is a very slight peak near 200°C. In addition, there will be a large peak between 600 and 700°C, but this is beyond the temperature range of the DSC.

Thermal diffusivity was determined using the laser flash diffusivity method. Thermal conductivity is calculated as the product of diffusivity, specific heat, and density. Thermal diffusivity results are given in Table 2 and are plotted in Figure 8. The thermal diffusivity curve has a plateau between 600 and 700°C.

Calculated thermal conductivity values are shown in Table 3 and are plotted in Figure 9. The conductivity values also exhibit a plateau near 600°C. These values have not been corrected for thermal expansion in keeping with common practice.

Thermal expansion results are given in Table 4 and are plotted in Figure 10. The expansion curve has an inflection near 600°C. Average coefficient of expansion values are included in Table 4 and are plotted in Figure 11. The expansion becomes linear at 600°C.

4.2.3.3 Chemical Analysis

The targeted composition of the Alcoa cermet 5324/17% Cu is 17% Cu, 28% Fe, and 33.72% Ni with a ratio %Fe/%Ni of 0.83. The analysis of random samples of PNL cermets and ELTECH production cermets are shown below.

	PNL Cermets			
Sample	%Cu	%Fe	%Ni	%Fe/%Ni
48-3	17.5	29.0	32.9	0.88
48-11	18.6	28.1	32.0	0.88
51-5	18.2	28.5	32.5	0.87
			Mean	0.88
	ELTECH Production Cermets			
58-4	13.1	30.4	34.5	0.88
58-6	12.4	29.7	34.6	0.86
			Mean	0.87

Table 1. Specific Heat Results

Temperature (°C)	Specific Heat (W-s $g^{-1}K^{-1}$)
22.0	0.592
52.0	0.615
77.0	0.641
102.0	0.665
127.0	0.686
152.0	0.707
177.0	0.726
202.0	0.746
227.0	0.769
252.0	0.762
277.0	0.755
302.0	0.757
327.0	0.762
352.0	0.767
377.0	0.774
402.0	0.784
427.0	0.794
452.0	0.805
477.0	0.816
502.0	0.829
527.0	0.844
552.0	0.861
577.0	0.881
602.0	0.910

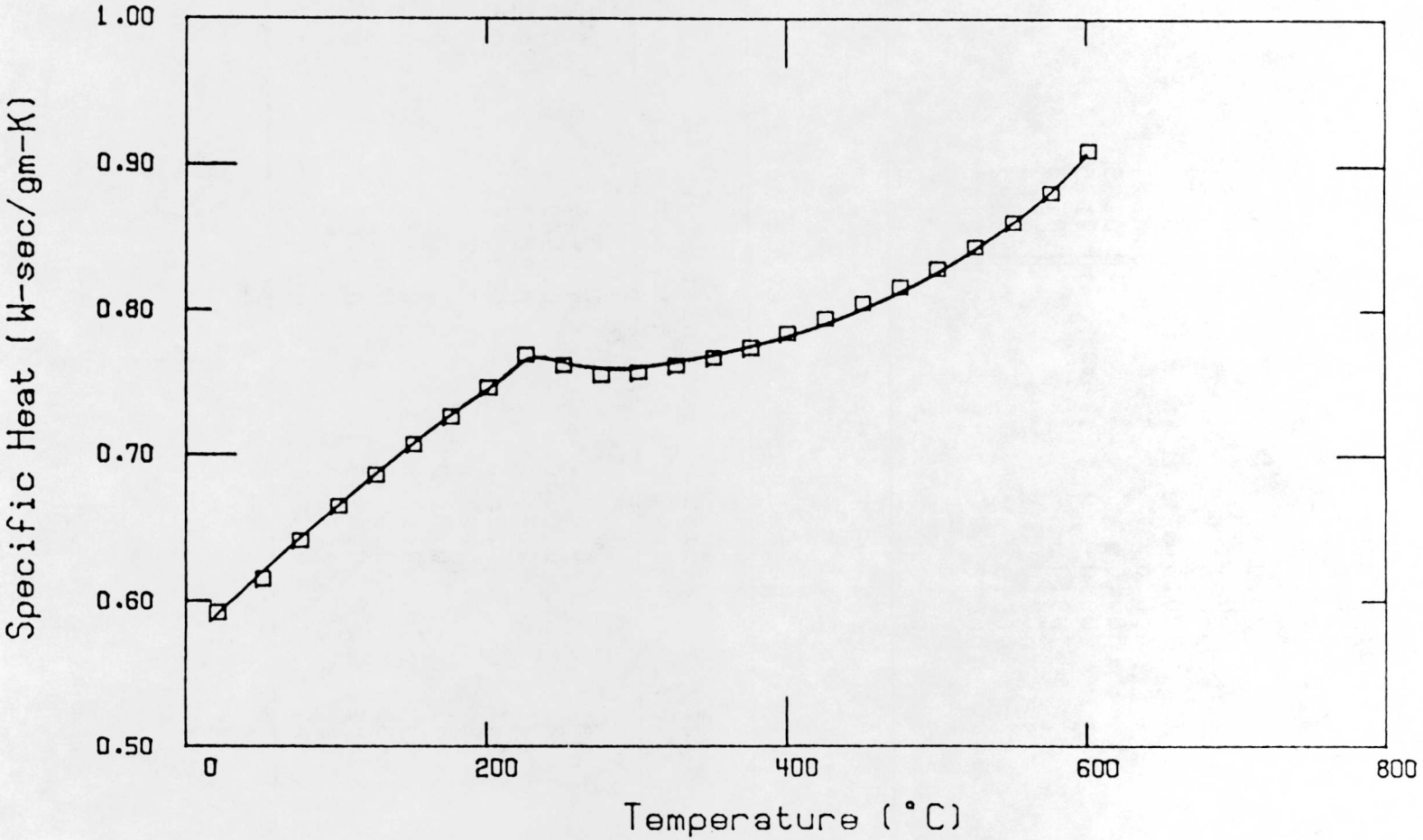

Figure 7 Specific Heat

Table 2. Thermal Diffusivity Results

	Temperature (°C)	Diffusivity ($cm^2 s^{-1}$)
	23.0	0.0415
	100.0	0.0347
	200.0	0.0274
	300.0	0.0235
	400.0	0.0214
	500.0	0.0185
	600.0	0.0175
	700.0	0.0173
	800.0	0.0164
	900.0	0.0152
	1000.0	0.0145
Cool	500.0	0.0180

Table 3. Thermal Conductivity Calculations

Temp. (°C)	Density ($g\ cm^{-3}$)	Specific Heat ($W\text{-}s\ g^{-1}K^{-1}$)	Diffusivity ($cm^2\ s^{-1}$)	Conductivity ($W\ cm^{-1}K^{-1}$)
23.0	5.681	0.5920	0.0415	0.13957
100.0	5.681	0.6640	0.0340	0.12825
200.0	5.681	0.7440	0.0275	0.11623
300.0	5.681	0.7550	0.0234	0.10037
400.0	5.681	0.7820	0.0215	0.09551
500.0	5.681	0.8270	0.0185	0.08692
600.0	5.681	0.9080	0.0175	0.09027
700.0	5.681	0.9140	0.0173	0.08983
800.0	5.681	0.9380	0.0164	0.08739
900.0	5.681	0.9590	0.0152	0.08281
1000.0	5.681	0.9760	0.0145	0.08040

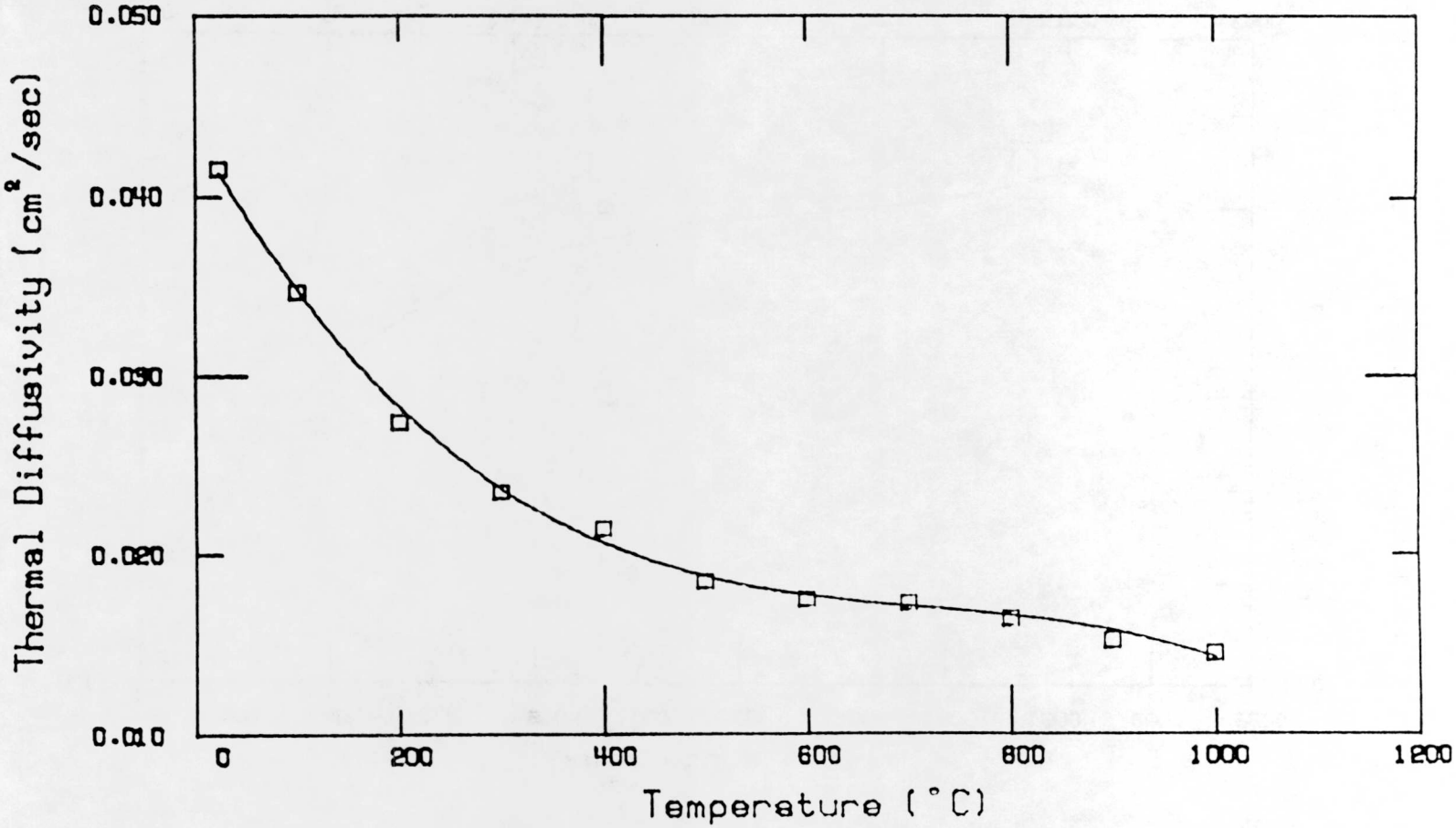

Figure 8 Thermal Diffusivity

Figure 9 Thermal Conductivity

Table 4. Thermal Expansion Results

Temperature (°C)	Expansion (in./in.)	Average Coefficient ($10^{-6}C^{-1}$)
22	00	--
47	225	--
97	295	--
147	1240	9.9
197	1777	10.2
247	2417	10.7
297	2983	10.8
347	3610	11.1
397	4224	11.3
447	4868	11.5
497	5547	11.7
547	6254	11.9
567	6558	12.0
587	6870	12.2
607	7173	12.3
617	7298	12.3
647	7703	12.3
697	8319	12.3
747	8946	12.3
797	9581	12.4
847	10180	12.3
897	10820	12.4
947	11450	12.4
997	12050	12.4

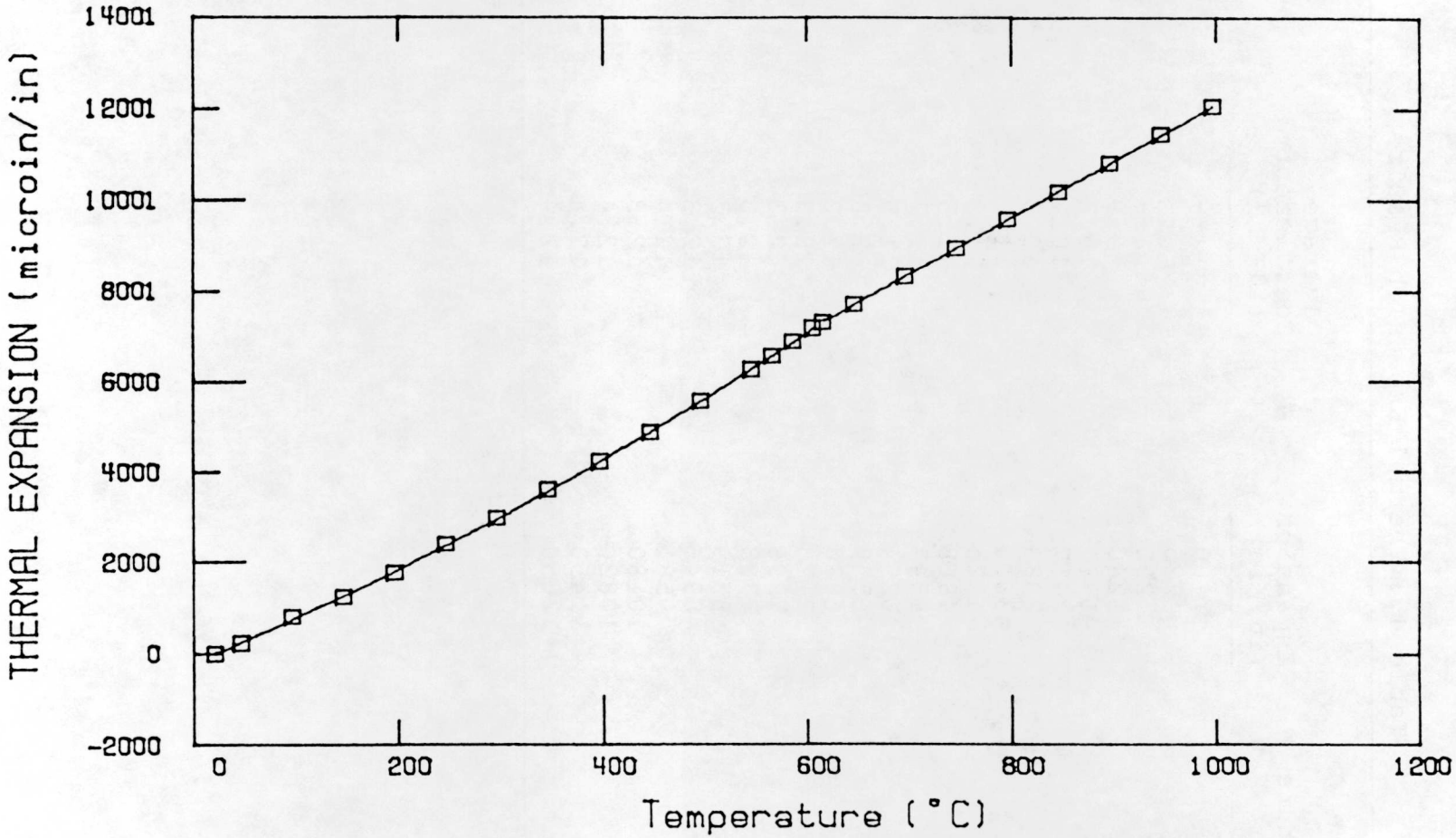

Figure 10 Thermal Expansion

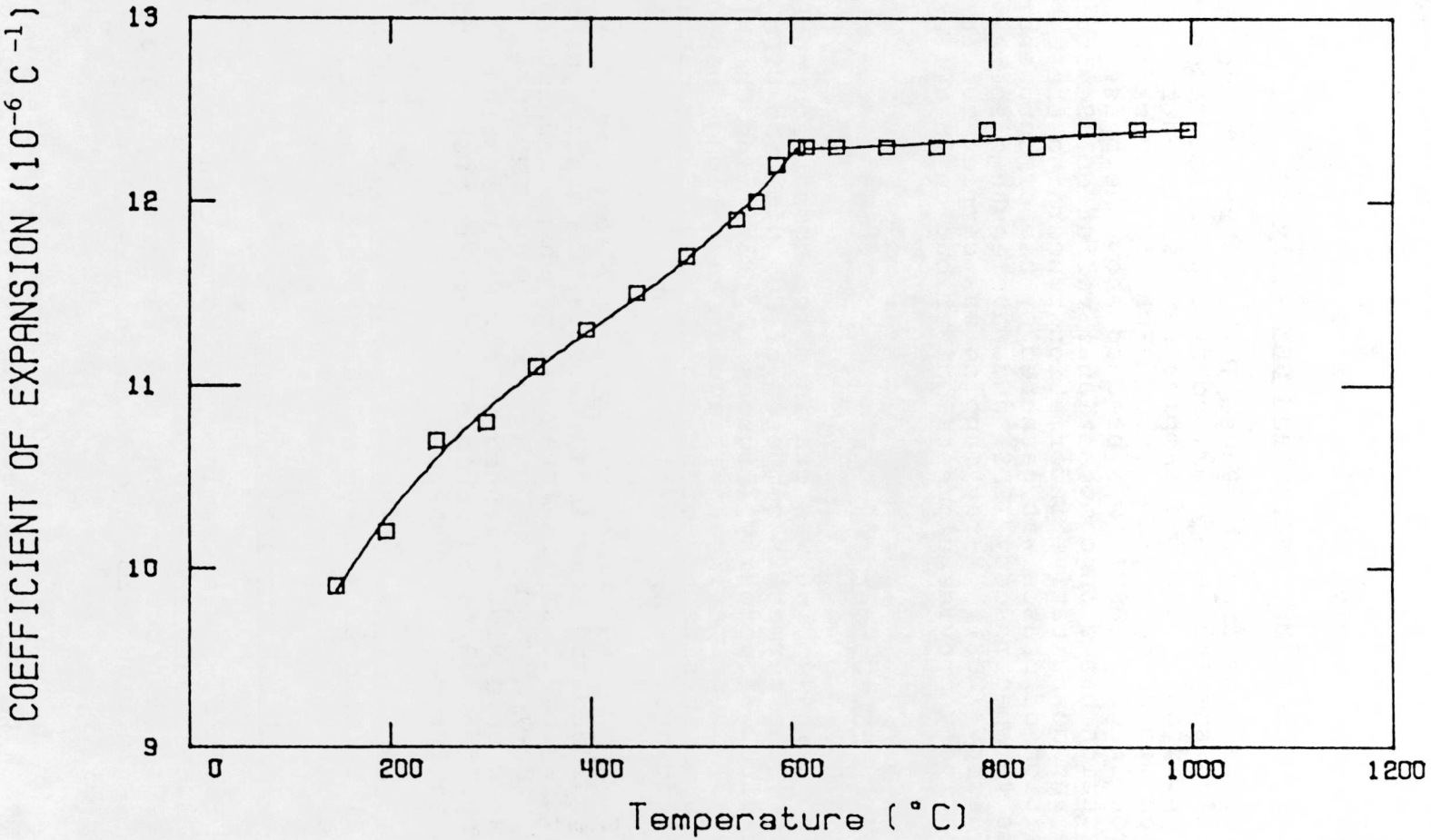

Figure 11 Coefficient of Expansion

PNL cermets used in Phase I are slightly Cu rich, whereas the ELTECH production cermets are slightly Cu poor because of Cu bleeding when sintering the greenforms. However, both cermet materials show equivalent %Fe/%Ni ratios.

4.2.3.4 Optical Microscopy and SEM Analysis

Both PNL samples from the Phase I Anode Project and ELTECH production samples were examined by optical microscopy with a Nikon Optiphot. Selected samples were analyzed by scanning electron microscopy (SEM) with a JEOL 35CX. Back scatter electron imaging (BSEI) was used to show the phase distribution based on compositional variation. Semiquantitative and quantitative information concerning the composition of phases was gathered by use of both energy dispersive spectroscopy (EDS) and wavelength dispersive spectroscopy (WDS). X-ray mapping was carried out to qualitatively provide elemental distribution in different phases.

4.2.3.4.1 PNL Cermet

PNL cermet 13474-31-6 was examined for comparison to ELTECH samples. The cermet is composed of Cu, NiO, and $NiFe_2O_4$ grains with ~3% porosity (Figures 12, 13). The Cu (A in Figure 13) is primarily as irregular and oblong shaped grains up to 75 µm in size. A minor amount of smaller roundish Cu grains, down to 5 µm, are also present.

The $NiFe_2O_4$ (B in Figure 13), typically 45 µm in size, is often equiaxed and sometimes encircles Cu grains while NiO (C), averaging 35 µm, is irregular in shape and interstitial to the $NiFe_2O_4$. There is some evidence of $NiFe_2O_4$ exsolution lamellae within NiO, oriented in several directions. Porosity, from 30 to 50 µm in diameter, is often roundish but sometimes irregular in shape.

Typical compositions of the phases are shown in Table 5. The Cu metal is alloyed with up to 20% Ni while the NiO contains some Fe.

4.2.3.4.2 ELTECH Production Cermet

Sample 13468-57-3 was examined for comparison to PNL cermets. The ELTECH cermets are also composed of Cu, NiO, and $NiFe_2O_4$ (Figures 14, 15) but contain up to 7% porosity. Typical Cu grains (A in Figure 15) are 30 µm in size with rare grains up to 175 µm.

$NiFe_2O_4$ (B in Figure 15) is 20 to 25 µm and equiaxed, sometimes with crystal faces. The NiO (C in Figure 15), 10 to 35 µm in size, are irregular in shape and contain lamallar exsolution of $NiFe_2O_4$ along crystallographic axes. Porosity is generally 20 to 30 µm in diameter and can be round, oval,

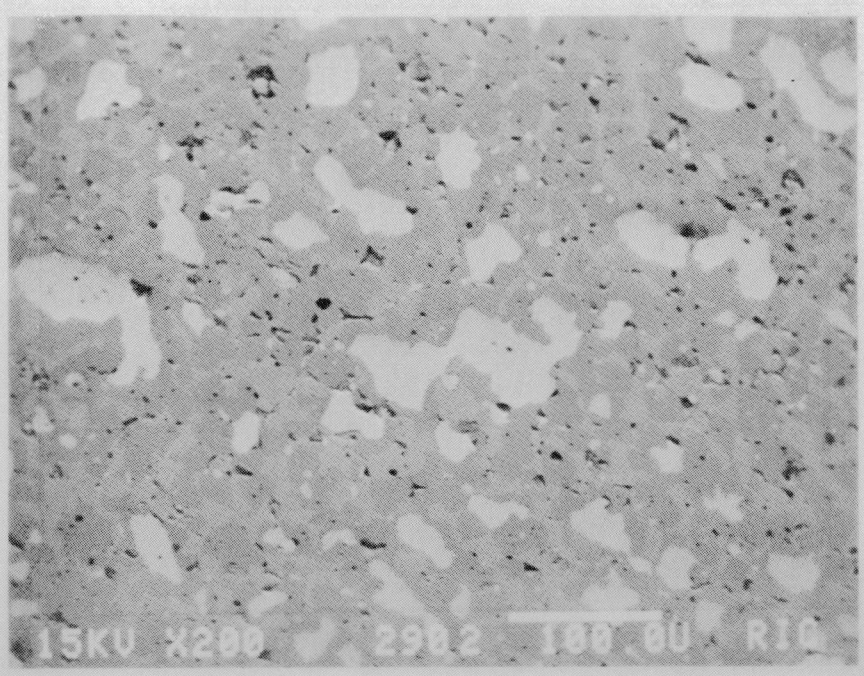

BSE 200X

FIGURE 12
Typical Microstructure of PNL
$NiFe_2O_4$/Cu Cermet
Sample 13479-31-6

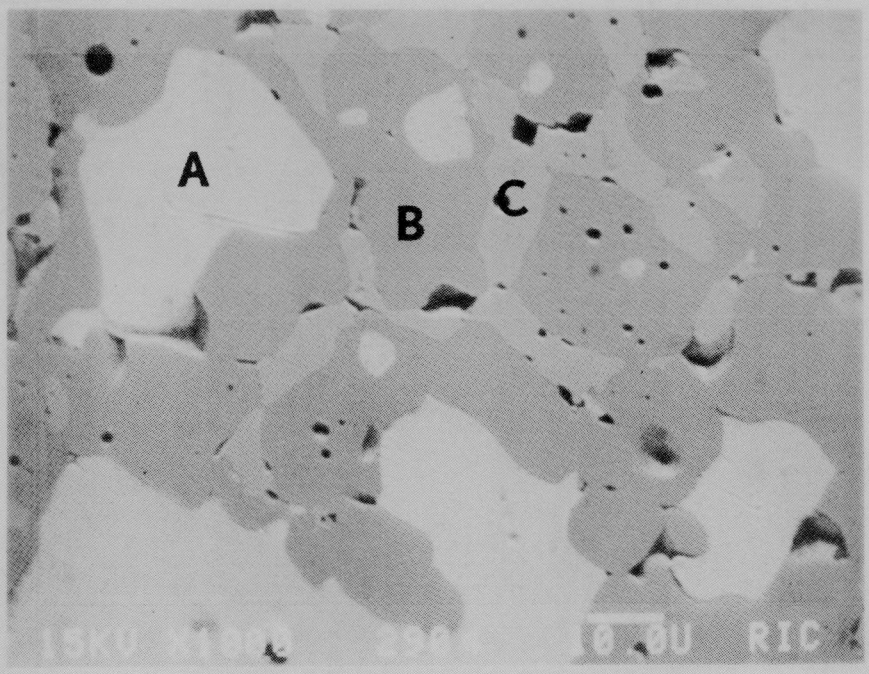

BSE 1000X

FIGURE 13
High Magnification of PNL
$NiFe_2O_4$/Cu Cermet
Sample 13474-31-6

Table 5. Typical Phase Composition Based on Semiquantitative EDS Analysis, in Wt%

Sample	Phase	Cu	Ni	Fe	O[a]
PNL 13474-31-6	Cu	77	20	3	-
	NiO	-	80	12	8
	$NiFe_2O_4$	-	20	54	26
ELTECH 13468-57-3	Cu	93	3	3	-
	NiO	-	82	11	7
	$NiFe_2O_4$	-	22	52	26

a. Calculated by difference

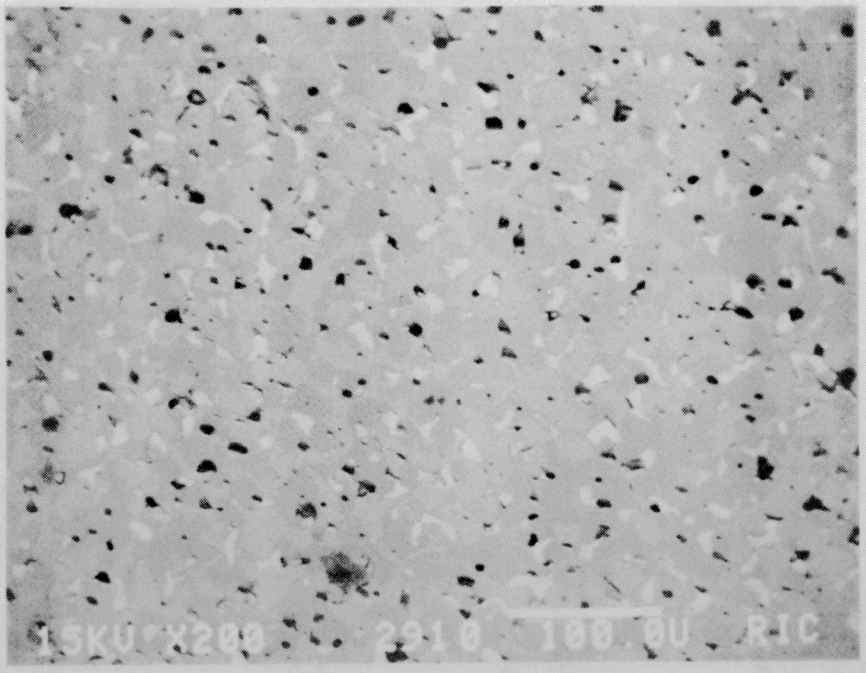

BSE 200X

FIGURE 14
Typical Microstructure of ELTECH
$NiFe_2O_4$/Cu Cermet
Sample 13468-57-3

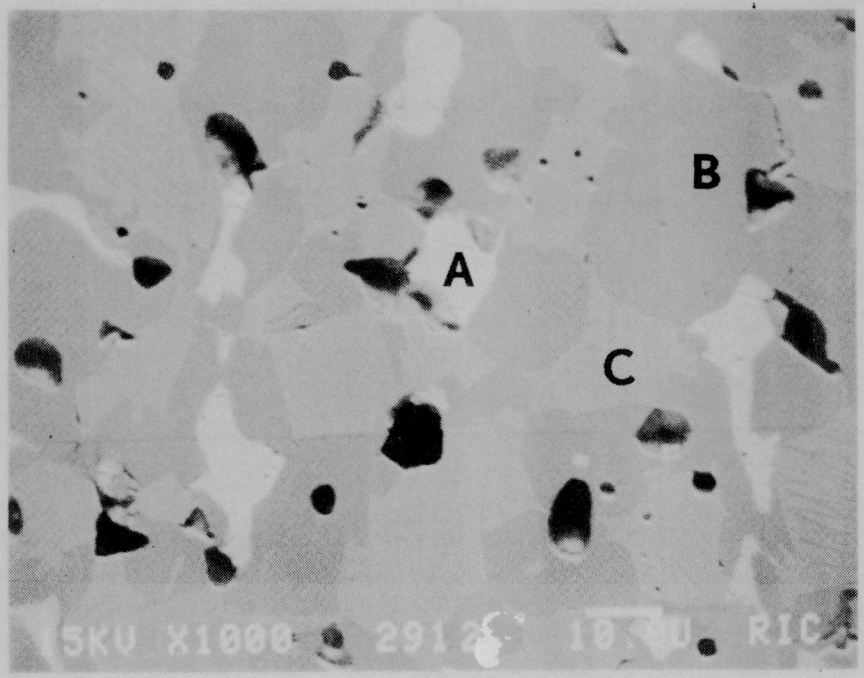

BSE 1000X

FIGURE 15
High Magnification of ELTECH
$NiFe_2O_4$/Cu Cermet
Sample 13468-57-3

or irregular in shape.

Typical phase compositions are shown in Table 5. The Cu is alloyed with a small amount of Ni and Fe (3 wt%). The NiO contains some Fe in solid solution.

4.2.3.4.3 PNL Versus ELTECH

Optical microscopy shows the sintered cermets have equivalent ferrite and oxide grain formation and grain sizes, however there is a difference in porosity and Cu metal distribution that can be attributed to the pre-sintering powder history. Namely, the PNL calcined powders were spray dried before blending with Cu powder and isopressing. The spray dried powder resulted in a flowable powder that compacted more uniformly when isopressed. When these uniformly compacted greenforms were sintered, the resulting anode had high density and low porosity and no Cu metal bleeding during sintering. In contrast, the ELTECH calcined powders were not spray dried and thus not as flowable, and the sintered greenforms produced a slightly more porous anode that suffered loss of Cu metal through bleeding. The melting of the Cu and subsequent grain boundary diffusion out of the anode gave a highly dispersed interconnected Cu network throughout the cermet that accounts for the metallic characteristic in the resistivity measurements.

In summary of the materials characterization, the cermets are equivalent in physical properties and performance and the slight differences in porosity and densities can be attributed to differences in pre-sintering powder processing techniques.

4.2.4 Test Cells and Operating Protocol

Two different test cells were used. The short term test cell was identical to that operated in phase I of the DOE project and was operated for up to 10 h. The long term test cell was designed during phase 2 of the project and was operated for test durations of 50 and 100 h.

4.2.4.1 Short Term Cell Design

In phase I of the DOE program, the bulk of the tests were at alumina saturation and were run for a nominal 10 h. The short-term test cell used a large 750 mL 99.8% Al_2O_3 crucible 7.5 cm in diameter that fitted into a short carbon liner. A small 998 alumina crucible 3 cm diameter X 3 cm tall was placed inside the large alumina crucible to hold the aluminum cathode. The aluminum cathode made contact through an alumina sheathed carbon contact and an Inconel 600 current feeder rod assembly. The cell also incorporated an aluminum reference electrode in an alumina tube with a molybdenum current feeder rod. The cermet anode, connected to a Inconel

601 current feeder rod, was suspended above the cryolite bath. The cell assembly is shown in Figure 16. The crucible contains 500 g of cryolite bath to a depth of 5-cm deep when molten.

4.2.4.2 Short Term Cell Operating Protocol

On the initial setup, the anode was suspended above the bath during the heatup. The cell was heated to 60°C above the operating temperature to ensure complete melting of the cryolite mixture. The bath temperature was then lowered to the operating temperature and the anode current set. The anode was lowered into the molten bath to a depth of 1/8 in. and the electrolysis was immediately started. The operating protocol is summarized in Figure 17 for the Standard Bath (BR (BR 1.35). The Standard Bath consists of commercial grade cryolite with 5% CaF_2 at a BR of 1.35, and saturated with alumina at 980°C.

4.2.4.3 Long Term Test Cell Design

An extensive effort was made to use the bench-scale cell design as shown in Figure 16 for long term alumina saturated tests. However, after an exhaustive effort it became obvious that it was impossible to prevent the cell from crusting over after 50 h of operation. One reason is that, in the short term cell, the alumina sheathed feeder rods for the aluminum cathode and the alumina covering the reference electrode acted as sites for crust formation. Secondly, feeding mixtures of NaF, AlF_3, and alumina caused crust formation that encapsulated and seized the anode. Thus a new long-term cell design was needed to eliminate these problems and a cell operating protocol was needed to prevent crust formation.

The long-term cell design (Figure 18) included a tall carbon 8 cm diameter crucible with a conical tapered bottom for the aluminum pool, that became the cathode through electrical contact made with the carbon crucible. A well defined cathode at the bottom of the crucible was maintained by an inert alumina liner insulating the sides of the crucible. The anode, attached to a current feeder rod was suspended in the cryolite bath. This cell design removed all of the alumina sheathing that acted as sites for crust formation.

4.2.4.4 Long Term Test Operating Protocol

During operation of the long term test cell the cryolite became more acidic because of sodium adsorption by the carbon crucible. This loss of sodium was quite pronounced during the first two days of operation and led to wide swings in bath ratio during that time. The most effective way to

FIGURE 16
SHORT TERM
TEST CELL

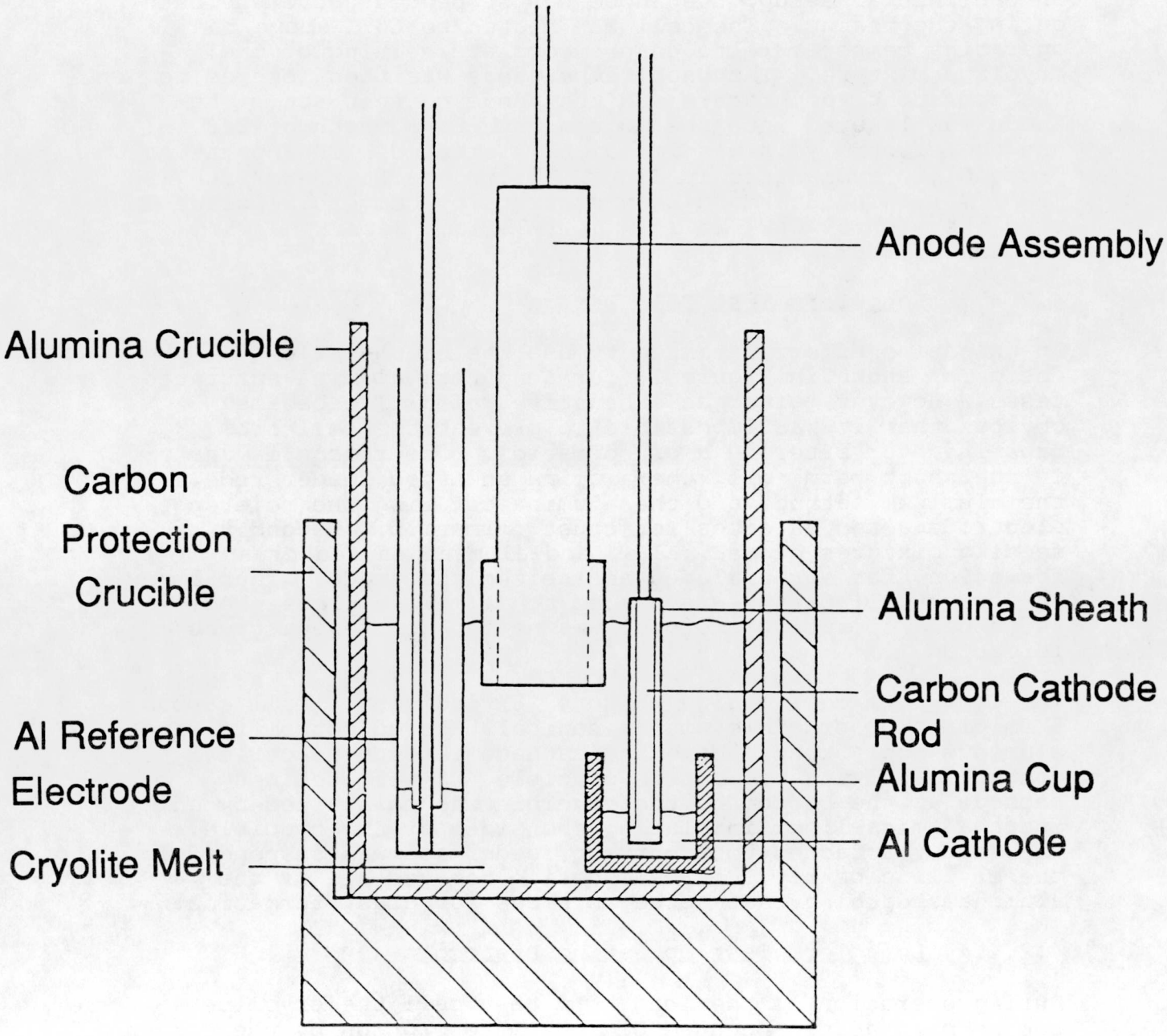

FIGURE 17

SHORT TERM TEST

CELL OPERATING PROTOCOL

STANDARD BATH RATIO - 1.35

ALF_3 - 6.5%

ALUMINA - 8%

CaF_2 - 5%

INITIAL HEATUP 1040°C (ANODE ABOVE MELT)

COOL TO 980°C (LOWER ANODE INTO MELT)

SET CURRENT DENSITY

FEED ALUMINA/CeF_3 MIXTURE

FIGURE 18
LONG TERM TEST CELL

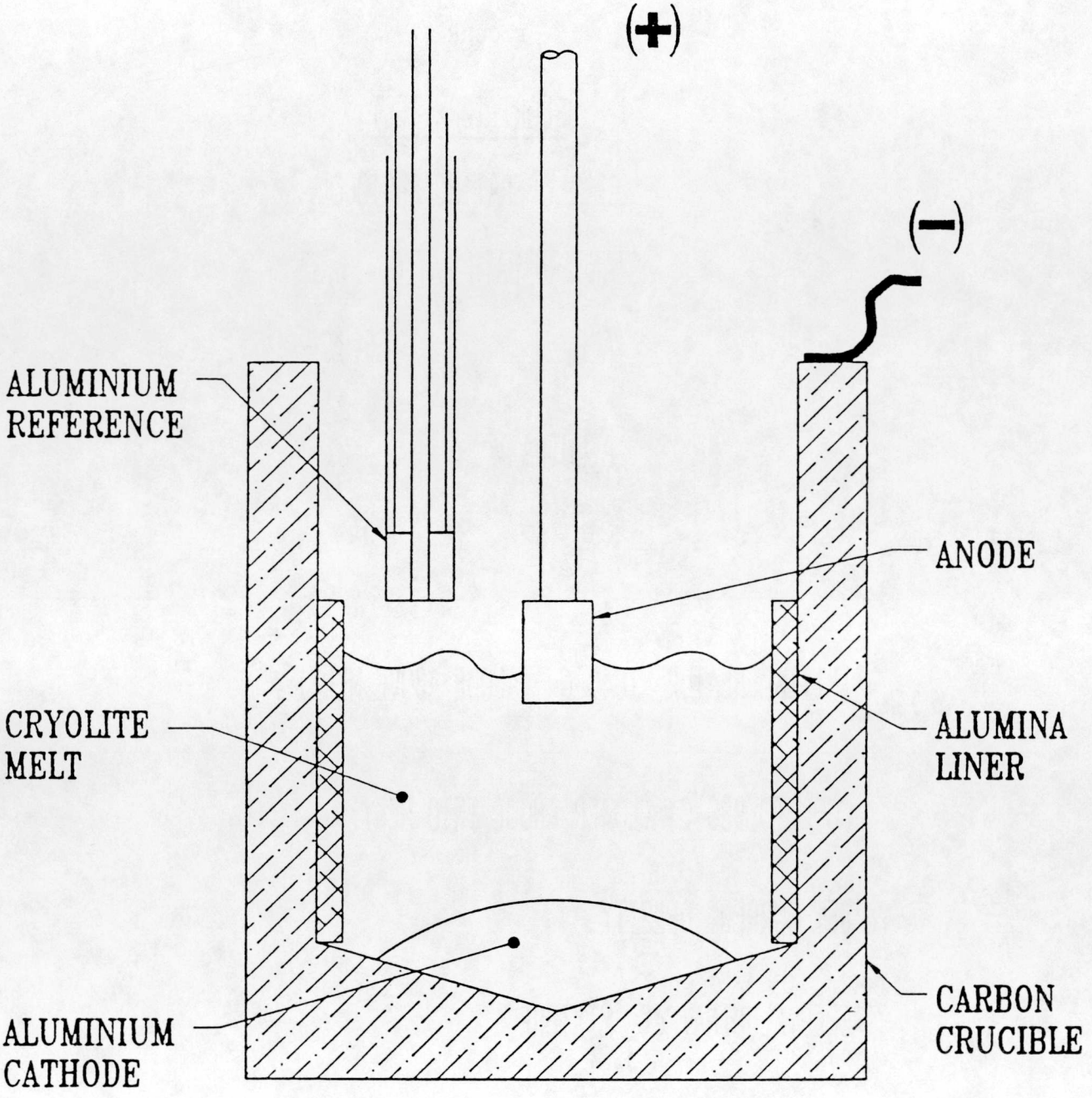

LONG TERM TEST CELL

control the bath acidity was by the slow addition of Na_2CO_3, which minimized crust formation by the reaction

$$3\ Na_2CO_3 + 2\ AlF_3 = 6\ NaF + Al_2O_3 + 3\ CO_2\ (gas). \quad (14)$$

Bath ratio determinations were made from analyses every 24 h and the bath ratio and level maintained by additions of the targeted bath compositions. The long term operating protocol is summarized in Figure 19.

4.2.5 Background Corrosion

Because CEROX coating protection was determined from metal and bath contamination by cermet components, it is important to know the background levels of the corrosion products that were being contributed by the system.

The aluminum cathode material obtained from Morton Thiokol, Inc. is 99.999% pure while the Al_2O_3 liners from McDanel are 99.8% Al_2O_3 with low levels of impurities. The tall carbon crucibles obtained from Stackpole have a reported impurity of 0.03% Fe. The Al_2O_3 powder added to the bath was from Fisher Scientific (A-591) and reportedly contains 0.002% Fe.

For an evaluation of corrosion products introduced by the system, including bath and additives, cell components and the anode holder, the long term cell was heated and cooled to operating temperature and then the bath and metal were sampled and analyzed for Fe, Ni, and Cu by ICP (inductive coupled plasma). The long-term cell constituents were sampled with both the anode assembly held above the bath during heatup and without an anode assembly above the bath during heatup. The analytical results are:

System Corrosion

		%Fe	%Ni	%Cu
Morton Thiokol (99.999%) Aluminum Cathode		0.002	0.000	0.000
American Fluoride Co. Synthetic Cryolite		0.005	0.000	0.000
Long term cell	Metal	0.020	0.000	0.000
Heatup--no anode	Cryolite	0.000	0.002	0.004
Long term cell	Metal	0.075	0.002	0.010
Heatup--anode above Melt	Cryolite	0.003	0.013	0.000
Total calculated background corrosion (in grams)		0.05 g	0.08 g	0.004 g

FIGURE 19

LONG TERM TEST

100 h

CELL OPERATING PROTOCOL

STANDARD BATH RATIO - 1.35

ALUMINA - 8%

CaF_2 - 5%

INITIAL HEATUP 1040°C (ANODE ABOVE MELT)

COOL TO 980°C (LOWER ANODE INTO MELT)

SET CURRENT DENSITY

FEED ALUMINA / CeF_3 MIXTURE

ADJUST BATH RATIO WITH Na_2CO_3

ADJUST BATH DEPTH WITH TARGETED BATH / 24 HOURS

The only appreciable contaminant in the long-term cell heatup without the anode assembly is the Fe from the carbon crucible. The long-term cell heatup with the anode assembly above the melt shows more of the anode composite elements present. This may be due to the reflux action of volatile $NaAlF_4$ condensing and attacking the anode and anode holder (which contains Fe, Ni, and Pt plated Cu). The total background corrosion, in grams, was calculated from the percentage of the components in the bath and metal.

4.2.6 Analytical Protocol

During long term testing, bath composition monitoring was necessary because of sodium adsorption by the carbon crucible and losses of volatile components, mainly as sodium aluminum tetraflouride ($NaAlF_4$). For half-saturated alumina tests, the alumina concentration was periodically determined.

4.2.6.1 Cryolite Bath Ratio Analysis

Bath levels were adjusted every 24 h by addition of the targeted bath composition. In addition, the bath was sampled and analyzed every 24 hours and appropriate additions made to correct the BR. The bath analysis procedures are described below.

Step 1. Digestion

A cryolite sample was obtained from the cryolite bath with a hollow alumina rod. The cryolite was ground into a fine powder and a 1.0 g sample weighed into a 400 mL beaker. Potassium hydroxide (8.00 mL of 1.0 N solution) was added along with 30 mL of deionized water. The beaker was covered with a watch glass and heated to boiling. The digestion proceeded for 1/2 h. During the digestion, excess AlF_3 reacted with KOH to form potassium cryolite and aluminum hydroxide giving us

$$2\ AlF_3 + KOH = K_3AlF_6 + Al(OH)_3. \qquad (15)$$

After complete digestion, the solution was rapidly cooled to room temperature using an ice bath.

Step 2. Acidification

KCl was then added to the cooled digest, in excess over the KOH used during digestion. A convenient addition was 90 mL of 0.1 N HCl. This amount was 1 mmole (milli-mole) excess over the initial KOH addition.

Step 3. Titration

The acidified solution was subsequently back titrated with a standard KOH solution (0.1 N). The endpoint was determined

when the pH reached 8.3. The easiest way to do this was to add the KOH in 1 mL aliquots and record the pH. The solution was stirred vigorously during titration in order to stabilize the pH reading. When the pH reached 4 to 5, smaller aliquots were used. By graphing the pH versus volume of KOH, the endpoint could readily be determined.

Step. 4 Calculations

The minimum volume of KOH added during titration was found to be 10.0 mL (1 mmole), because this is the amount of excess HCl used during acidification. The volume of KOH used in excess of 10 mL was that required for titration of AlF_3. Therefore,

$$Vcor = Vtitr - 10.0 \text{ mL}. \quad (16)$$

The mmole of AlF_3 in the sample was then calculated by

$$\text{mmole } AlF_3 = Vcor \times 0.1 \text{ mole KOH}/1 \times 2 \text{ mole } AlF_3/3 \text{ moles KOH}. \quad (17)$$

The weight of AlF_3 in the sample became

$$\text{wt } AlF_3 = \text{mmoles } AlF_3 \times 83.98 \text{ g/mole}/1000. \quad (18)$$

The wt% AlF_3 was the weight of AlF_3 divided by the sample weight multiplied by 100. For a 1.0 g sample this became

$$\text{wt\% } AlF_3 = \text{wt } AlF_3 \times 100. \quad (19)$$

4.2.6.2 Bath Ratio Determination

The graph in Figure 20 shows the bath ratio as a function of wt% AlF_3. This assumes a bath containing 5% CaF_2 and 8% Al_2O_3. Should these vary, the curve would be slightly shifted. However, because these are the standard concentrations during our tests, the bath ratio could be read directly from the graph.

4.2.6.3 Wet Chemical Determination of Free Alumina

A sample of cryolite bath was crushed in a mortar to -100 mesh, and a 1 g sample was digested in 50 mL of a 30 wt% solution of aluminum chloride hexahydrate for 30 min. The solution was boiled on a hot plate with a magnetic stirrer in a 100 mL beaker with a watch glass cover containing cold water. After digestion, the hot solution was allowed to cool for 30 min before filtration and careful washing. The precipitate was washed with deionized water until free of chloride ion ($AgNO_3$ test). The precipitate was then dried in an oven at 110°C and gravimetrically determined by normal procedures.

FIGURE 20
Bath Ratio as a Function of
Wt % AlF_3

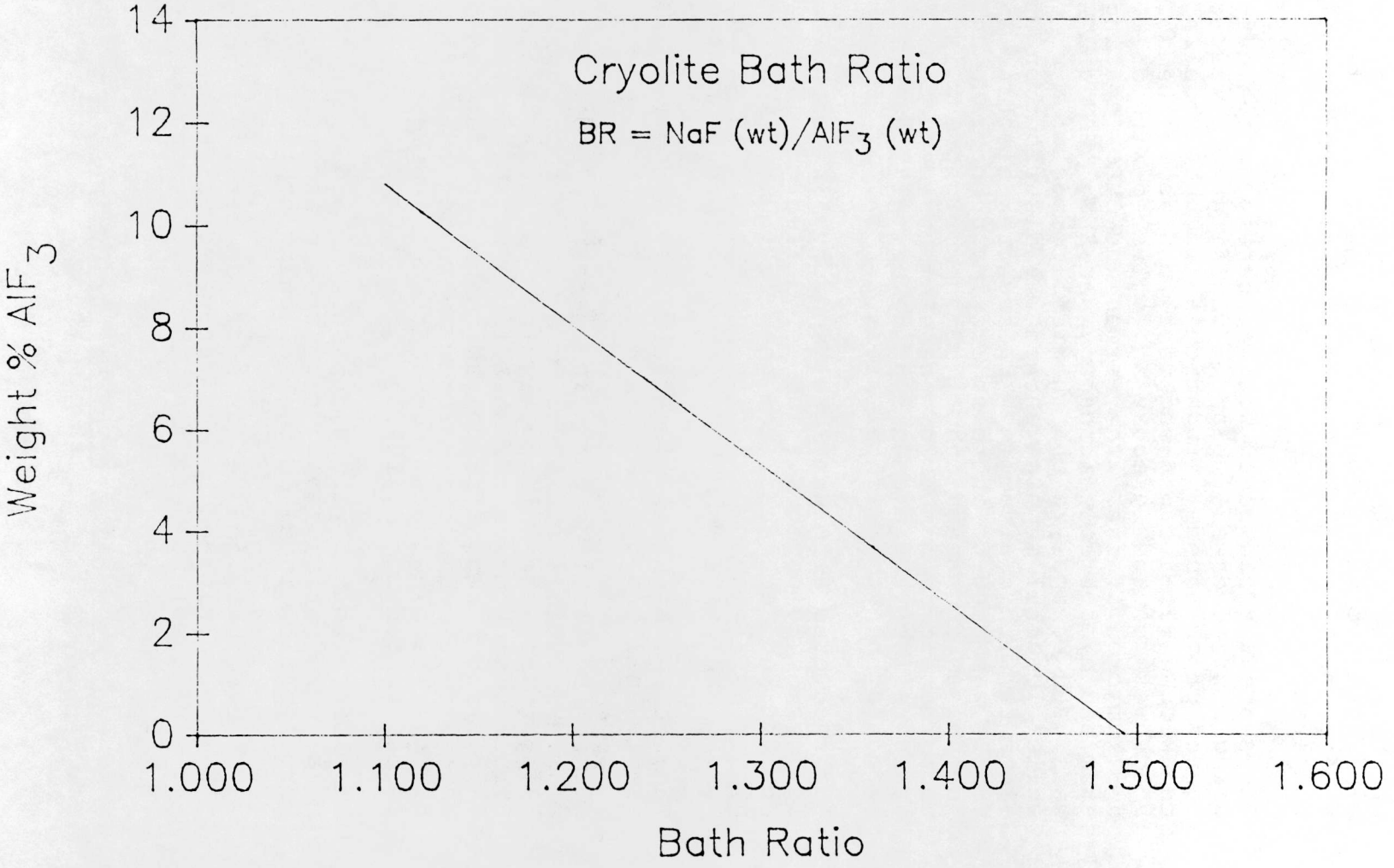

4.2.6.4 Analytical Methods for Tested Samples

At the end of the test period, the anode was raised from the bath, the electrical current and the furnace were shut OFF, and the cell and its contents were allowed to cool to room temperature.

The anode was sectioned with a Buehler Isomet cut-off saw using a diamond wafer blade. The first cut was across the center of the anode perpendicular to the anode surface and the second was a cross-sectional cut above the meltline. The anode was mounted in epoxy and polished with diamond grit to a 0.1 micron finish. The cermet and CEROX coating were examined by optical microscopy and SEM. EDX and WDX analyses were used to analyze the chemical composition of the samples while elemental mapping showed the distribution of particular elements within a sample. Backscatter electron imaging (BSEI) was used to increase the image contrast and delineate the phases from each other. Image brightness is dependent upon the atomic number of the elements detected. Darker areas reflect the presence of relatively lower at. wt elements than the lighter areas.

The recovered aluminum metal and cryolite bath were analyzed for cermet components. The solidified cryolite bath was crushed and separated from the aluminum cathode ball and the dispersed aluminum particles. The bath was ground with a mortar and pestle and then screened through a 50 mesh screen.

The crushed bath was mixed uniformly and a representative sample analyzed by ICP.

All of the aluminum particles were remelted together in an alumina crucible at 1000°C in argon. After cooling to room temperature, the uniform aluminum ball was sectioned with a Struer Discotom cut-off saw with a SiC blade. A heart-cut sample was taken. The contaminants were removed from all the cut surfaces of the sample by polishing on a 180 grit SiC cloth. The clean aluminum heart-cut sample was analyzed for cermet components by ICP.

The ICP corrosion values for Fe, Ni, and Cu in the bath and metal were normalized to project the industrial metal purity. Normalization involved the following steps:

1. The Fe, Ni, and Cu ICP analyses for the bath and metal were multiplied by the recovered weight of bath and metal (in grams) to determine the Fe, Cu, and Ni contamination in grams

   $$\text{wt of Al metal recovered} \times \frac{\text{\% Fe, Ni, or Cu in Al}}{100} = \text{g of Fe, Ni, or Cu in the Al}$$

wt of cryolite recovered X $\frac{\%\ Fe,\ Ni, or\ Cu\ in\ bath}{100}$ = g of Fe, Ni, or Cu in the cryolite

2. The contamination of each element in the bath and Al metal were added together

g of Fe, Ni, or Cu in Al metal + g of Fe, Ni, or Cu in the cryolite = Total grams of Fe, Ni, or Cu

3. The background corrosion was subtracted

Total g of Fe, Ni, or Cu - background corrosion of Fe, Ni, or Cu = "Corrected" g of Fe, Ni, or Cu due to corrosion of the anode

4. The corrosion was normalized for the theoretical amount of aluminum produced at the given current density, for the given amount of time, and assuming 95% current efficiency

$\frac{g\ of\ Fe,\ Ni,\ or\ Cu}{g\ of\ Al\ (theor.)}$ X 100 = % of impurities of Fe, Ni, or Cu projected in an industrial Al pool

A sample calculation is given in Appendix 1 for the 100 h Ce-free test operated at 1 A/cm^2 and a BR of 1.35.

4.2.7 Alumina/CeF_3 Feeder

The semi-automated feeder, as shown in Figure 21, had a mounted carousel with 20 dumpable plastic vials each with a maximum 10 gram capacity. The carousel was rotated by a programmed air powered cylinder that was controlled by a electrically powered solenoid switch. The feed rates were programmed for hourly additions.

4.3 SHORT TERM TESTS

The objective of the short term testing was to evaluate the CEROX coating quality formed under a variety of cell operating conditions. The dosing regimen tests were performed to establish a regimen for CeF_3 additions that would maintain a desired CEROX coating thickness in the Standard Bath. Next, the coatings with targeted thicknesses (1 mm) were produced in the Standard Bath and then exposed to quasi-commercial electrolytes for a total of 8 h. Contamination of the Al metal by Fe, Ni, and Cu was measured and the microstructure of the cermet and CEROX coating examined. Finally, half saturated Al_2O_3 tests were attempted in CeF_3-containing baths.

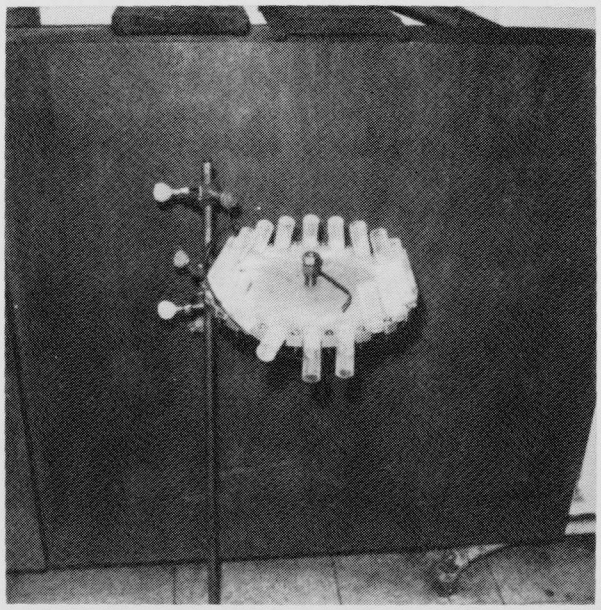

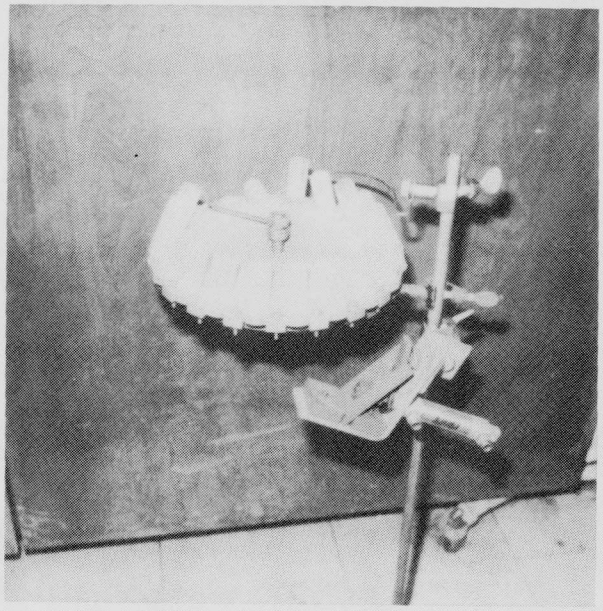

FIGURE 21
Alumina Feeder

4.3.1 CEROX Dosing Regimen

The first set of tests were designed to determine the amount of CeF_3 necessary to maintain in the bath in order to maintain a targeted CEROX coating thickness in the Standard Bath (BR 1.35).

4.3.1.1 Experimental Design

An array of 18 tests, nominally 8 h each, were performed and are summarized below. Two approaches to obtain targeted coating thicknesses were evaluated: in the first approach, the calculated amount of CeF_3 for a given coating thickness was added to the bath before the start of the test and periodic additions were made during operation to maintain the coating thickness; in the second approach, the test was started with no CeF_3 in the bath and periodic additions of CeF_3 were made to form and maintain the coating after an initial period (10 to 15 minutes) of operation without the protective CEROX coating.

The CEROX dosing program is summarized in the array of tests below:

CEROX Dosing Regimen Tests

Current Density, A/cm^2	% CeF_3 Initially Present	Targeted Thickness 0.5 mm	1.0 mm	1.5 mm
0.6	100	1[a]	1[a]	1[a]
1.0	100	1	1	1
1.4	100	1	1	1
0.6	0	1[a]	1[a]	1[a]
1.0	0	1[a]	1	1
1.4	0	1[a]	1	1

a. Resulted in cermet-to-cermet delamination.

In Phase I of this contract, it was established that when CeF_3 was added to the cryolite bath, cerium deposition on the anode substrate would not take place until a certain equilibrium concentration was reached in the aluminum pool and the cryolite bath. Analysis of cerium in the aluminum and the cryolite identified the partition coefficient for the BR 1.35 to be 2% Ce (Al): 0.3% Ce (bath) (partition coefficient of 6.67). In this work, the relationship between coating and CeF_3 addition confirmed the partition coefficient

established in Phase I for a bath ratio of 1.35.

4.3.1.2 Results and Discussion

The relationship between CeF_3 added to the bath and CEROX coating thickness was independent of current density and was found to be:

Coating Thickness (mm)	CeF_3 wt%
± 0.5	0.5
± 1.0	1.0
± 1.5	1.5

The coating thicknesses were maintained by periodic addition of CeF_3 along with the alumina feed to satisfy the partition coefficient for the electrowon aluminum produced.

When 100% of the CeF_3 was initially present, coatings were uniform and of targeted thicknesses for each of the current densities, as illustrated in Figure 22a for the 1.4 A/cm^2, 1.5% CeF_3 experiment. However, in the three experiments at 0.6 A/cm^2, a cermet-to-cermet delamination took place, as shown in Figure 22b.

In experiments where the bath was initially Ce-free and periodic additions of CeF_3 were made to form the CEROX coating, cermet-to-cermet delamination also occurred. However, delamination was prevented at 1.0 and 1.4 A/cm^2 current densities and 1.0 and 1.5 mm thicknesses if the addition of CeF_3 was started in <5 min. Cermet-to-cermet delamination still occurred, regardless of how quickly the CeF_3 was added, in the 0.6 A/cm^2 experiments and in the experiments with 0.5 mm coating thickness (Figure 23). Experiments that developed delamination are delineated with an asterisk in the table on page 45. The CEROX coatings from the tests that were initially Ce-free appeared similar in microstructure to those achieved with the CeF_3 initially present and were uniform and of targeted thickness.

4.3.1.3 Conclusions

Uniform CEROX coatings of the desired thickness were obtained by adding CeF_3 to the bath. At equilibrium, dissolved cerium was partitioned between the bath and the aluminum according to the partition coefficient determined in Phase I, and a stable CEROX coating formed on the anode; the thickness of the CEROX coating was proportional to the concentration of cerium in the bath. For a given cerium concentration in the bath, the coating thickness was independent of current density.

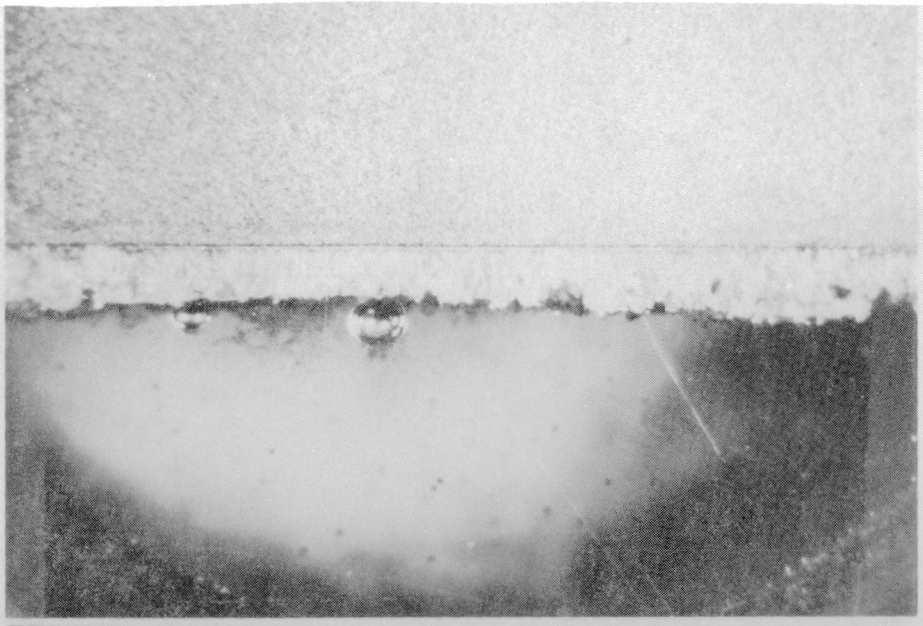

FIGURE 22a 8X
100% CeF_3 Initially
1.4 A/cm^2 1.5% CeF_3
Target 1.5 mm thick
Standard Bath

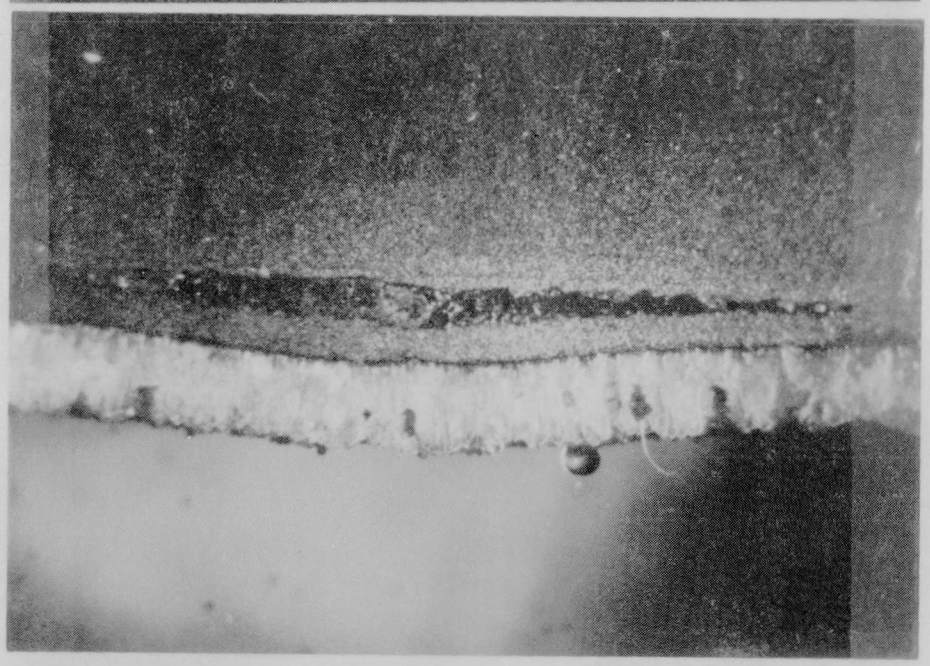

FIGURE 22b 8X
100% CeF_3 Initially
0.6 A/cm^2, 1.5% CeF_3
Target 1.5 mm thick
Standard Bath

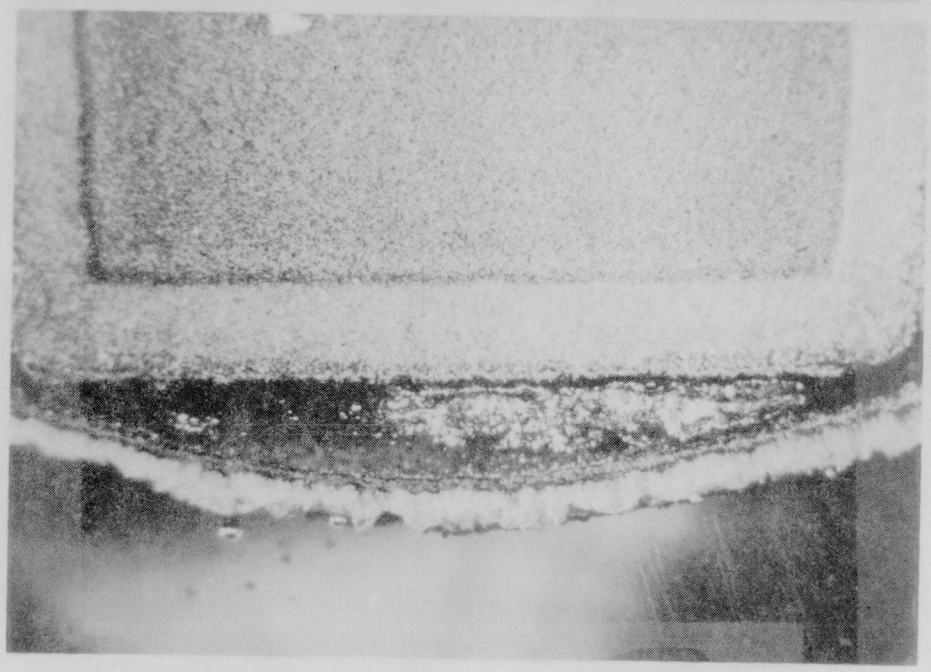

FIGURE 23 8X
0% CeF_3 Initially
1.4 A/cm^2 0.5% CeF_3
Target 0.5 mm
Standard Bath

For experiments at 0.6 A/cm^2, cermet anode corrosion was observed for all baths with Ce initially present and for all those initially Ce-free; theses results limit the usefulness of the CEROX coating for low current density operations. The cermet corrosion observed at higher current densities with delays in addition of CeF_3 (ie., initially Ce-free) shows the need for sufficient CeF_3 in the bath at all times during cell operation and for when a new cell is brought on-line.

4.3.1.4 Electrical Resistance of the CEROX coating

The additional electrical resistance caused by the CEROX coating on the anode was estimated from the change in the iR component of the anode potentials, measured at the beginning and during each of the short term dosing regimen experimental runs. Data and calculations are given in Table 6 and shown in Figure 24. In all cases with CeF_3 in the bath, anode potentials rose during the first 2 h of electrolysis. The anode potentials peaked within 2 h and then decreased to a plateau over the next 6 h.

The magnitude of the rise is dependent on both the concentration of CeF_3 in the bath (i.e. coating thickness) and current density. Resistance increases with increasing CeF_3 and increasing current density. One experiment at 1.4 A/cm^2 and 1.5% CeF_3, which should have the highest resistance, initially peaked with the highest resistance but then plateaued lower than several of the other experiments. This could be caused by changes in the microstructure of the coating (density) or to variation of the thickness with time.

The resistance results contrasts with the reported results in "Cerium Oxide Coated Anodes For Aluminum Electrowinning" by J. K. Walker and supported by DOE.[31] In those 8 h tests, there was a decrease in resistivity as well as coating thickness and density with increasing current density.

The increase in anode resistance can be attributed to the presence of the CEROX layer as well as the development of an O_2 bubble layer, which would increase with increasing current density. We do not have a method of measuring the resistance components because of the bubble layer and therefore are unable to accurately determine the resistance caused by the CEROX coating alone.

4.3.2 Quasi-Commercial Electrolytes at Alumina Saturation

Four tests were performed to determine the effect of different electrolyte compositions on the CEROX coating quality, as compared to the Standard Bath (BR 1.35).

Table 6. CEROX Coating Resistance (ohm-cm2)

%CeF_3	A/cm^2	$\frac{\Delta E\ (v)}{i\ (A/cm_2)}$[a]				
		0 h	2 h	4 h	6 h	8 h
1.5	1.4	0	0.500	0.357	0.314	0.382
1.0	1.4	0	0.471	0.414	0.407	0.407
0.5	1.4	0	0.250	0.240	0.260	0.270
1.5	1.0	0	0.400	0.370	0.350	0.360
1.0	1.0	0	0.320	0.260	0.240	-
0.5	1.0	0	0.144	0.100	0.110	0.150

a. $\Delta E = V_{time} - V_{initial}$

FIGURE 24

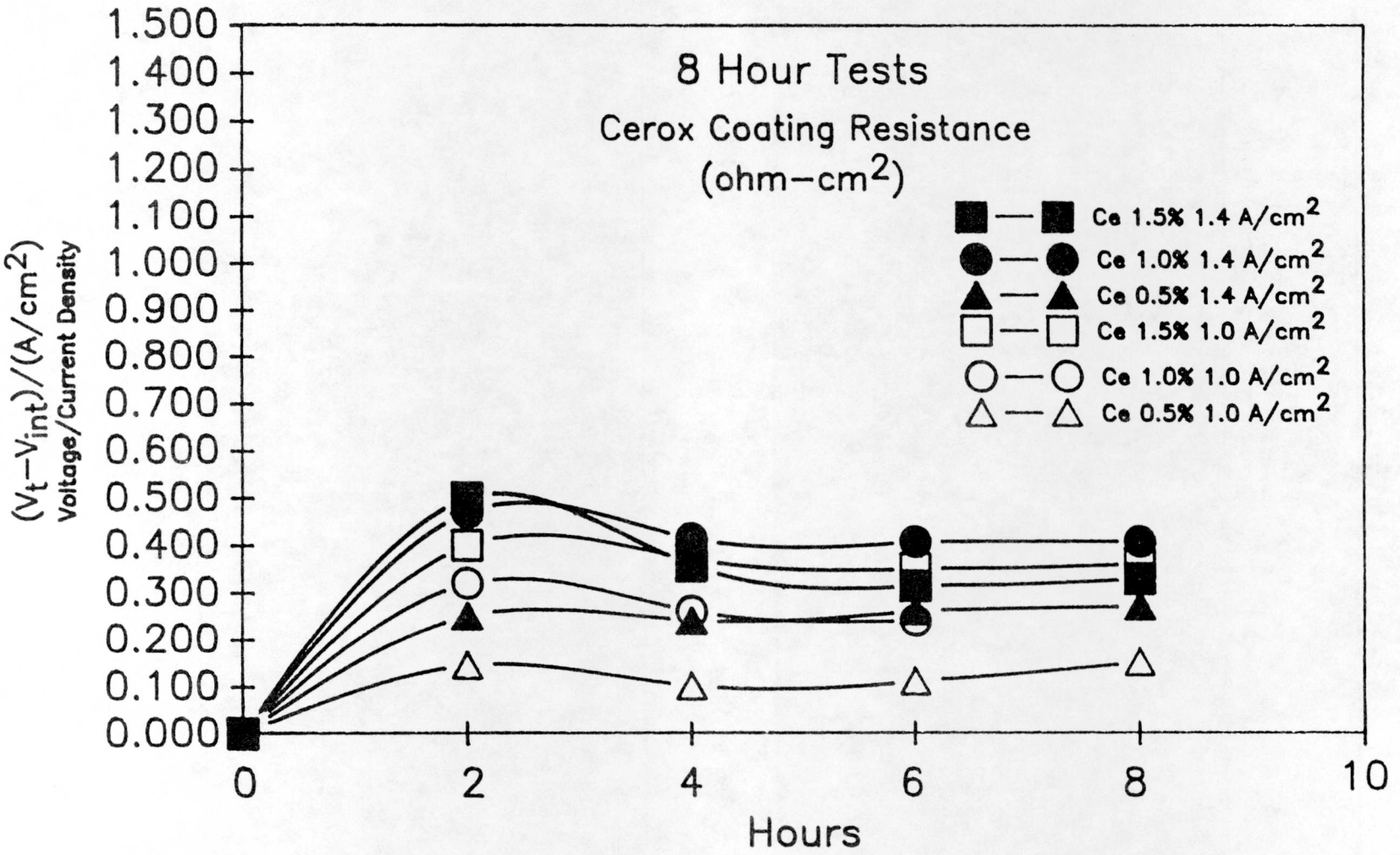
8 Hour Tests
Cerox Coating Resistance
(ohm-cm2)
Ce 1.5% 1.4 A/cm2
Ce 1.0% 1.4 A/cm2
Ce 0.5% 1.4 A/cm2
Ce 1.5% 1.0 A/cm2
Ce 1.0% 1.0 A/cm2
Ce 0.5% 1.0 A/cm2
(Vt-Vint)/(A/cm2)
Voltage/Current Density
1.500
1.400
1.300
1.200
1.100
1.000
0.900
0.800
0.700
0.600
0.500
0.400
0.300
0.200
0.100
0.000
0
2
4
6
8
10
Hours

4.3.2.1 Outline of Experiments

Four short term cell tests were evaluated to compare the standard bath (BR 1.35) to three DOE-specified saturated alumina electrolytes with 1.0% CeF_3 at a current density of 1.0 A/cm^2.

Three of the four short term tests were initiated under standard bath conditions at BR 1.35 with 1.0% CeF_3 at a current density of 1.0 A/cm^2 at 980°C. After 2 h of operation, when the anodes had achieved a CEROX coating thickness of 1.0 mm, temperature adjustments and additions to the bath were made to meet the DOE specified conditions and then the cell was operated at those conditions for 6 h. A fourth test at standard conditions was run for 8 h for comparison. The composition of the baths are:

Quasi-Commercial Electrolytes

	Bath 1	Bath 2	Bath 3	Std Bath
% Al_2O_3	8	8	8	8
Bath Ratio	1.07	1.4	1.15	1.35
% CaF_2	6	3	5.5	5
% MgF_2	0.05	3.5	0.0	0.0
% LiF	0.0	3	0.0	0.0
Temp°C	955	945	965	980

4.3.2.2 Results and Discussion

Table 7 summarizes the microscopy and SEM/EDX/WDX analyses. Figure 25 A-D compares the samples at low magnification.

4.3.2.2.1 Coating Thickness

CEROX coatings were deposited at a current density of 1.0 A/cm^2 at a BR 1.35 with 1% CeF_3 added to the cryolite. It was determined that after 2 h of operation under these conditions, a 1 mm thick coating developed on the nickel ferrite substrate. Samples were than exposed to quasi-commercial electrolytes. After exposure to the different baths, the CEROX coating was uniform and ranged from 0.35 mm thick in Bath 1 to 0.9 mm thick in Bath 2.

It was discovered that thin CEROX coatings resulted from operation in acid baths (ie. low bath ratios). Analysis of the metal and the bath showed an inverse relationship between the bath ratio and the concentration of cerium in the metal:

Table 7. Comparison of Anodes from DOE Baths and Standard Bath

Bath	CEROX Coating mm	Cu depleted layer thickness, μm	Phases in Cu depleted layer	Other Layers
1	0.35	<100 bottom 500 sides Porous	$NiFe_2O_4$(4%Cu) NiO(21%Cu,11%Fe) Cu oxide Ni-Cu-Fe Aluminate	Cu oxide layer between CEROX and cermet
2	0.90	400 to 600 Slightly porous	$NiFe_2O_4$(4%Cu) NiO(16%Cu,10%Fe) Ni-Cu-Fe Aluminate	Cu oxide layer between CEROX and cermet
3	0.60	700 Slightly porous	$NiFe_2O_4$(6%Cu) NiO(14%Cu,14%Fe) Cu oxide	CeF_3 and Cu oxide layer with some $NiFe_2O_4$ between CEROX and cermet
Std.	0.71	400 Dense	$NiFe_2O_4$(<1%Cu) NiO(21%Cu,10%Fe) Ni-Cu-Fe Aluminate	Gray layer (not identified) between CEROX and cermet

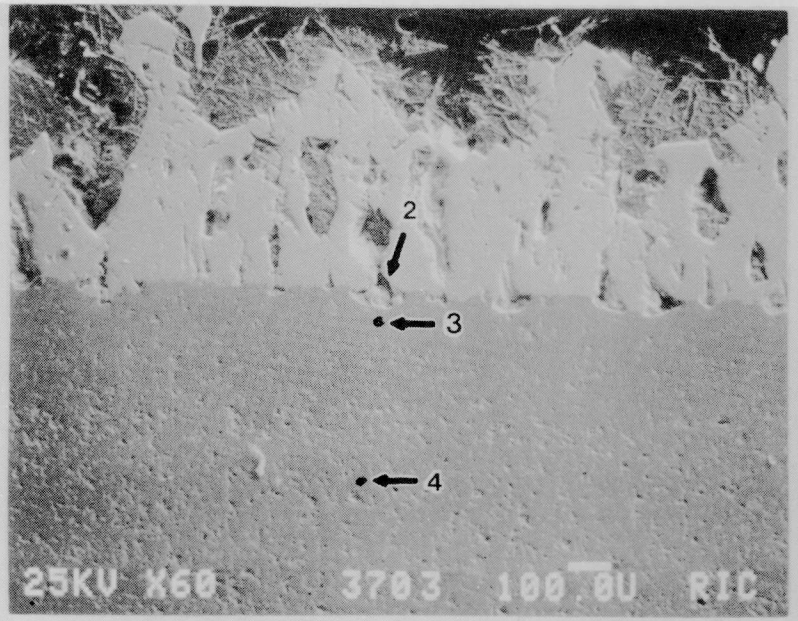

FIGURE 25A 60X
#13505-28 Standard Bath

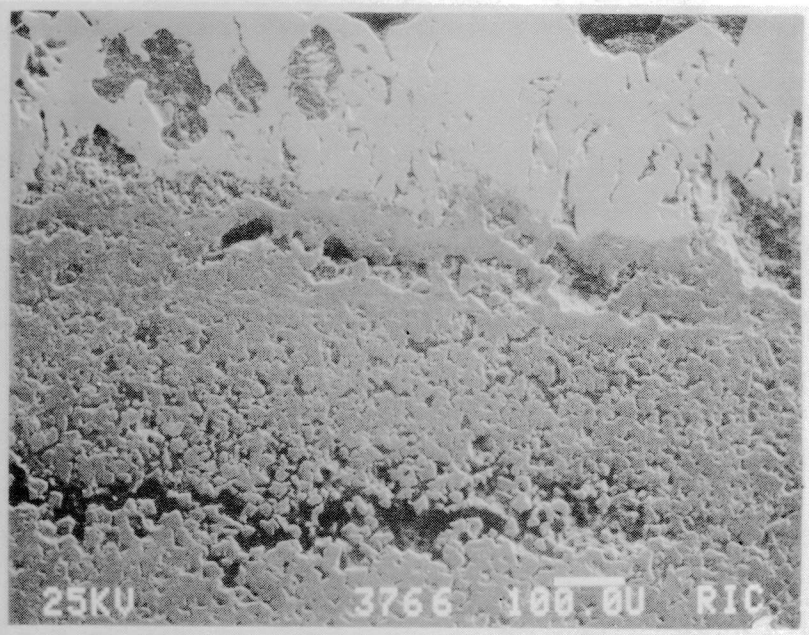

FIGURE 25B 100X
#13505-30 Bath 1

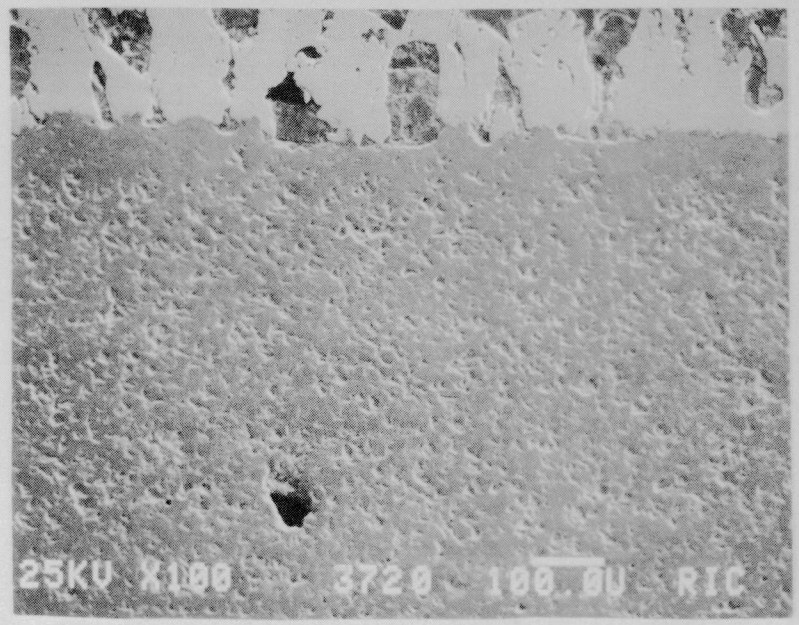

FIGURE 25C 100X
#13505-32 Bath 2

FIGURE 25D 48X
#13505-34 Bath 3
BEI

at lower bath ratios, more cerium was found in the metal as well as in the bath (Table 8). It is evident that the increased AlF_3 activity shifts the equilibrium between $Ce_{(Al)}$, $Ce_{(bath)}$, and Ce in the CEROX coating toward the two dissolved species.

This shift in the cerium partitioning is the first evidence of a correlation between the CEROX coating stability and the AlF_3 activity. Operation with lower bath ratios (ie., high AlF_3 activities) results in thinner coatings. The increase in the cerium concentration in the metal and the bath, resulting in the thinnest coating, demonstrates that the dynamic equilibrium of the CEROX coating is sensitive to the AlF_3 activity.

No correlation between other additives and coating thickness or quality was evident. The SEM analysis revealed that coatings were somewhat porous with cryolite penetration to the cermet interface. No evidence of the bath additives was detected in the CEROX coating.

4.3.2.2.2 Phase Assemblage and Layers

The interior of all the tested samples, as typified in Figure 26, consists of $NiFe_2O_4$ (A), $(Ni_{0.8}Fe_{0.2})O$ (B), and Cu with up to 6% Fe and 2% Ni alloyed in (C). A trace of a Cu oxide is occasionally found. This composition is similar to the untested samples.

There is Cu metal depletion in an exterior layer of each cermet anode, averaging around 500 µm, but not of a uniform thickness within each sample. The Cu depletion zone tends to be more extensive on the corners of the anode and less extensive on the bottom surface. The thickness of the layer does not appear to vary between the different baths. The redistribution of the copper is evident in the x-ray elemental map of the sample from Bath 2 (Figure 27).

The Cu metal depleted zone, as illustrated in Figure 28, consists of $NiFe_2O_4$ with up to 4% Cu in solid solution (A), (Ni,Cu,Fe)O with up to 20% Cu in solid solution (B), and occasionally a trace of Cu oxide or Ni-Fe-Cu aluminate (C). Porosity is somewhat higher in this region than in the untested anodes in the samples from Baths 1, 2, 3, and some grain delamination occurred in Bath 1. Cryolite was present within pores in this region.

A Cu oxide-rich layer, up to ~15 µm thick, was present between the CEROX coating and the cermet substrate in the anodes from Baths 1 and 2. Bath 3 also had an additional exterior layer, 100 µm thick, developed between the CEROX coating and the cermet (Figure 29). The layer consisted primarily of CeF_3 and Cu oxide, with some $NiFe_2O_4$. The layer is thickest along the edges and sides of the anode, and thins

Table 8. Cerium Partitioning

BR	Temp. °C	%CaF_2	%MgF_2	%LiF	%$Ce_{(Al)}$	%$Ce_{(Bath)}$	P.C.[a]
1.40	945	3	3.5	3	1.69	0.31	5.45
1.35	980	5	0	0	2.14	0.29	7.30
1.15	965	5.5	0	0	2.75	0.32	8.71
1.05	955	6	0.5	0	2.21	0.36	6.07

a. Partition Coefficient

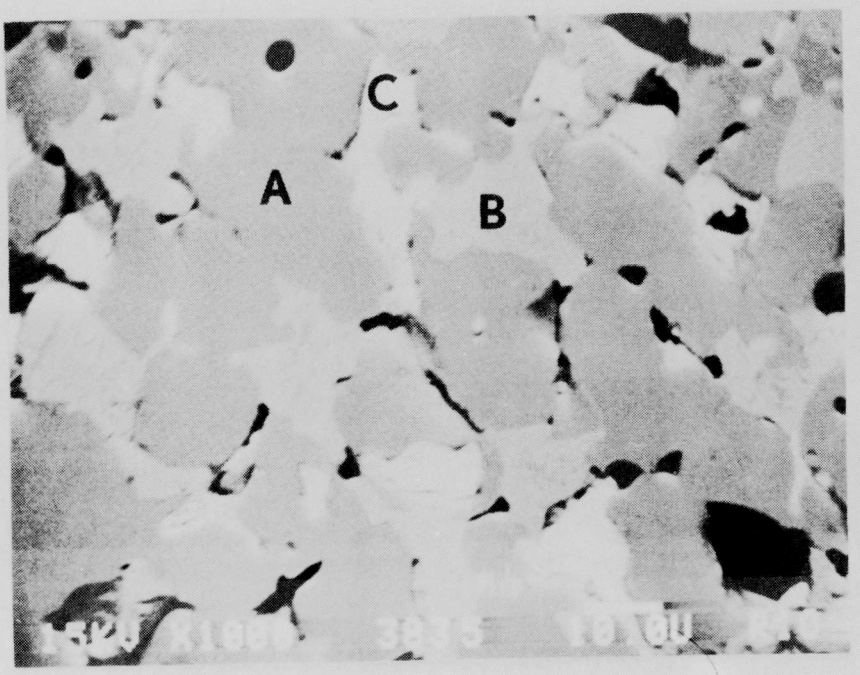

BEI 1000X

FIGURE 26

Interior of Tested Samples
#13505-28, Standard Bath

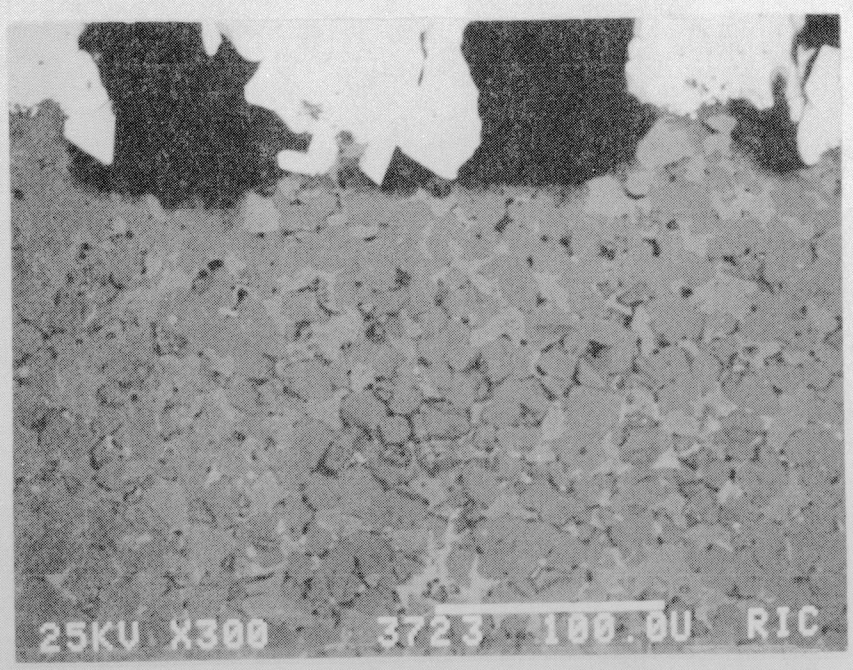

a. BEI 300X

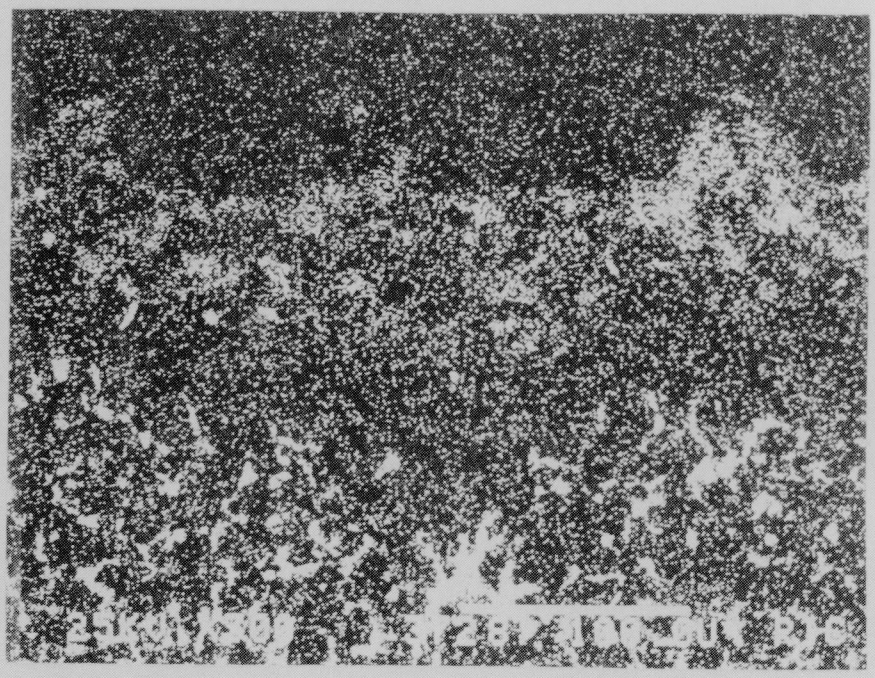

b. Cu Elemental X-ray Map 300X

FIGURE 27
Edge of Cermet Next to
CEROX Coating
#13505-32, Bath 2

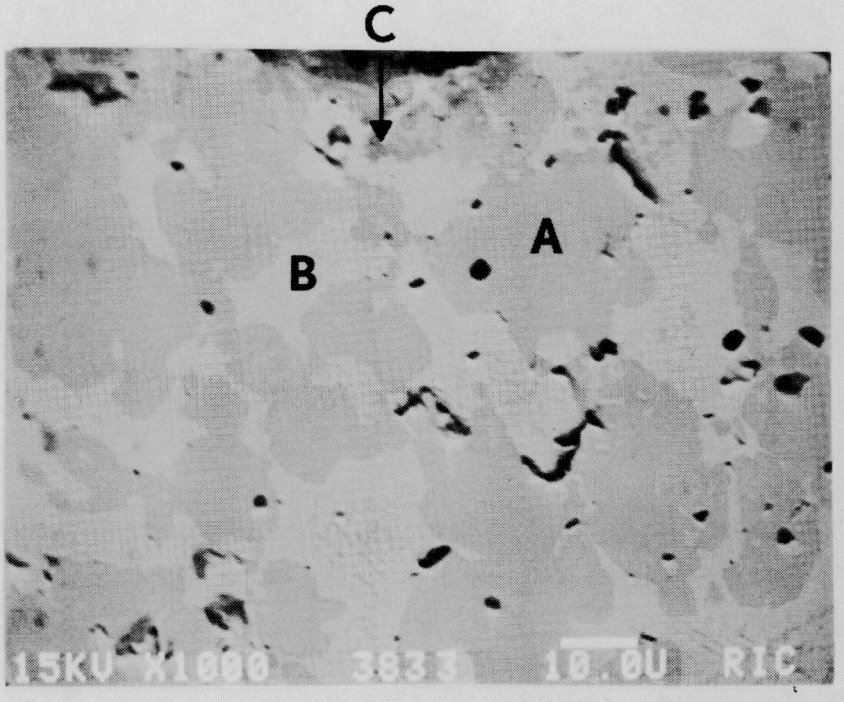

BEI 1000X

FIGURE 28

Cu Depleted Zone
#13505-28, Standard Bath

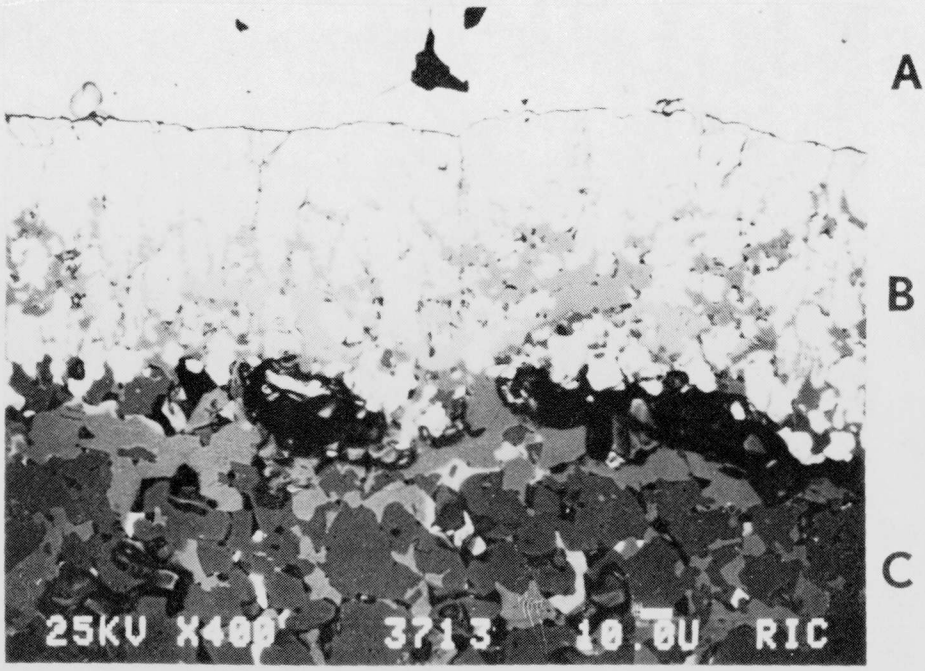

BEI 400X

FIGURE 29
The CeF_3 and CuO Layer (B)
Developed Between the
CEROX Coating (A) and
Ni-ferrite Substrate (C)
#13505-34
Bath 3

out and disappears across the center of the anode surface. This disruption at the interface is unusual for a 10 h test, which is generally characterized by a uniform CEROX coating across the surface of the anode. It appears that the addition of a significant quantity of AlF_3 to raise the acidity of the bath had a destabilizing effect on the CEROX coating.

There was no evidence of phases containing the bath additives, either in the exterior or interior of the cermet.

4.3.2.2.3 Corrosion

Fe, Ni, and Cu contamination of the Al metal and cryolite in the four baths was determined by ICP analysis. The Fe contamination was normalized (as described in the Methods and Materials section) and is shown in Figure 30. The highest Fe contamination occurred in the Standard Bath. It is obvious that the additives had no detrimental effect on the corrosion of the cermet.

4.3.2.3 Conclusions

The quasi-commercial baths selected did have some observable effects on the CEROX coating and its protection of the cermet substrate.

1. No evidence of bath additives was detected in the CEROX coating, at the CEROX-cermet interface, or within the cermet

2. Additives did not have a negative effect on the corrosion of the cermet

3. Tests in acidic baths demonstrated that AlF_3 activity affects the dynamic equilibrium of the CEROX coating

4. Because of the shift in the CEROX partitioning in the acidic bath, cerium additions will have to be adjusted to maintain adequate CEROX coating thickness on the cermet in the long term acidic bath tests

4.3.3 Half-Saturated Alumina Tests

Experiments were performed to identify a suitable cell liner material for use in the half saturated tests. However, no inert liner material suitable for long-term testing in half-saturated cryolite was identified. Several candidate materials thought to be suitable as liners failed under test. The following materials were evaluated.

FIGURE 30

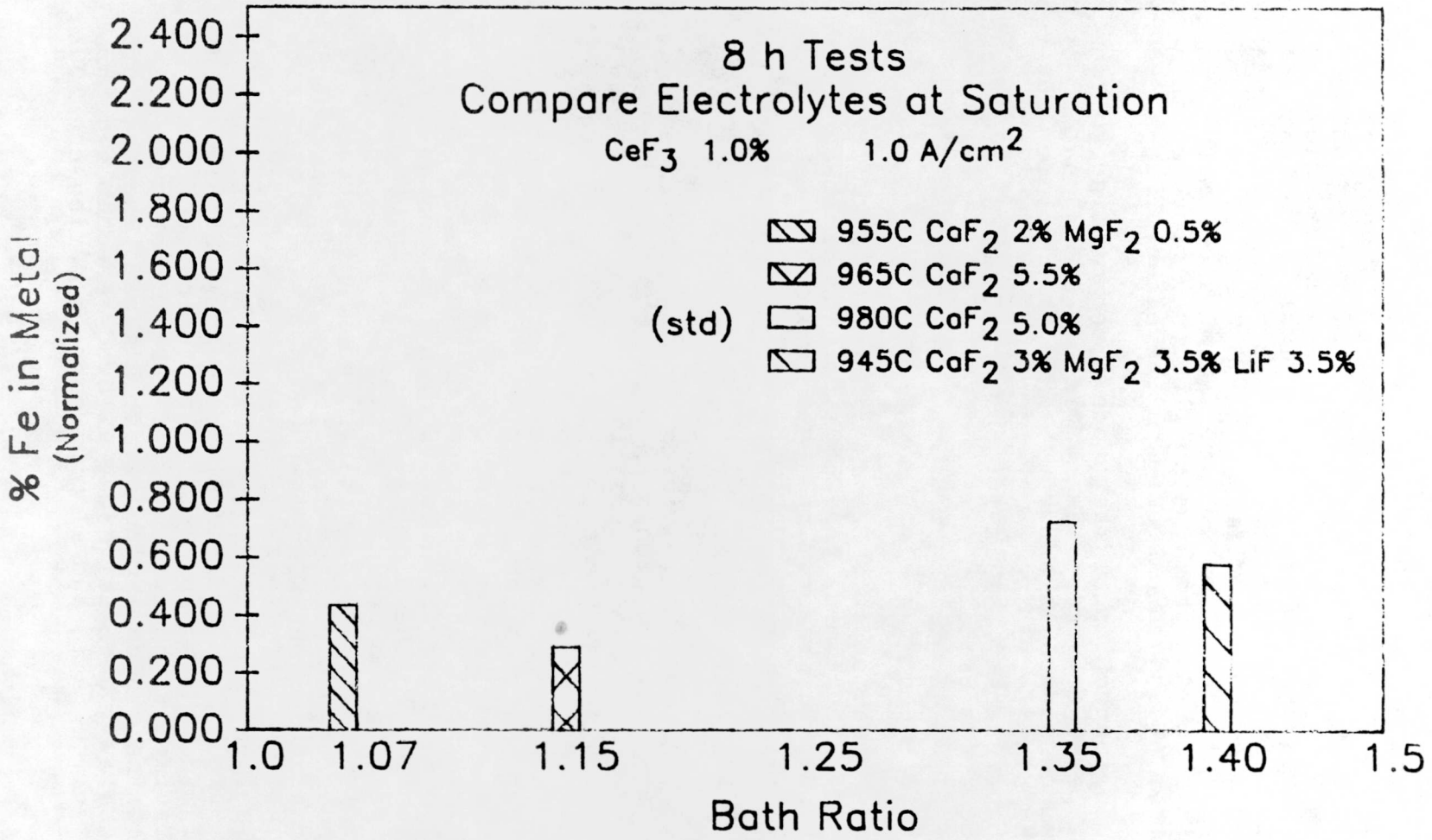
8 h Tests
Compare Electrolytes at Saturation
CeF3 1.0% 1.0 A/cm2
955C CaF2 2% MgF2 0.5%
965C CaF2 5.5%
(std) 980C CaF2 5.0%
945C CaF2 3% MgF2 3.5% LiF 3.5%
% Fe in Metal
(Normalized)
2.400
2.200
2.000
1.800
1.600
1.400
1.200
1.000
0.800
0.600
0.400
0.200
0.000
1.0
1.07
1.15
1.25
1.35
1.40
1.5
Bath Ratio

4.3.3.1 Boron Nitride

A half-saturated alumina test with a BR 1.35 at 1 A/cm^2 was attempted with a BN liner for 100 h. The test ran very well with a fairly constant voltage (3 V) and control of the bath ratio required the addition of minimum amounts of Na_2CO_3. However, after 96 h, the BN liner showed signs of deterioration where portions of the liner had collapsed into the bath. The test was stopped after 97 h, and an attempt was made to extract the liner. When slight pressure was applied to the hooked liner, a section of the liner was torn away, showing that the BN liner had poor mechanical strength after prolonged exposure to the electrolyte at 980°C.

Upon inspection of the anode after cooling to room temperature, there was no visible CEROX coating on the anode and considerable anode wear had taken place (20% reduction of the diameter). Very little Al metal was produced. Unfortunately, BN is not compatible with CeF_3, causing to occur the reaction

$$6BN + CeF_3 = CeB_6 + 3N_2. \quad (20)$$

The formation of CeB_6 was confirmed by XRD. As CeF_3 in the bath is consumed, the CEROX coating becomes progressively thinner to preserve the equilibrium between dissolved cerium and cerium in the coating.

4.3.3.2 Silicon Nitride

A 100 h test was initiated and run to completion at alumina half-saturation with a BR 1.35 at 1 A/cm^2. The liner was composed of a high density, low porosity silicon nitride. Unfortunately, the anode had no CEROX coating at the end of the test cycle and was tapered as with anodes operated in cerium free baths. Little Al metal was produced and the liner deteriorated.

After the first 24 h, tests showed the bath contained 4% alumina; however, after 48 h, silica contamination was detected in the alumina. From 48 h on, the silica contamination began to have significant effects on the analysis for the bath ratio and alumina content. The silica interference for the cryolite ratio was backed out by subtracting out KOH consumed in the back titration up to pH 6.8. The silicic acid, which remained suspended in the aluminum chloride digest, was decanted off in the supernatant liquid. Tube Excited Fluorescence Analysis (TEFA) for alumina showed some silica contamination remaining but the gravimetric analysis showed a total residual mass of 6% alumina, which includes some silica. These efforts were not totally quantitative but allowed reasonable control over the cryolite ratio and alumina content during the 100 h test.

4.3.3.3 Aluminum Nitride

An aluminum nitride coupon was tested in a 50 h solubility test at 980°C in a standard bath (no current was applied). The coupon dissolved.

No other materials were identified that might make suitable liners for evaluation of in-situ CEROX coated anodes in cryolite not saturated with alumina.

4.4 LONG TERM ALUMINA SATURATED TESTS

CEROX coating stability and anode protection was evaluated on nickel ferrite/Cu cermet anodes in nine long term tests of 100 h and compared to a nickel ferrite/Cu cermet tested for 100 h without a CEROX coating.

4.4.1 Outline of Experiments

The objective of these tests was to demonstrate that the CEROX coating, which has been shown to provide protection to the cermet substrate in short term tests, would continue to provide protection to the cermet in long term tests. In addition, comparisons of the metal contamination could be made for various operating conditions.

The tests were operated at 980°C in alumina saturated baths (10% alumina) with 5.0% CaF_2 (Table 9). Tests were run at current densities of 0.6, 1.0, and 1.4 A/cm^2 and BR of 1.35 (Standard Bath), 1.2 (acidic), and 1.6 (non-acidic). The preferred CEROX coating thickness of (nominally) 1.0 mm was maintained by additions of CeF_3 to the bath throughout the experiments. The cerium-free experiment was performed at BR 1.35 and current density of 1.0 A/cm^2. Bath ratio and composition were monitored and maintained as described in the Materials and Methods section.

4.4.2 Results and Discussions

Cell voltage was monitored throughout the tests and gave an indication of the CEROX coating resistance. The tested anodes were cross-sectioned and examined microscopically for changes in the phase assemblage or structure. Contamination of the Al metal by Fe, Ni, an Cu was measured and used as an indication of the amount of deterioration of the cermet anode.

4.4.2.1 Cell Voltage

Cell voltage was monitored over the course of the tests (Table 10) and is shown in Figures 31, 32, and 33. The cerium-containing cells have a rapid voltage rise in the first 8 h asthe CEROX coating develops. Generally, the

Table 9. Long Term Tests

100 h, 5% CaF_2, 10% Al_2O_3, 980°C

CEROX[a] (mm)	BR	Current Density A/cm^2
0	1.35	1.0
1	1.35	0.6
1	1.35	1.0
1	1.35	1.4
1	1.20	0.6
1	1.20	1.0
1	1.20	1.4
1	1.60	0.6
1	1.60	1.0
1	1.60	1.4

a. Nominal Thickness.

Table 10. Cell Voltage Versus Hours (100 h)
1.0% CeF_3, Alumina Saturated

	Cell Voltage					
A/cm^2	Start	8 h	24 h	48 h	72 h	100 h
			BR 1.60 (1015°C)			
0.6	0.6	1.7	1.8	1.8	2.0	2.1
1.0	2.0	3.5	3.7	3.5	3.5	3.6
1.4	3.0	4.2	4.3	4.6	4.7	4.7
			BR 1.35 (980°C)			
0.6	2.0	2.8	2.6	2.7	2.7	2.7
1.0	3.0	3.8	3.8	4.0	4.0	4.2
1.4	3.0	3.9	4.0	4.8	5.0	5.2
			BR 1.20 (980°C)			
0.6	1.7	2.5	2.7	2.7	2.8	2.8
1.0	2.8	3.0	3.4	3.4	3.5	3.4
1.4	3.5	3.8	3.9	3.8	3.8	3.5
			BR 1.35 (980°C)			
1.0	3.2	3.2	3.3	3.5	3.4	3.5

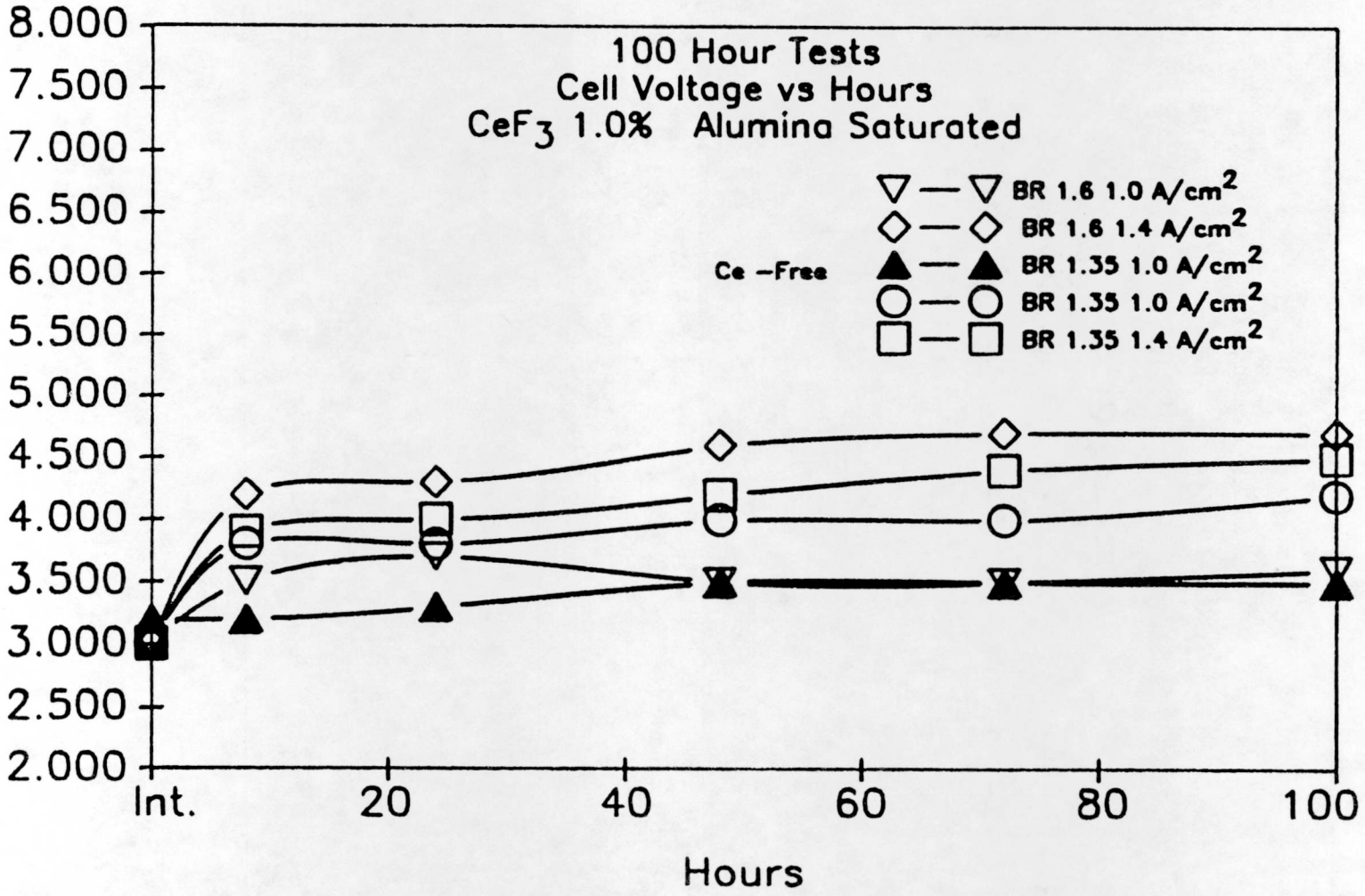
100 Hour Tests
Cell Voltage vs Hours
CeF_3 1.0% Alumina Saturated
Ce -Free
BR 1.6 1.0 A/cm²
BR 1.6 1.4 A/cm²
BR 1.35 1.0 A/cm²
BR 1.35 1.0 A/cm²
BR 1.35 1.4 A/cm²
Volts
8.000
7.500
7.000
6.500
6.000
5.500
5.000
4.500
4.000
3.500
3.000
2.500
2.000
Int.
20
40
60
80
100
Hours

FIGURE 31

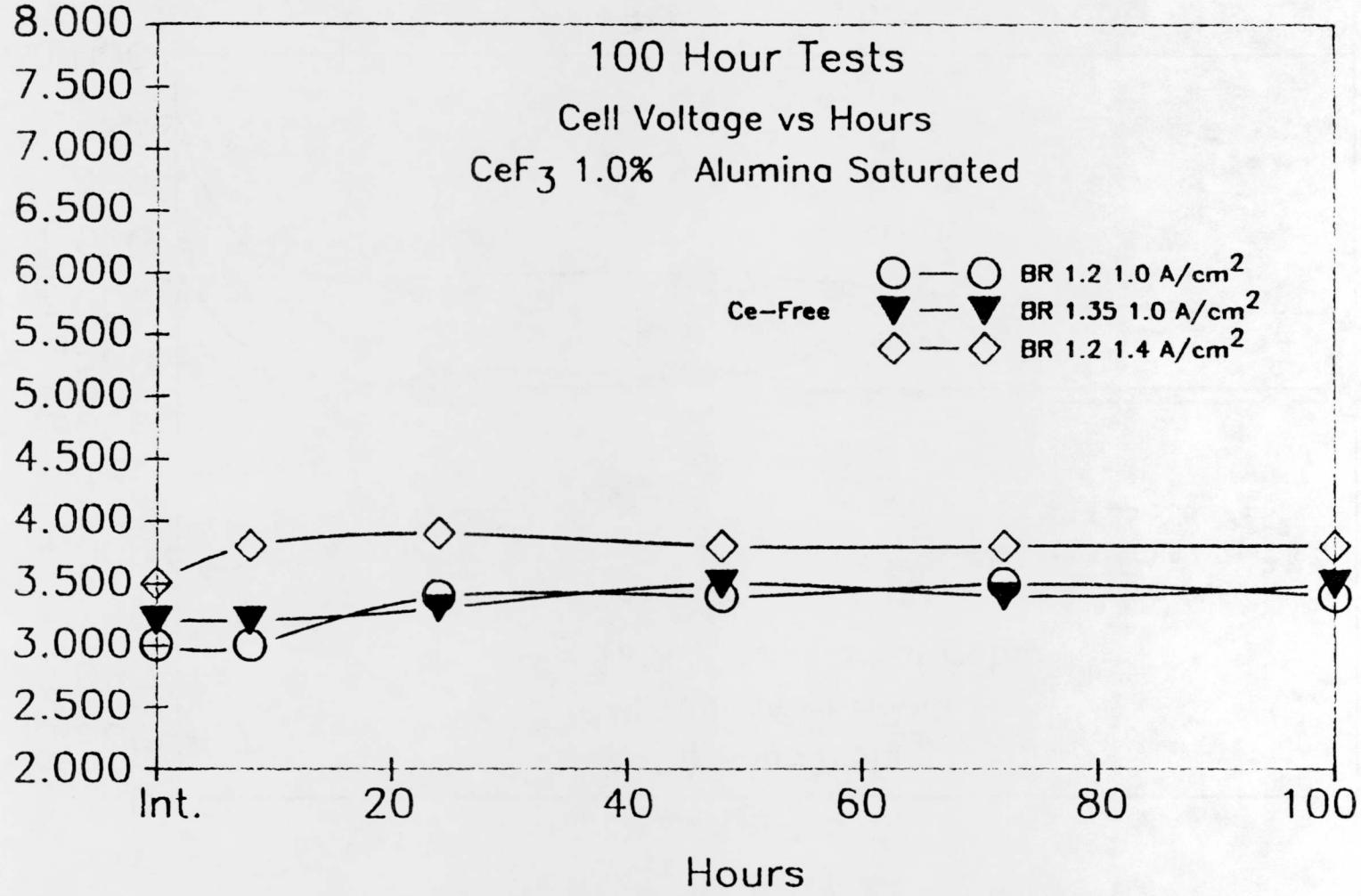
100 Hour Tests
Cell Voltage vs Hours
CeF3 1.0% Alumina Saturated
Ce-Free
BR 1.2 1.0 A/cm2
BR 1.35 1.0 A/cm2
BR 1.2 1.4 A/cm2
Volts
8.000
7.500
7.000
6.500
6.000
5.500
5.000
4.500
4.000
3.500
3.000
2.500
2.000
Int.
20
40
60
80
100
Hours

FIGURE 32

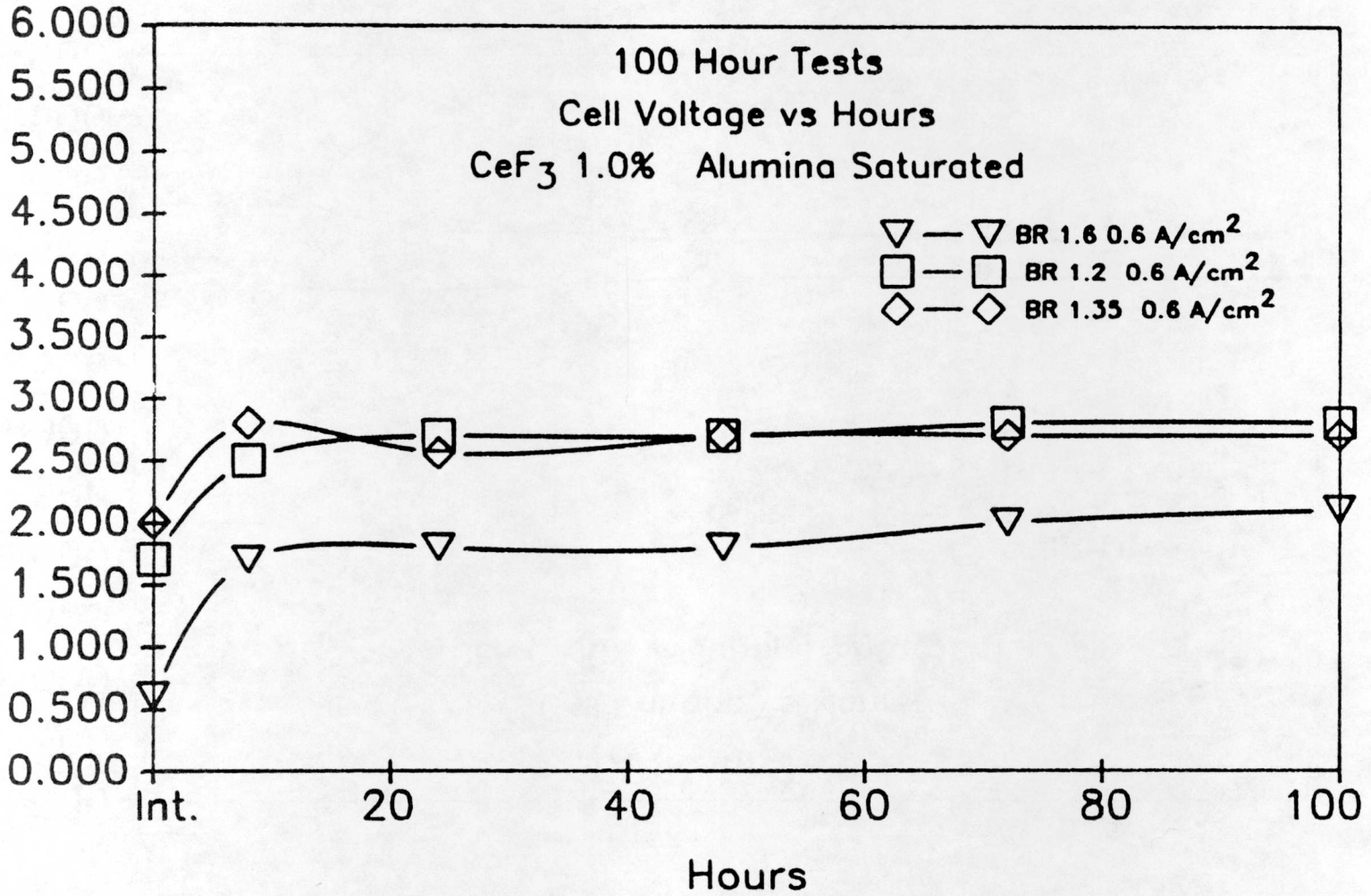
100 Hour Tests
Cell Voltage vs Hours
CeF3 1.0% Alumina Saturated
BR 1.6 0.6 A/cm2
BR 1.2 0.6 A/cm2
BR 1.35 0.6 A/cm2
Volts
6.000
5.500
5.000
4.500
4.000
3.500
3.000
2.500
2.000
1.500
1.000
0.500
0.000
Int.
20
40
60
80
100
Hours

FIGURE 33

voltage then increases slowly with time or levels off. In one experiment (BR 1.2, 1.4 A/cm^2) there was a slight decrease in cell voltage after the initial rise. The cerium-free experiment also showed a slight increase in voltage, from 3.2 to 3.5 V.

Tests operated at current densities of 1.0 and 1.4 A/cm^2 and for BR 1.35 and 1.6 are shown in Figure 31, and for BR 1.2 are shown in Figure 32. All tests operated at 0.6 A/cm^2 current density are shown in Figure 33.

As expected, higher current densities result in higher cell voltages. Tests operated at BR 1.35 resulted in the highest cell voltages, while voltages from tests at BR 1.6 were usually greater than or equal to those at 1.2, for a given current density. An exception is at the 0.6 A/cm^2 current density, where the cell voltage at BR 1.2 and 1.35 were similar, while those at 1.6 were lower. For tests operated at 1 A/cm^2, the test with BR 1.35 had the highest voltage, but those operated at bath ratios of 1.6 and 1.2 were very close to the cerium-free cell voltages.

The largest increase of voltage, from an initial voltage of 3.2 to 5.2 V, occurred in the 100 h cerium-containing tests at BR 1.35 and a current density of 1.4 A/cm^2. The smallest voltage increase was 0 to 0.4 V in the test operated with BR 1.2 and current density of 1.4 A/cm^2. Higher current density not only led to higher cell voltages, but also led to a greater increase in voltage over time in the BR 1.35 and 1.6 tests.

Cell voltage changes can be attributed to oxidation or changes in the substrate, the development of oxygen bubbles during electrolysis, as well as from the added resistance of the CEROX coating. It is not possible to determine the change because of the CEROX coating itself.

4.4.2.2 Microscopy

A summary of CEROX coating thickness, Cu metal depletion thickness, and other features are shown in Table 11. Cryolite penetrates the pores of the substrates and CEROX coatings in all samples.

4.4.2.2.1 0.6 A/cm^2

All anodes from the 0.6 A/cm^2 tests demonstrated some loss of integrity of the cermet substrate, ranging from an increased porosity layer at BR 1.2 (Figure 34) to complete delamination at BR 1.35 and 1.6 (Figures 35a and 36). The delaminated CEROX layer is attached to a thin ferrite-containing layer of 60 to 330 μm thickness, showing that the loss of adhesion was within the ferrite material and not between the CEROX and the ferrite. The delaminated ferrite layer consists of dense

Table 11. Long Term Test Results

Experiment	CEROX Thickness (mm)	Cu Metal Depletion Thickness (mm)	Distance From Edge to Porous (P) or Cracked (C) Zone (mm)
0.6 A/cm^2			
BR 1.2	0.3 to 1.2 (side)	1.4	-
BR 1.35	0.35	0	-
BR 1.6	1.0 to 1.25	0	-
1.0 A/cm^2			
BR 1.2	0.1 to 0.42	3.5	3(p), 3.5(c)
BR 1.35	0.13 to 0.85	4.5 to 5	3.5(c)
BR 1.35 Ce-free	0	4	4(c)
BR 1.6	0.2 to 1.2	4.5	4(p)
1.4 A/cm^2			
BR 1.2	0.1 to 0.4	2.1	2.1
BR 1.35	0.4 to 0.95	-	1,3.75,5.5(p)
BR 1.6	0.1 to 1.1	-	1.3(p),4.6(pc) 6.6(c)

a. 20X

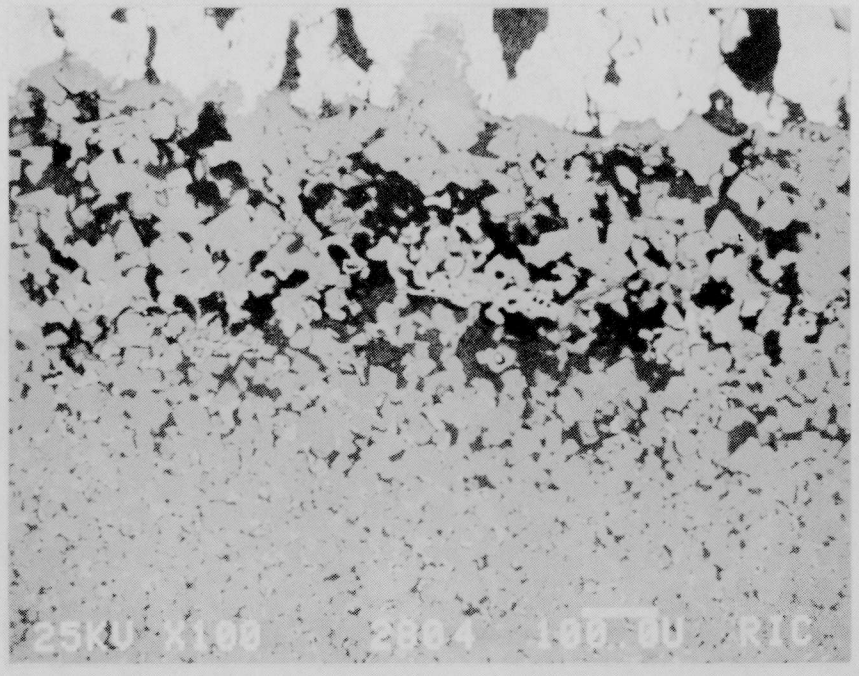

b. BEI 100X

FIGURE 34
BR = 1.2, 0.6 A/cm^2
#13505-52

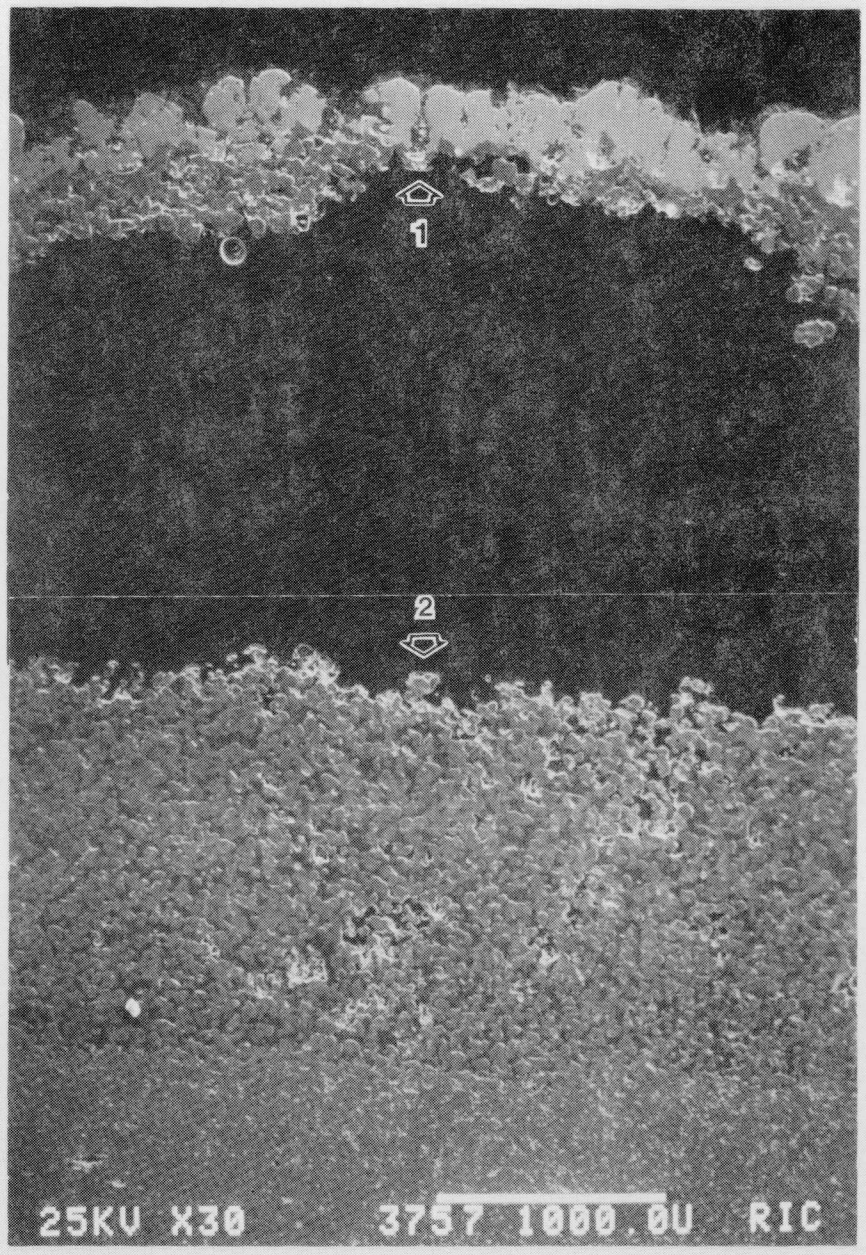

30X

FIGURE 35a
BR = 1.35, 0.6 A/cm^2
#13505-18

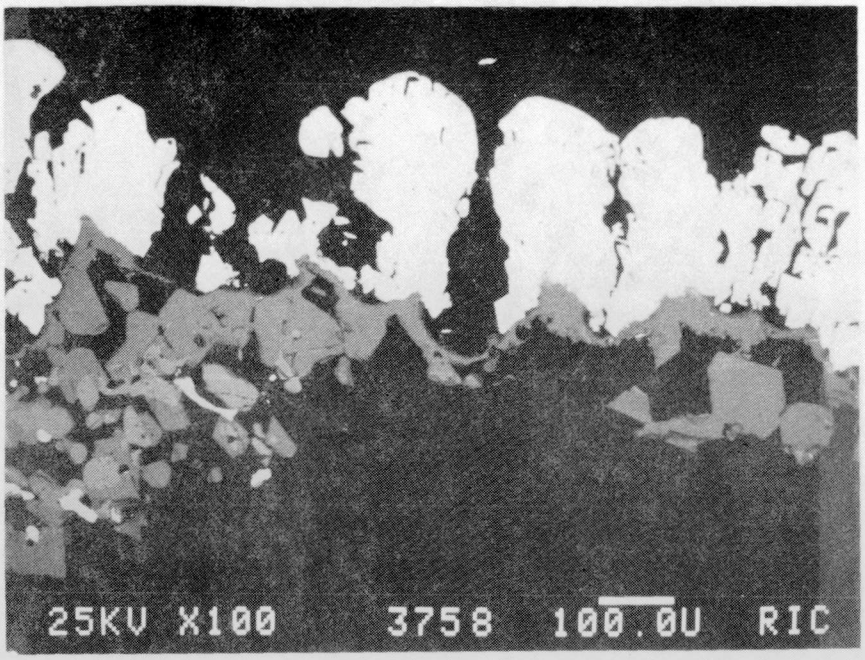

a. BEI 100X

Area 1

FIGURE 35b

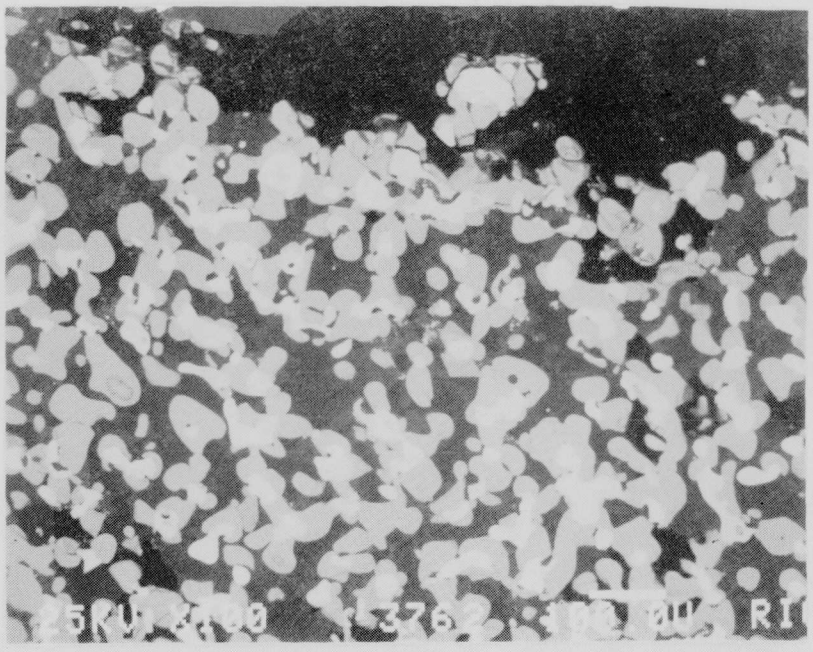

b. BEI 100X

Area 2

FIGURE 35c

FIGURE 35 b & c

BR = 1.35, 0.6 A/cm^2

#13505-18

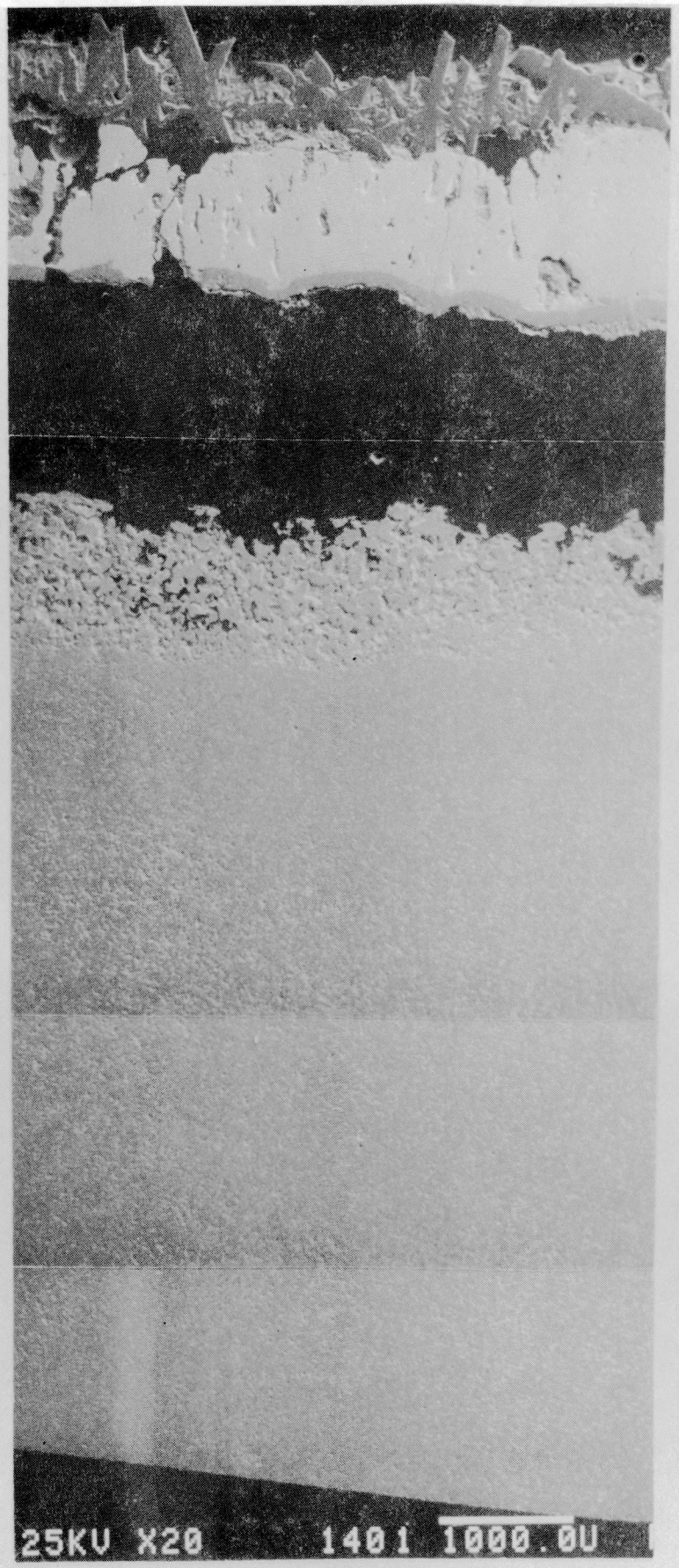

20X

FIGURE 36
BR = 1.6, 0.6 A/cm^2
#13505-64

$NiFe_2O_4$ in the BR 1.6 sample (Figure 37 a) but is of a typical cermet composition (Cu, NiO, and $NiFe_2O_4$) in the sample from BR 1.35 (Figure 35 b).

An outer region of the ferrite substrate depleted in Cu metal is common in tests at other current densities, but only occurs in the BR 1.2 sample at the 0.6 A/cm^2 current density, and in that test the thickness developed is less than in other tests. The anodes from BR 1.35 and 1.6 do not have a Cu metal depleted region, but instead have exterior layers, 1 to 1.7 mm thick, in which there is Cu metal of increased grain size (130 µm versus 30 m in the interior) occurring with coarse NiO grains (Figures 35 c and 37 b). In addition, in the exterior layer, the Cu metal is alloyed with higher amounts of Ni. The Cu composition (in weight percent) in the BR 1.6 sample is 61 Cu-39 Ni in the coarse exterior grains and decreases in Ni content within the fine grained substrate down to 94 Cu-3 Ni-3 Fe on the interior. The change in the Cu and Ni distribution and grain size is evident in Figure 38 a to d where X-ray mapping of Cu, Ni, and Fe is shown.

The BR 1.2 sample, which has Cu metal depletion, contains a Cu oxide phase that is most abundant in the porous layer, but also occurs within the substrate. There is abundant cryolite within the porous region. In addition, the NiO contains Cu in solid solution, with a composition (in wt%) of 83 NiO-10 FeO-8 CuO. A thin discontinuous layer of Ni-Fe aluminate, less than 5 microns thick, occurs next to the CEROX.

The CEROX coating is discontinuous, thin, variable in thickness, and dendritic-like on the BR 1.2 sample, increases in density in the BR 1.35 sample, and has an increased thickness and density in the BR 1.6 test. The interface between the CEROX and substrate is irregular.

4.4.2.2.2 1.0 A/cm^2

The cerium-free test was operated at BR 1.35 and current density of 1.0 A/cm^2. The tested anode is tapered and contains an exterior, Cu metal depleted region of up to 4-mm thick. That region consists of $NiFe_2O_4$ and NiO, of similar grain size as the interior of the sample, with a Cu oxide, probably Cu_2O, in the grain boundaries. There is increased porosity in the Cu metal depleted layer.

All CEROX coatings in the Ce-containing tests at 1.0 A/cm^2 were adherent with no indication of delamination. Coating thickness and density increases with increasing BR. The thickness of the coating along the surface varies. No difference in the CEROX coatings could be determined between those formed at 0.6 A/cm^2 and those at 1.0 A/cm^2 except at the BR 1.2, where coatings appeared slightly less dendritic at the higher current density (Figure 39).

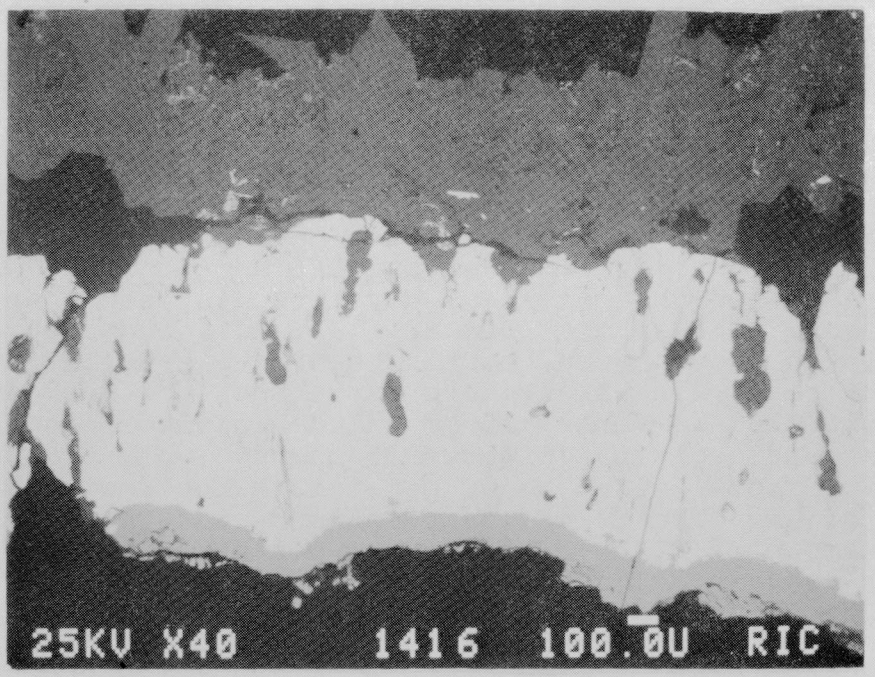

a. BEI 40X

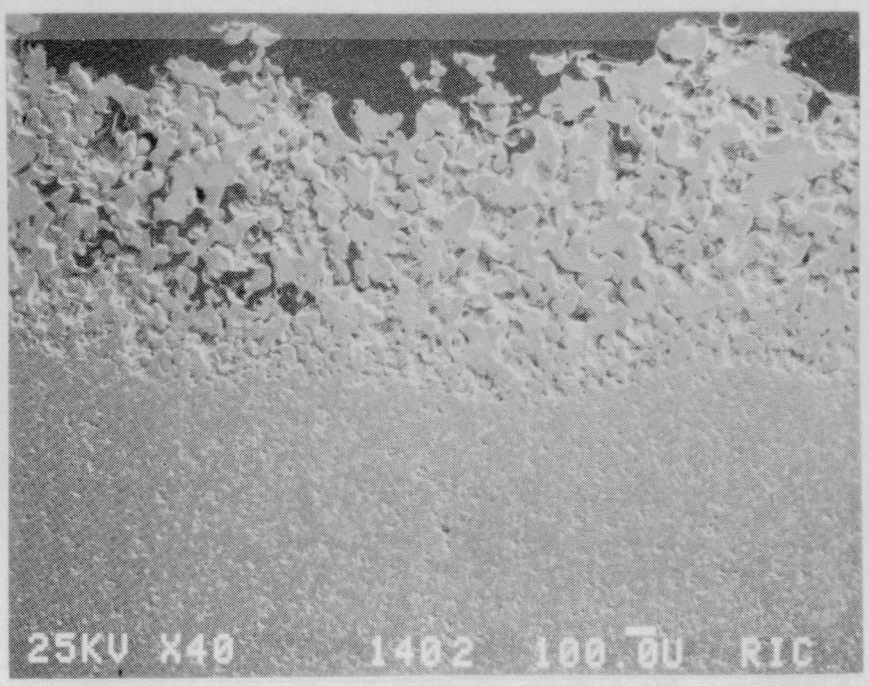

b. BEI 40X

FIGURE 37
BR = 1.6, 0.6 A/cm^2
#13505-64

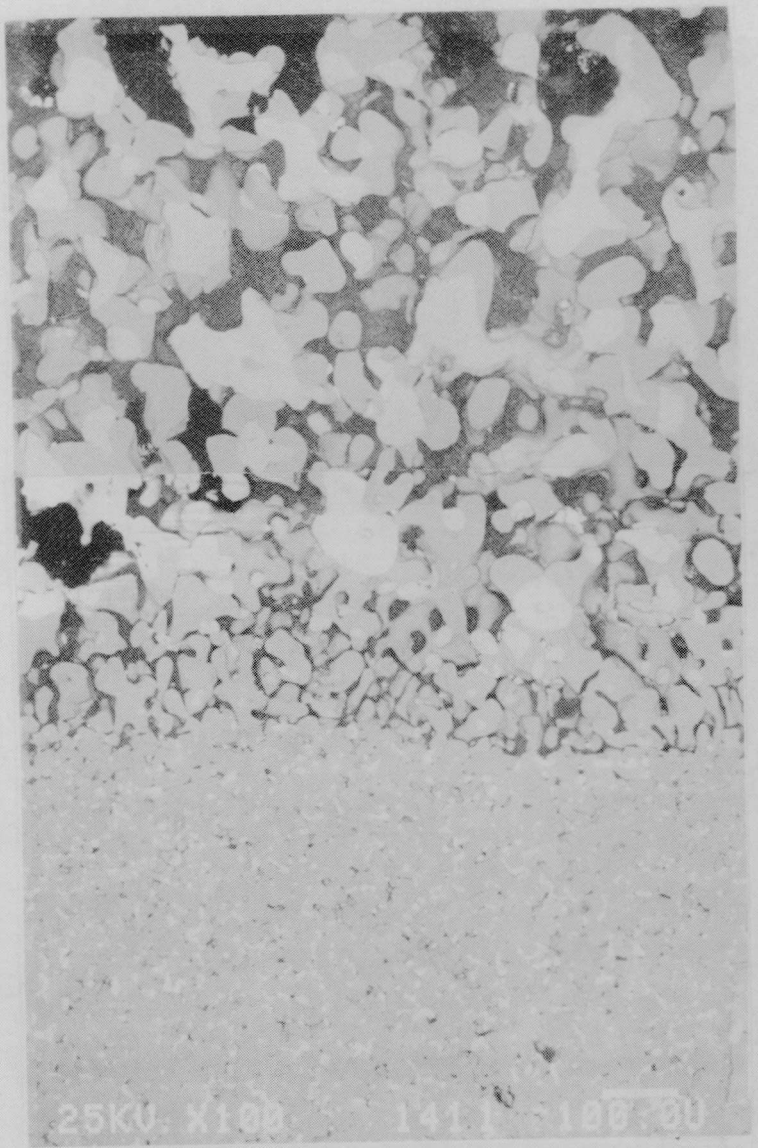

a. BEI 100X

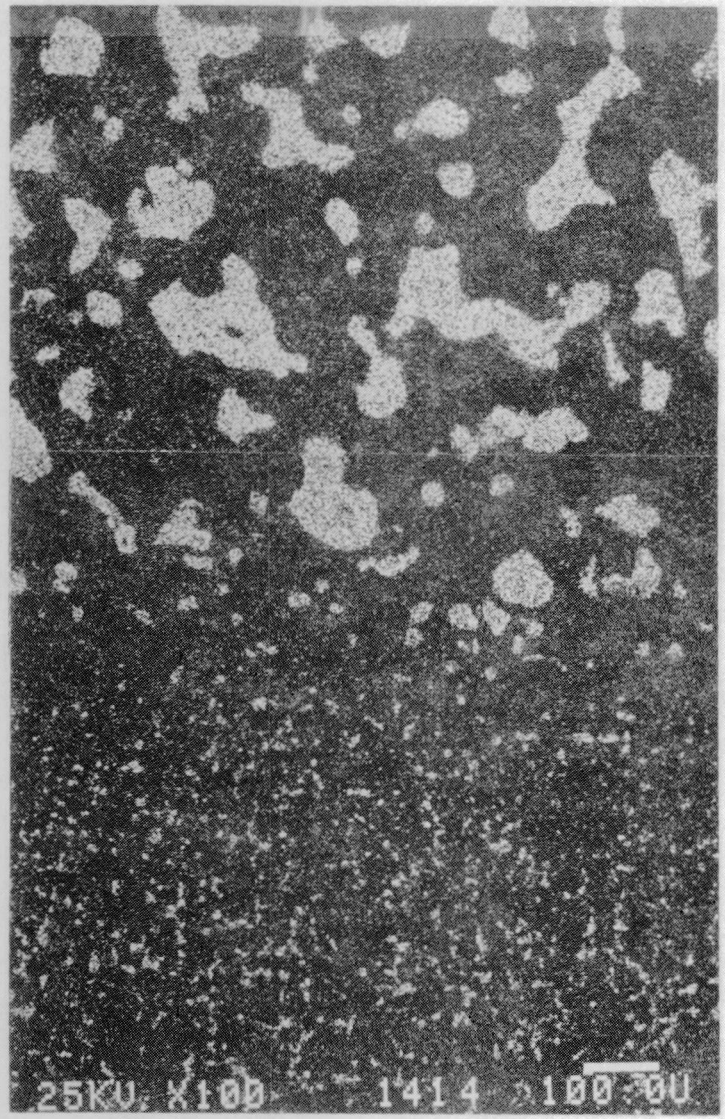

b. Cu Map 100X

FIGURE 38
BR = 1.6, 0.6 A/cm^2
#13505-64

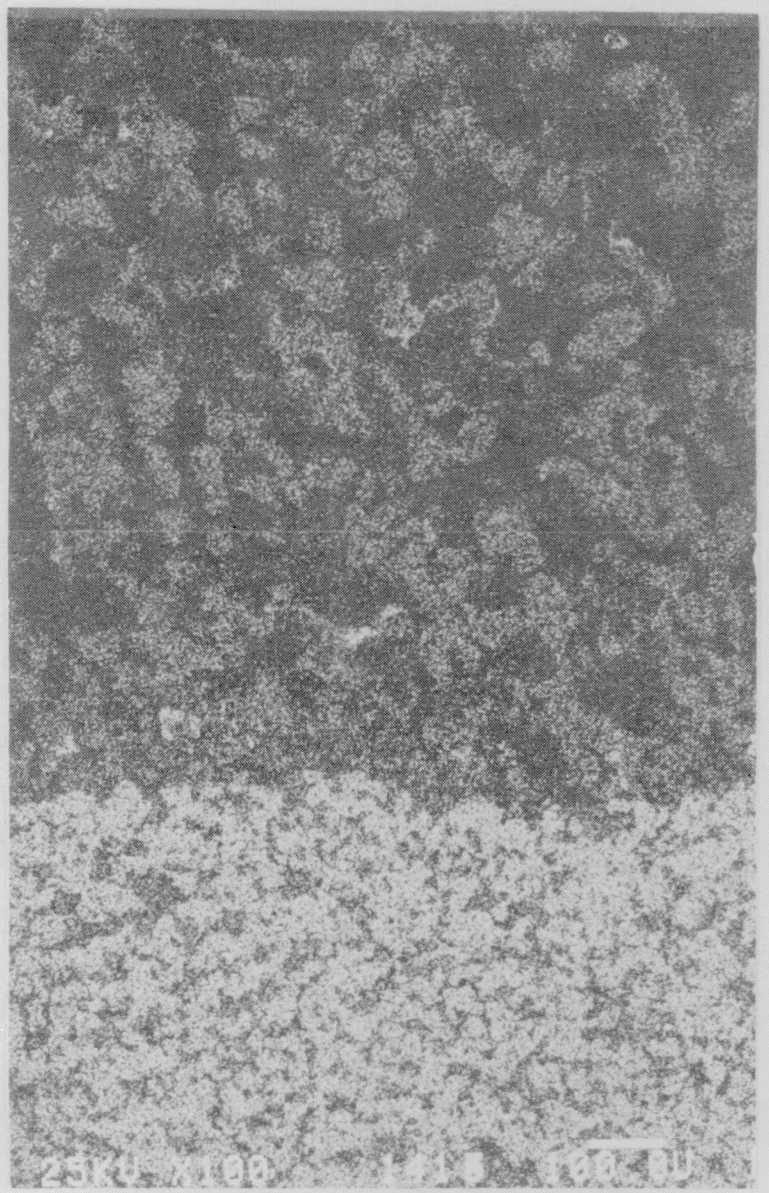

c. Fe Map 100X

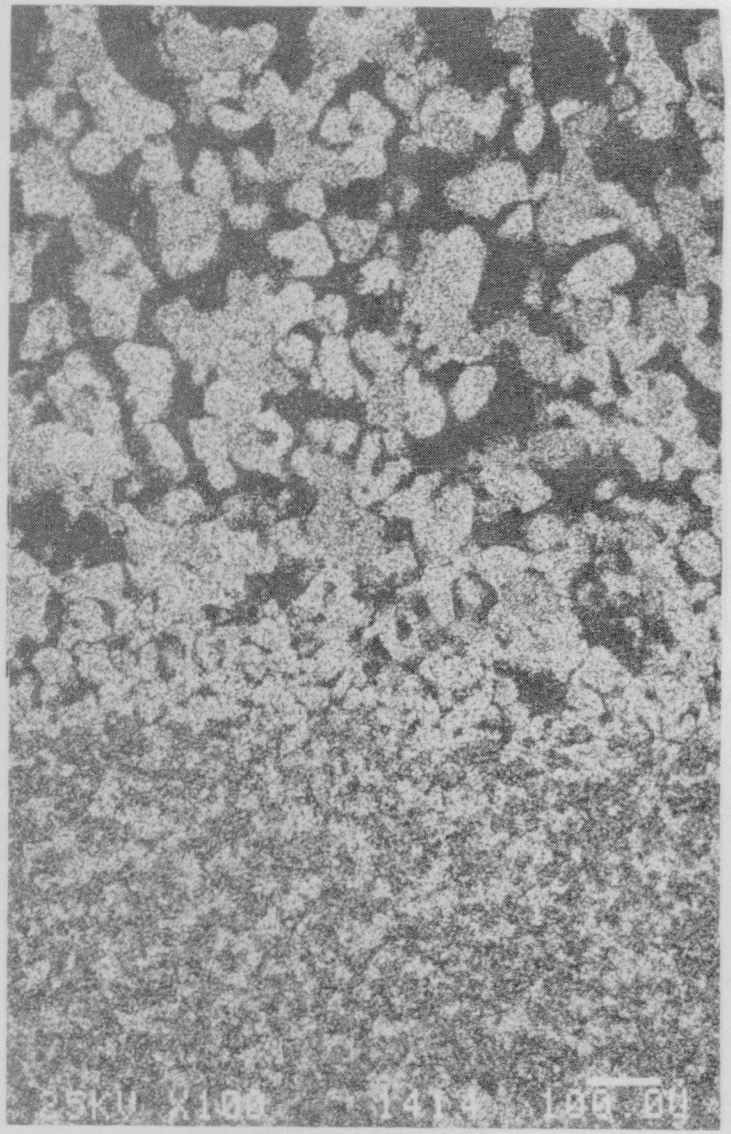

d. Ni Map 100X

FIGURE 38 (con't)
BR = 1.6, 0.6 A/cm^2
#13505-64

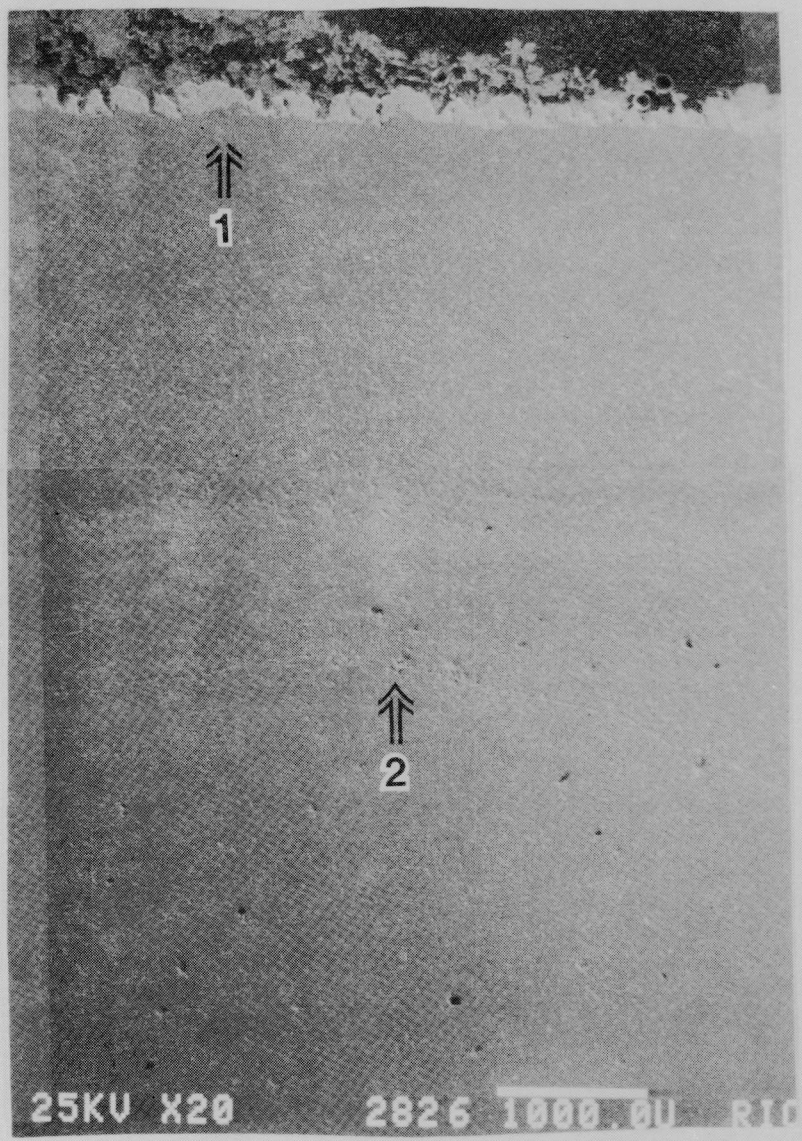

a. 20X

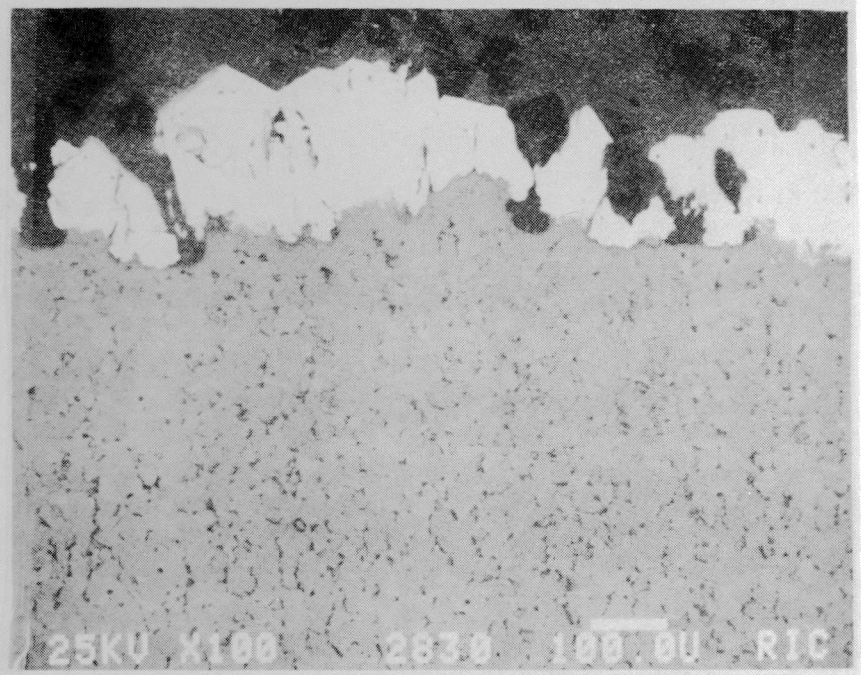

b. BEI 100X

FIGURE 39
BR = 1.2, 1.0 A/cm^2
#13505-50

The Cu metal depleted layer thickness ranges from ~3.5 mm to 5 mm, similar to that in the Ce-free sample. There is a slight increase in porosity within this region with a porous layer or crack (designated 2 in Figures 39, 40, and 41) near the boundary between the Cu metal depleted region and the Cu containing interior. The NiO contains Cu in solid solution in the outer region and some Cu oxide grains also occur, particularly near the CEROX coating. The outer edge of the substrate is irregular next to the CEROX coating.

There is a thin (<10 μm) discontinuous Ni aluminate layer between the CEROX and the substrate in each sample. The aluminate also contains small amounts of Cu or Fe.

4.4.2.2.3 1.4 A/cm^2

The high current density samples have an increased amount of porous areas at BR 1.35 and 1.6 compared to the 0.6 and 1.0 A/cm^2 tests (indicated by 2, 3, and 4 in Figures 44 and 47). In the acidic bath there is a distinct boundary (Figure 42 area 2) between the Cu metal depleted region and the Cu-containing interior. In the BR 1.35 and 1.6 tests, the boundary is less clear. Little Cu metal is found in the small BR 1.6 sample mounted for microscopy, while Cu metal and Cu oxide occur together in the porous regions of the BR 1.35 sample. Generally, Cu metal is reduced or absent from the most porous zones in that sample. The NiO contained Cu in solid solution with up to 12 to 21 wt% CuO within the NiO. There are also small amounts of Cu oxide in some grain boundaries.

In addition, in the BR 1.2 test, there is a dense $NiFe_2O_4$ layer in the substrate next to the CEROX (Figure 43 a to d) that contains inclusions of NiO next to the CEROX and Cu oxide in the center of the layer. The Standard Bath (BR 1.35) showed no change in the $NiFe_2O_4$ distribution in the exterior (Figure 45 a to d) but did show some Cu depletion at the exterior edge. The porous zones, by contrast, show a large change in the Ni, Cu, and Fe distribution. The X-ray mapping from region 2 of Figure 44 (~5.5 mm from the edge) is shown in Figure 46 a to d. The mapping indicates an increase in the grain size of NiO and $NiFe_2O_4$ and possible segregation into single-phase layers.

A thin (<10 μm), discontinuous Ni aluminate layer occurs next to the CEROX in all samples. In addition, some $NiAl_2O_4$ rims $NiFe_2O_4$ grains on the sides of the BR 1.2 sample.

As at the other current densities, the CEROX coating increases in thickness and density with increasing bath ratio. The thickness is variable across the anode. In the tests at BR 1.35 and 1.6, the CEROX is thin on the bottom of the anode with a recessed area, and increases in thickness

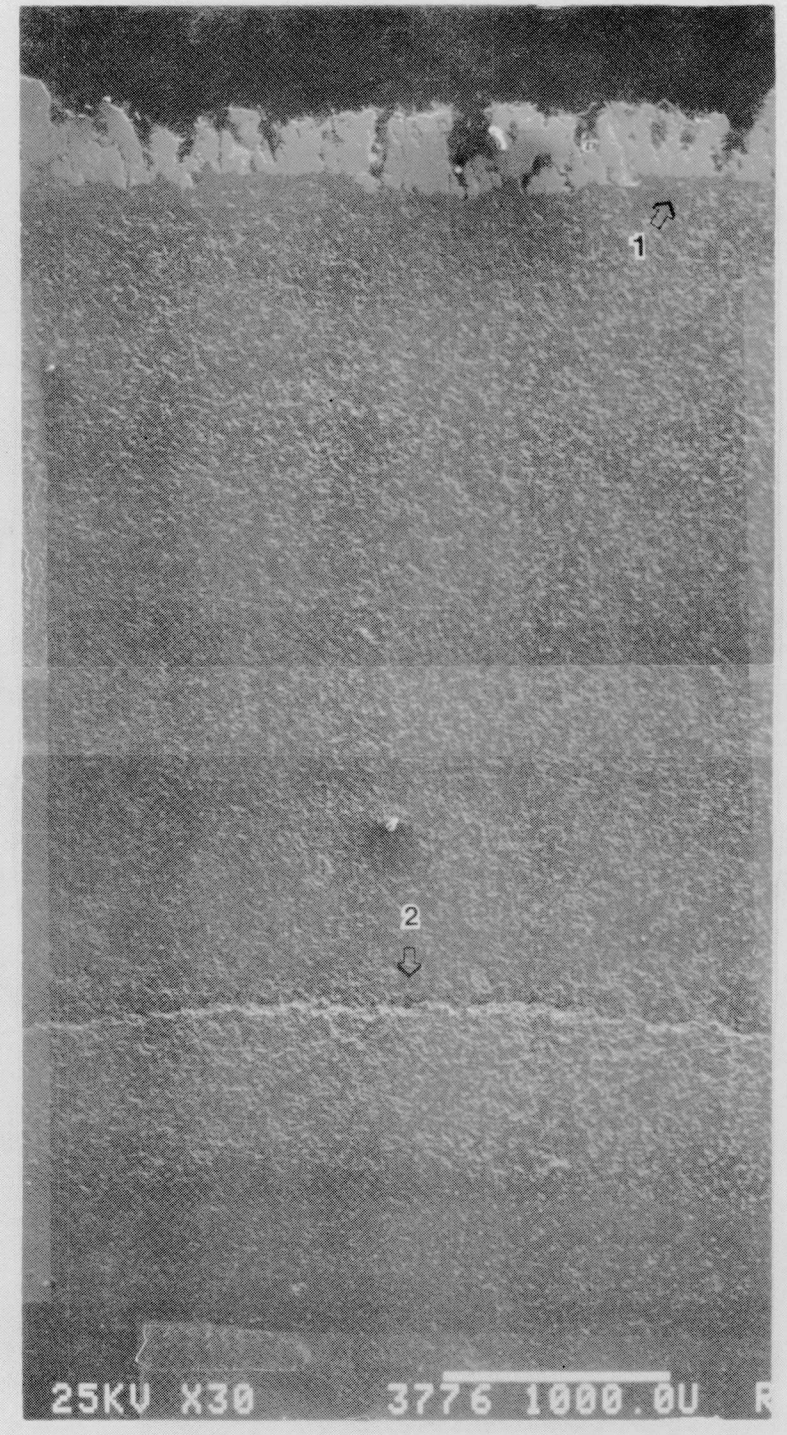

a. 30X

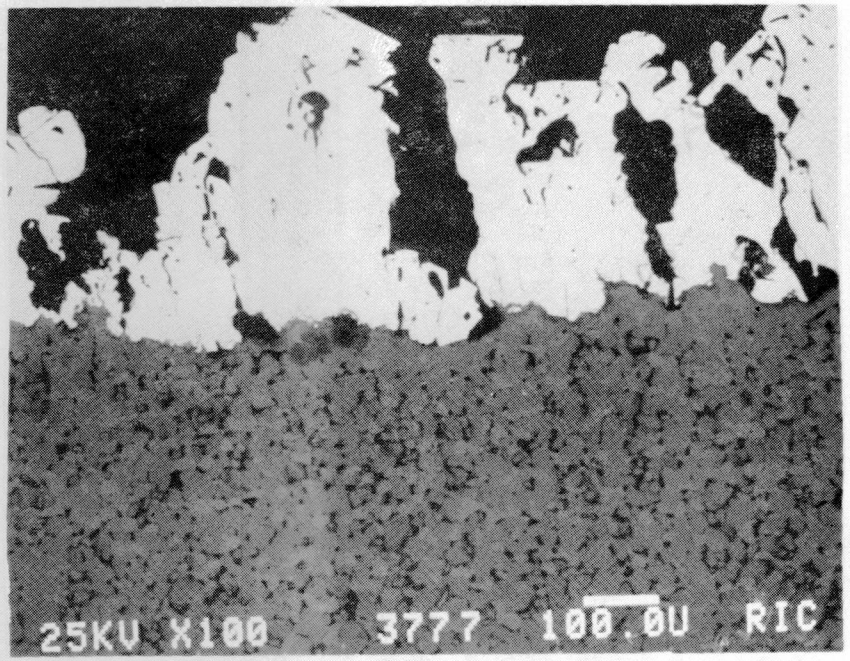

b. BEI 100X

FIGURE 40
BR = 1.35, 1.0 A/cm^2
# 13505-20

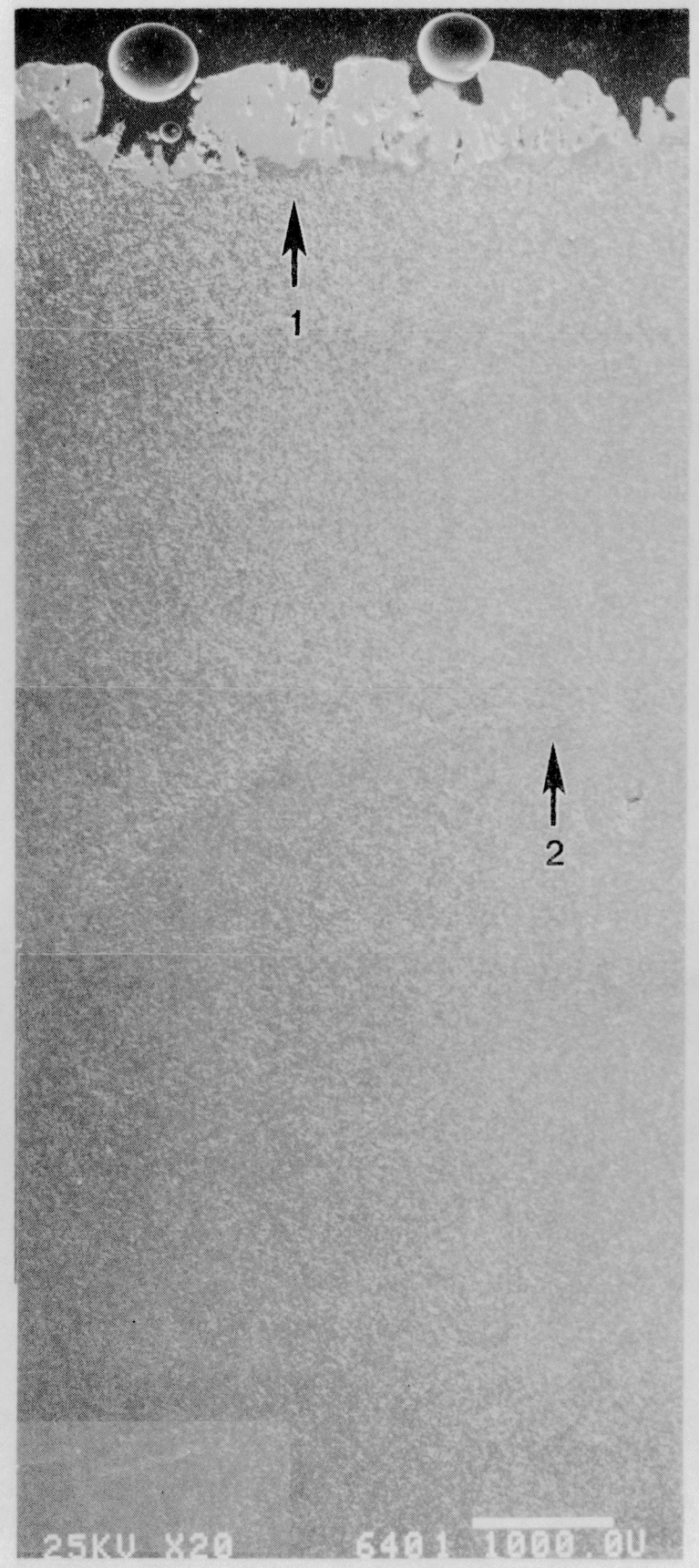

FIGURE 41 20X
BR = 1.6, 1.0 A/cm^2
#13505-60

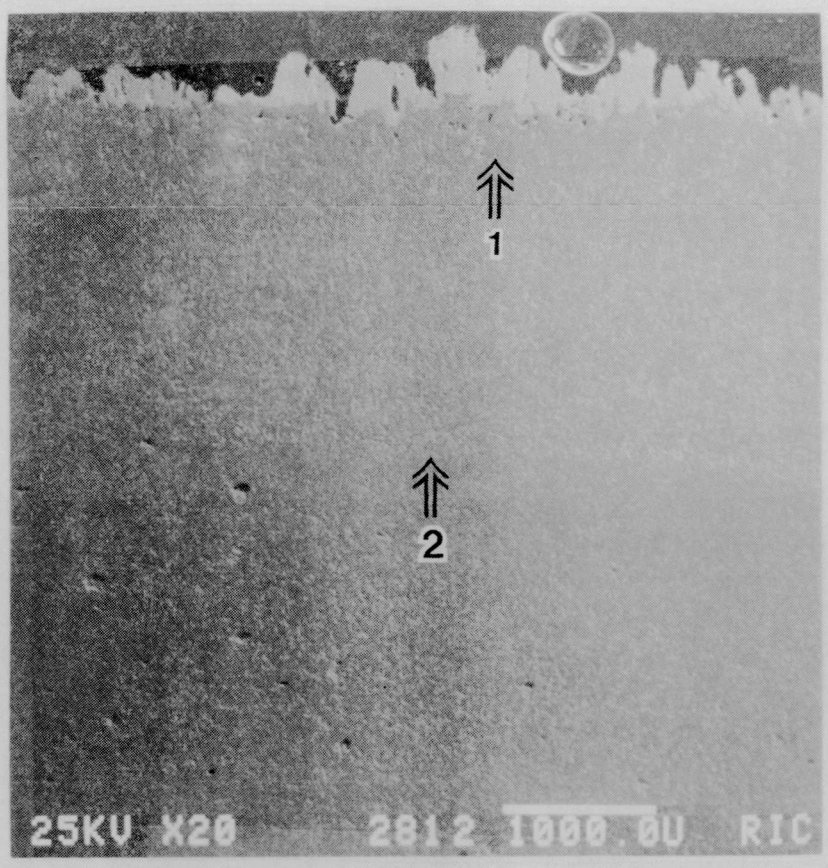

FIGURE 42 20X
BR = 1.2, 1.4 A/cm^2
#13505-48

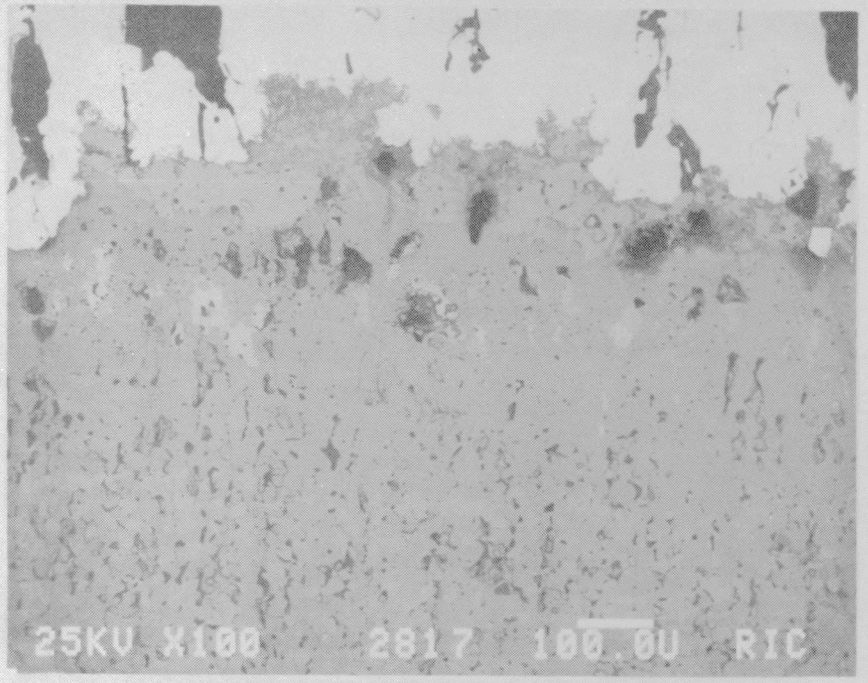

a. BEI 100X

b. Fe Map 100X

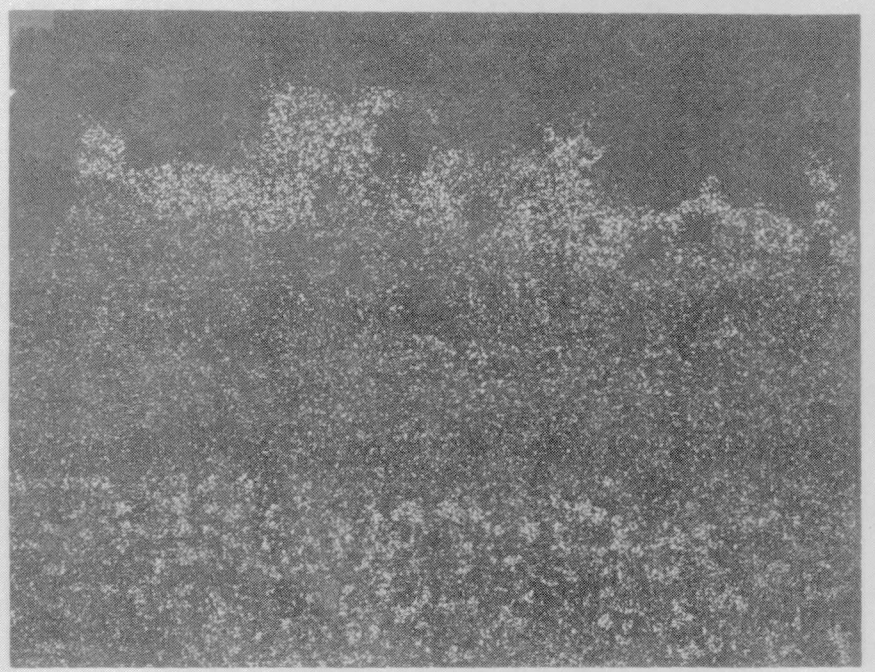

c. Ni Map 100X

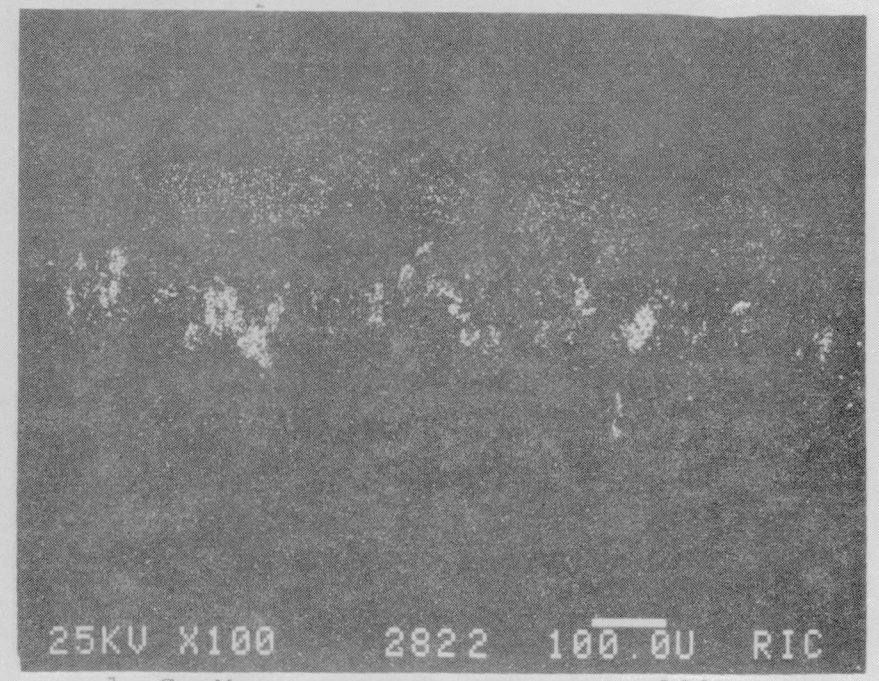

d. Cu Map 100X

FIGURE 43
BR = 1.2, 1.4 A/cm^2
#13505-48

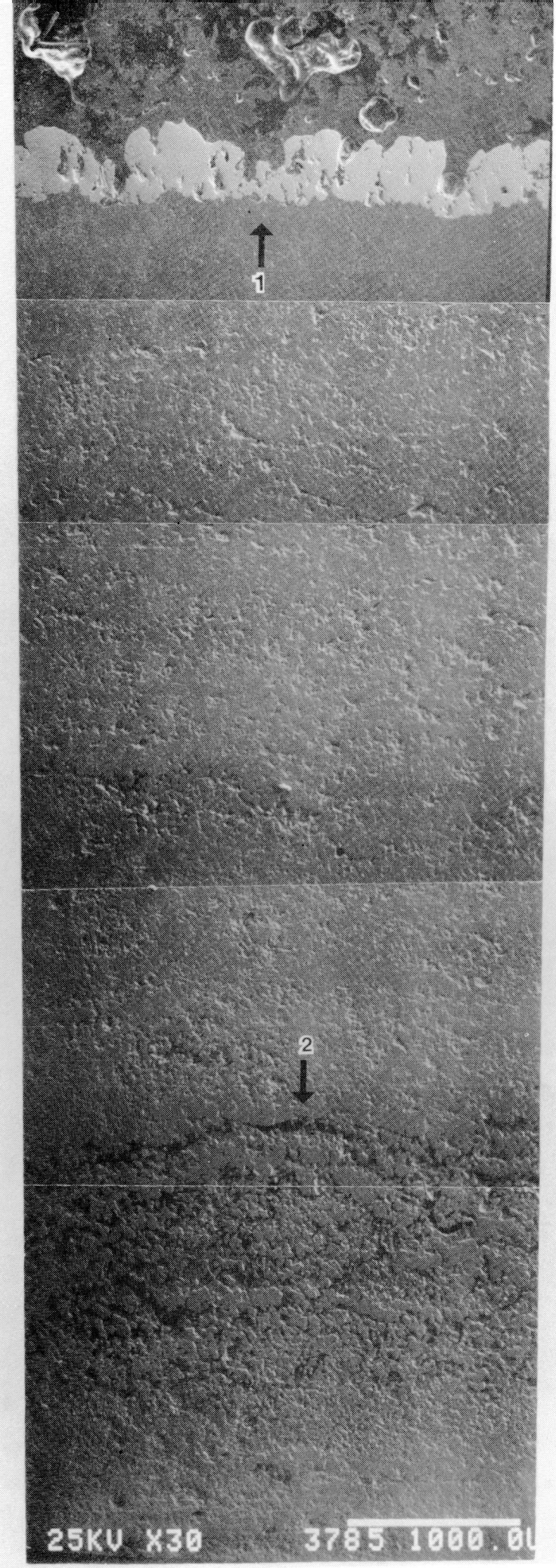

FIGURE 44 30X

BR = 1.35, 1.4 A/cm^2

#13505-26

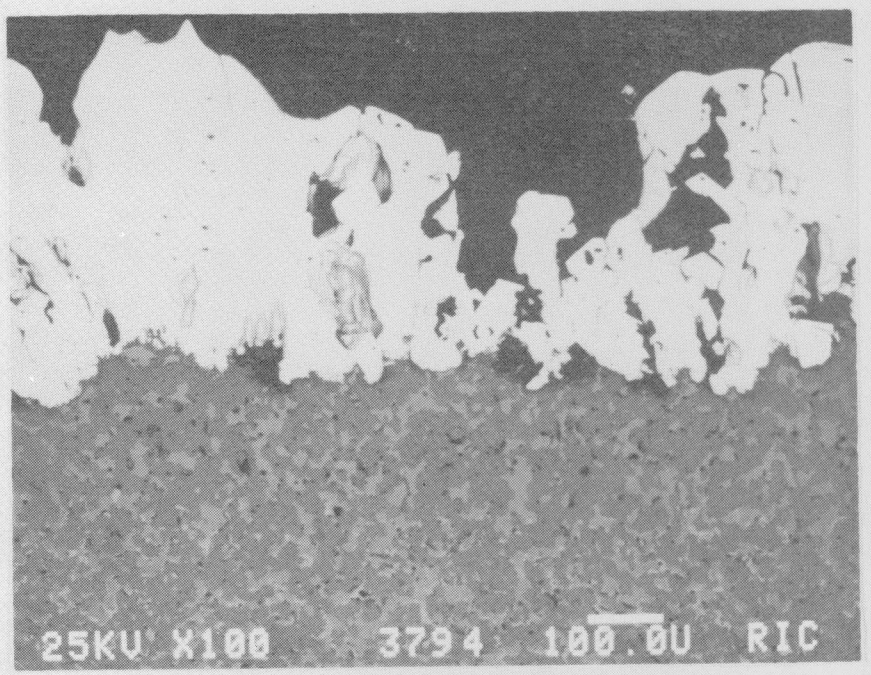

a. BEI 100X

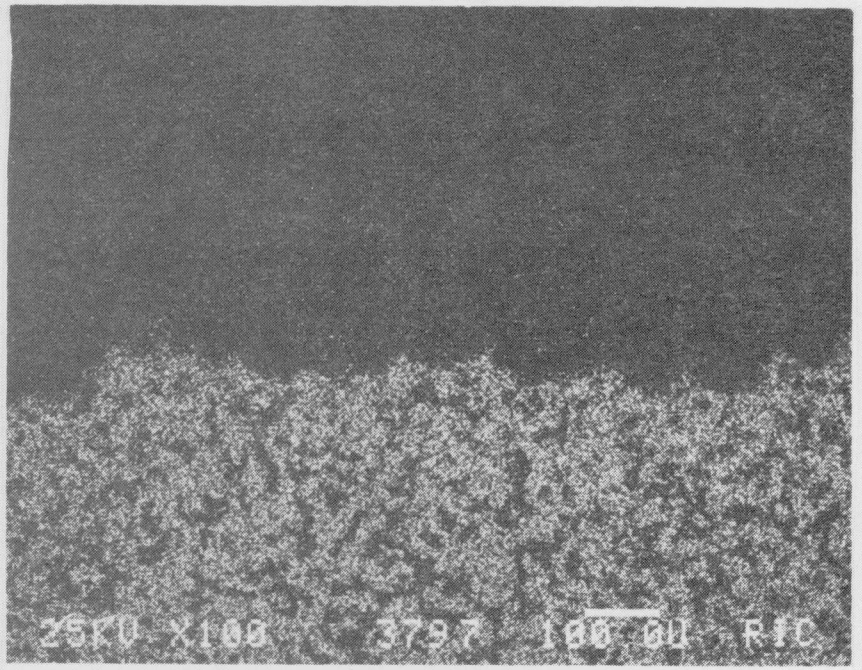

b. Fe X-ray Map 100X

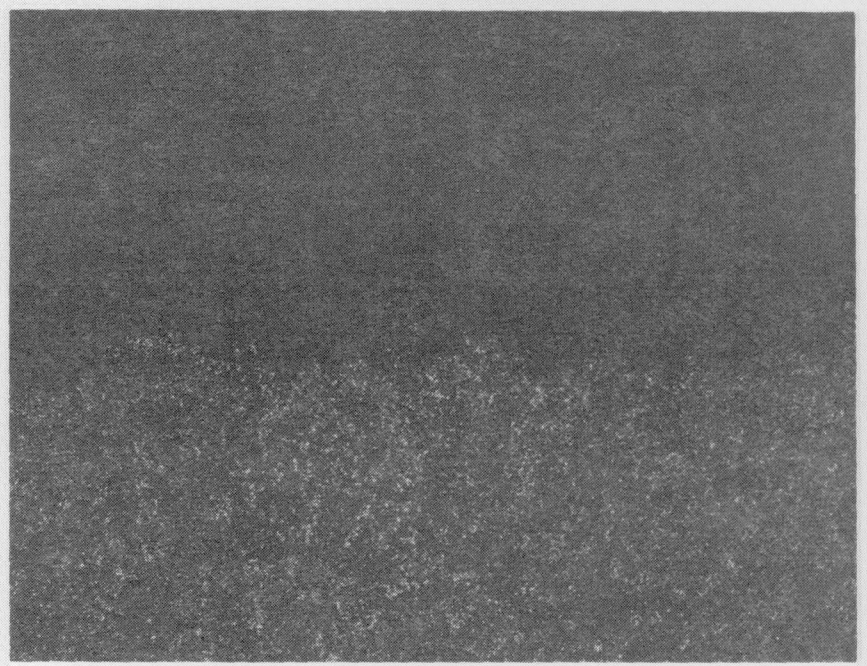

c. Ni X-ray Map 100X

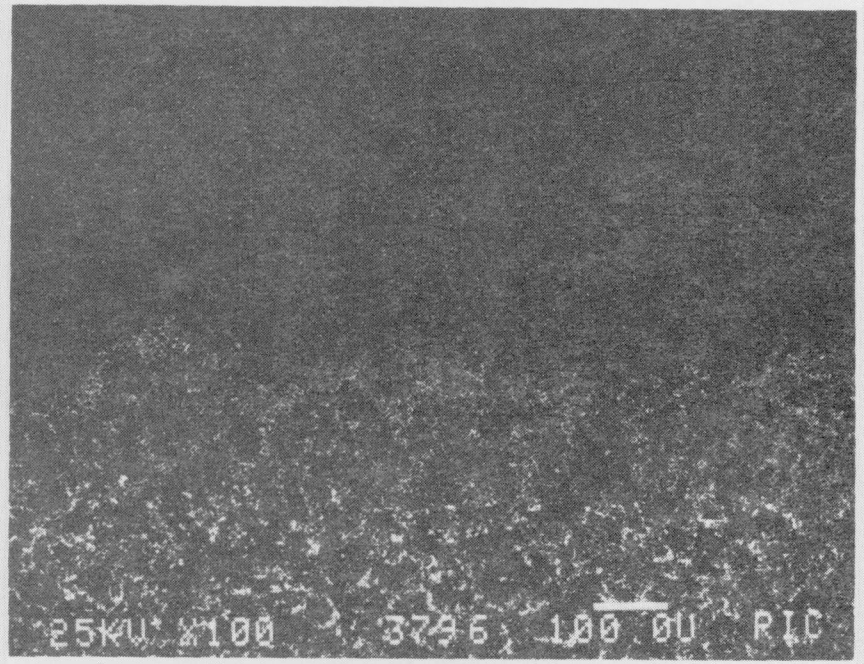

d. Cu X-ray Map 100X

FIGURE 45
BR = 1.35, 1.4 A/cm^2 - #13505-26

a. Fe X-ray Map 100X

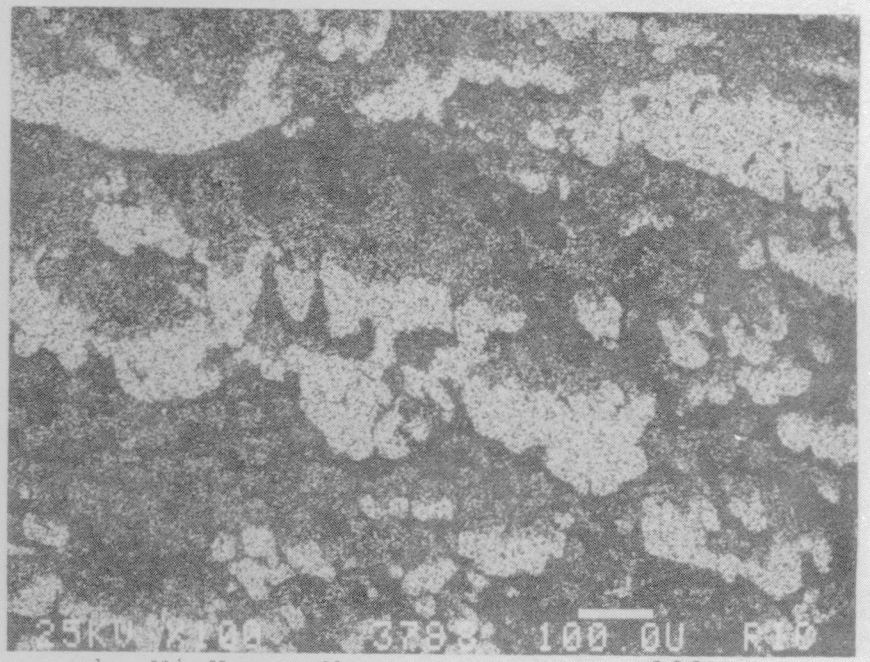

b. Ni X-ray Map 100X

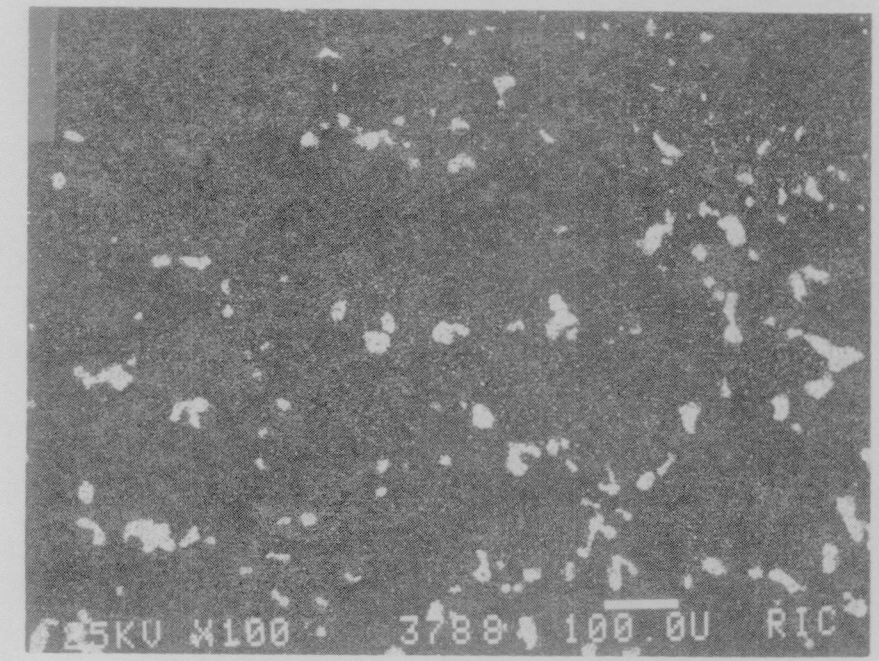

c. Cu X-ray Map 100X

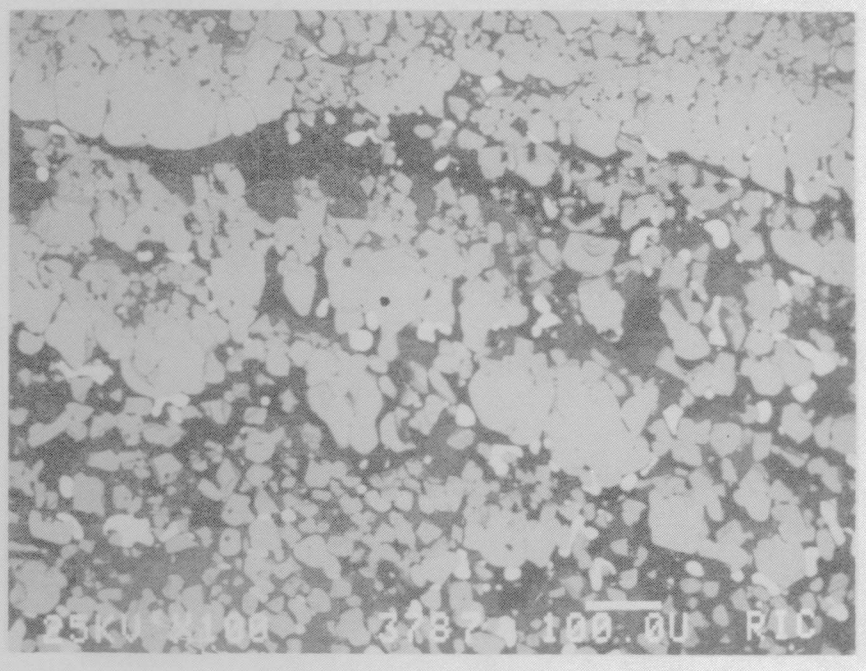

d. BEI 100X

FIGURE 46
BR = 1.35, 1.4 A/cm^2
13505-26 Area 2

FIGURE 47 20X

BR - 1.6, 1.4 A/cm^2

13505-74

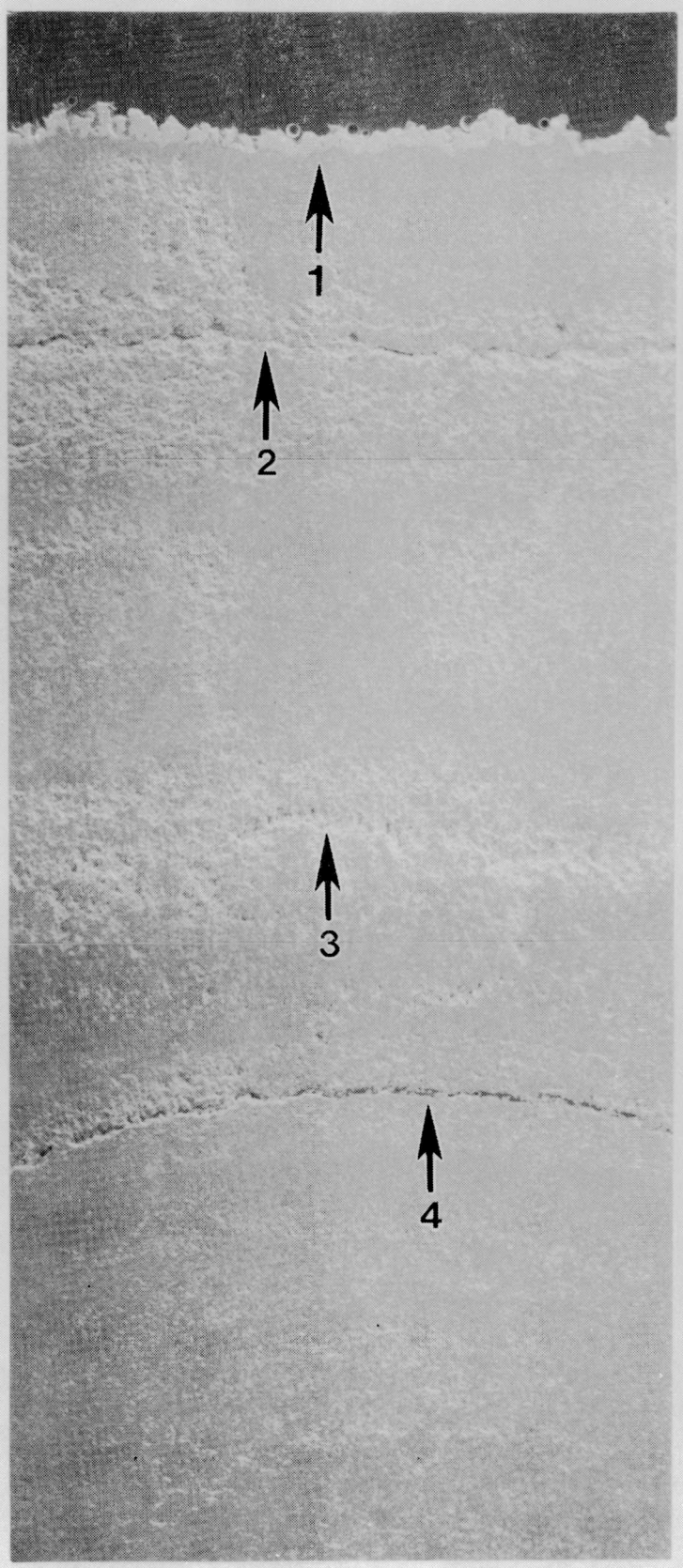

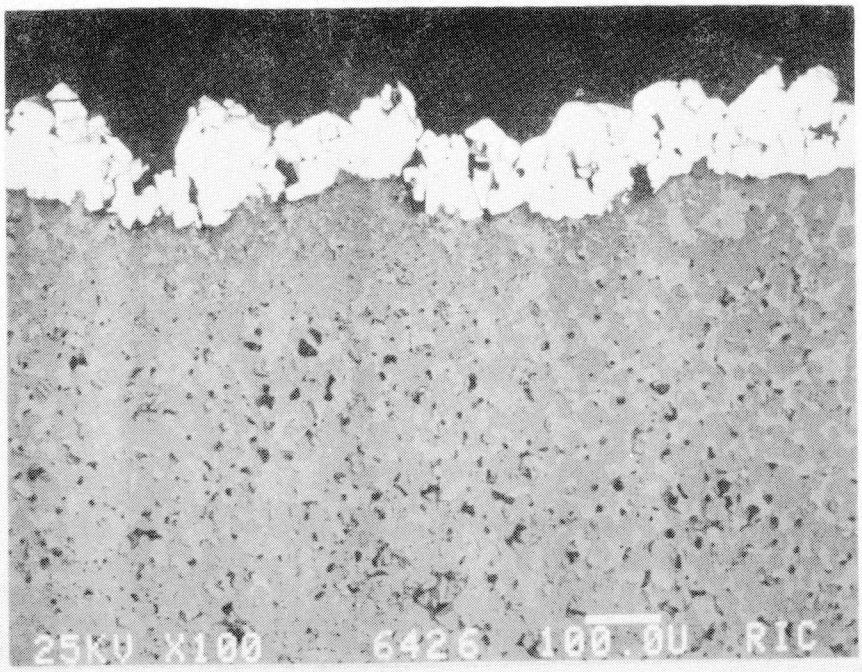

a. BEI Bottom 100X

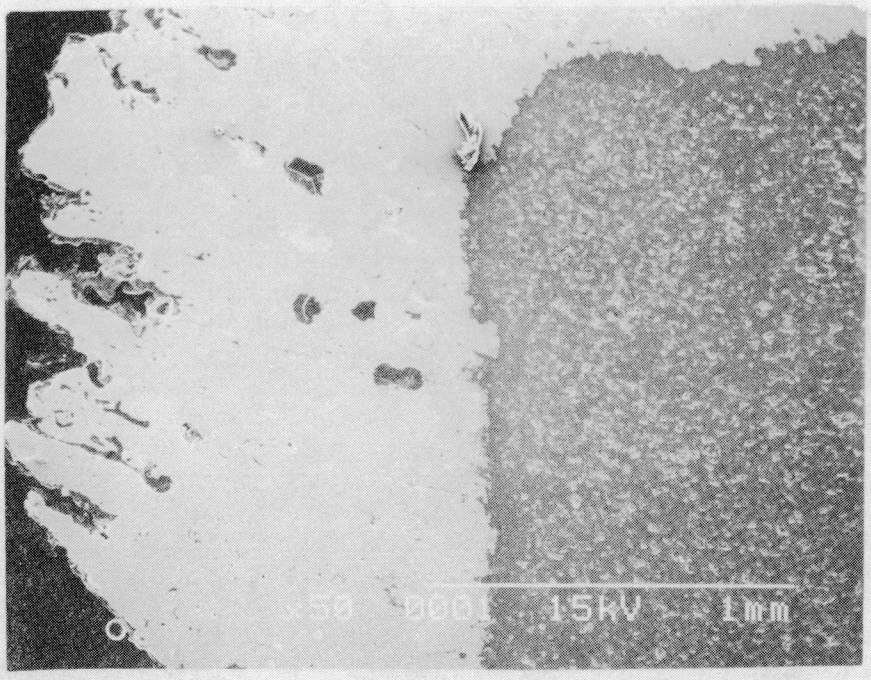

b. Corner 50X

FIGURE 48
BR = 1.6, 1.4 A/cm^2
#13505-74

and density at the edges and sides (Figure 48 a and b). The densest and thickest coating is present on the corners and sides of the BR 1.6 sample. As in other tests, the interface between the CEROX and the substrate is slightly irregular.

4.4.2.3 Corrosion

The cryolite bath and the aluminum from each test were analyzed by ICP and the analyses were corrected and normalized for Fe, Cu, and Ni contamination (as described in the "Materials and Methods" section).

Metal and bath analyses from anodes tested in the Standard Bath (BR 1.35) are shown in Table 12 and plotted in Figure 49. The anode tested at 0.6 A/cm^2 which resulted in cermet-to-cermet delamination produced abundant contamination, >2% of each component and a total of 8.15%. The samples tested at 1.0 and 1.4 A/cm^2 produced contamination levels of <0.8% of any one component and total impurities <1.04%. The Ce-free anode, operated at a BR of 1.35 and current density of 1.0 A/cm^2, had a very high Fe contamination and a total corrosion of 7.65%.

The analyses for the anodes tested in the acidic bath (BR 1.2) are shown in Table 13 and Figure 50. The contamination level from the anode tested at 0.6 A/cm^2 was a total of 1.49%, which was much lower than the anode at BR 1.35. The total contamination content at the other current densities were slightly less than in the BR 1.35 test.

For the samples operated in a non-acidic bath (BR 1.6) analyses are shown in Table 14 and Figure 51. As compared to other bath ratios, contamination was highest at the 0.6 A/cm^2 current density where cermet-to-cermet delamination occurred. Total contamination decreases with increasing current density. The smallest amount of corrosion products produced from all the long term tests was in the test operated with a BR 1.6 and current density of 1.4 A/cm^2. Total corrosion products produced in that test were 0.15% while Fe was 0.04%.

In Figure 52, Fe contamination for all tests operated at 1 A/cm^2 is shown for the different bath ratios. The cerium free test is included for comparison. The CEROX coating provides a 34-fold reduction in the Fe content at the BR 1.35. No cerium-free tests were operated at the other bath ratios and the Fe contamination level in those tests are also well below that of the cerium-free test.

When comparing the Fe, Ni, and Cu contamination values (Tables 12, 13, and 14) it is clear that the amount found in the bath versus the amount found in the metal varies among the tests. In general, the majority of the contamination is in the cryolite bath rather than the Al metal. This is

Table 12. Tests (100 h)
1.0% CeF_3, BR 1.35

Cermet Components in Recovered Metal and Bath (Normalized)

		$Fe_{(gms)}$	$Ni_{(gms)}$	$Cu_{(gms)}$	
Ce-Free		0.27	0.12	0.08	Metal
1.0 A/cm^2		5.18	0.61	0.47	Bath
	Total	5.45	0.73	0.55	
	Corrected	(5.40)	(0.65)	(0.54)	
	Normalized	6.27%	0.75%	0.63%	
0.6 A/cm_2		0.04	0.00	0.01	Metal
		1.39	1.20	1.72	Bath
	Total	1.43	1.20	1.73	
	Corrected	(1.38)	(1.12)	(1.72)	
	Normalized	2.67%	2.16%	3.32%	
1.0 A/cm_2		0.12	0.07	0.23	Metal
		0.09	0.08	0.43	Bath
	Total	0.21	0.15	0.66	
	Corrected	(0.16)	(0.07)	(0.65)	
	Normalized	0.18%	0.08%	0.75%	
1.4 A/cm_2		0.23	0.63	0.13	Metal
		0.12	0.14	0.15	Bath
	Total	0.35	0.77	0.28	
	Corrected	(0.30)	(0.69)	(0.27)	
	Normalized	0.25%	0.57%	0.22%	
System Contamination		0.05	0.08	0.004	

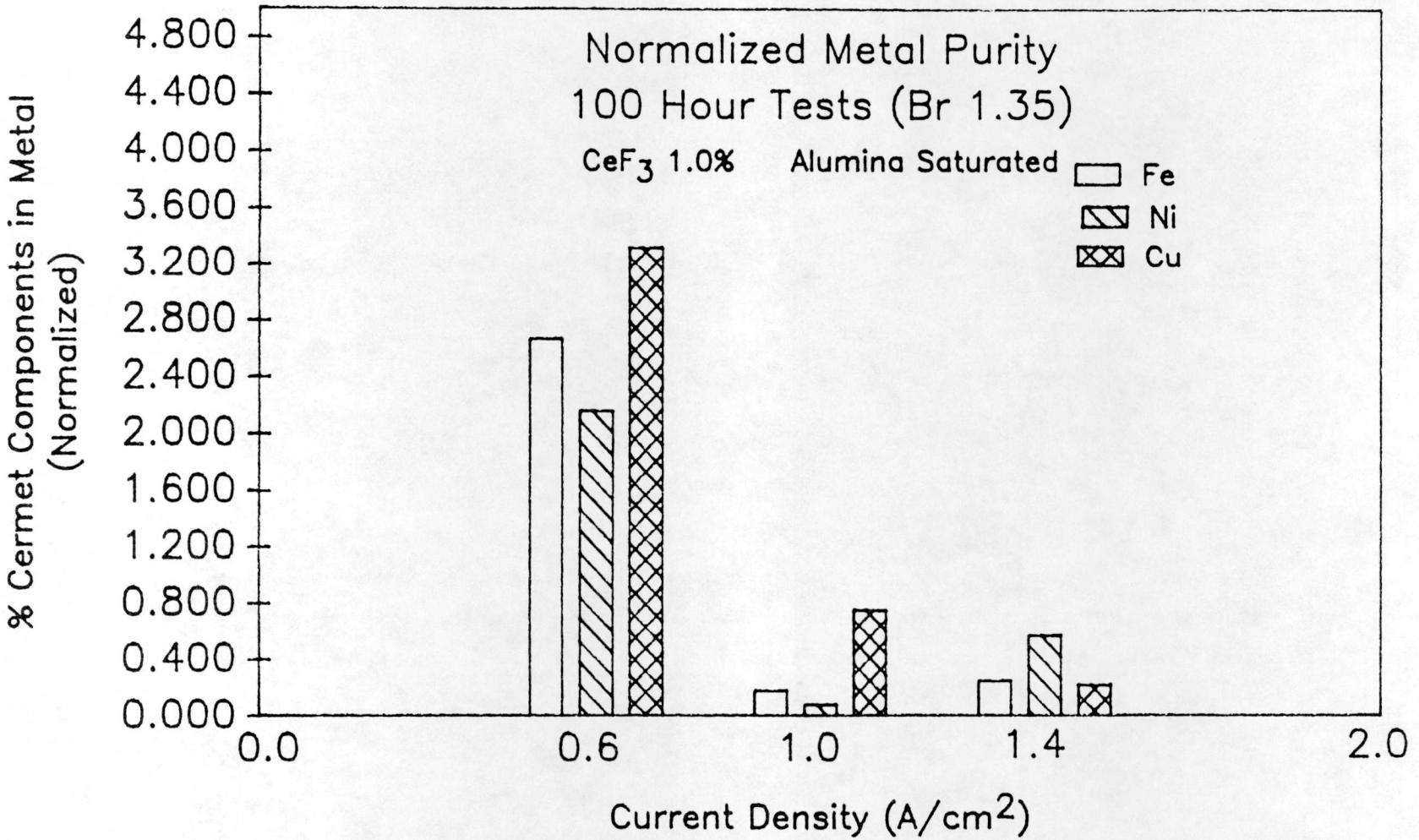
Normalized Metal Purity
100 Hour Tests (Br 1.35)
CeF_3 1.0%
Alumina Saturated
Fe
Ni
Cu
% Cermet Components in Metal
(Normalized)
4.800
4.400
4.000
3.600
3.200
2.800
2.400
2.000
1.600
1.200
0.800
0.400
0.000
0.0
0.6
1.0
1.4
2.0
Current Density (A/cm^2)

FIGURE 49

Table 13. Tests (100 h)
1.0% CeF_3, BR 1.20

Cermet Components in Recovered Metal and Bath (Normalized)

	$Fe_{(gms)}$	$Ni_{(gms)}$	$Cu_{(gms)}$	
0.6 A/cm_2	0.05	0.01	0.01	Metal
	0.45	0.10	0.29	Bath
Total	0.50	0.11	0.30	
Corrected	(0.45)	(0.03)	(0.29)	
Normalized	0.87%	0.06%	0.56%	
1.0 A/cm_2	0.03	0.01	0.03	Metal
	0.28	0.12	0.41	Bath
Total	0.31	0.13	0.44	
Corrected	(0.26)	(0.05)	(0.43)	
Normalized	0.30%	0.06%	0.50%	
1.4 A/cm_2	0.16	0.51	0.07	Metal
	0.16	0.10	0.25	Bath
Total	0.32	0.61	0.32	
Corrected	(0.27)	(0.53)	(0.31)	
Normalized	0.22%	0.44%	0.25%	

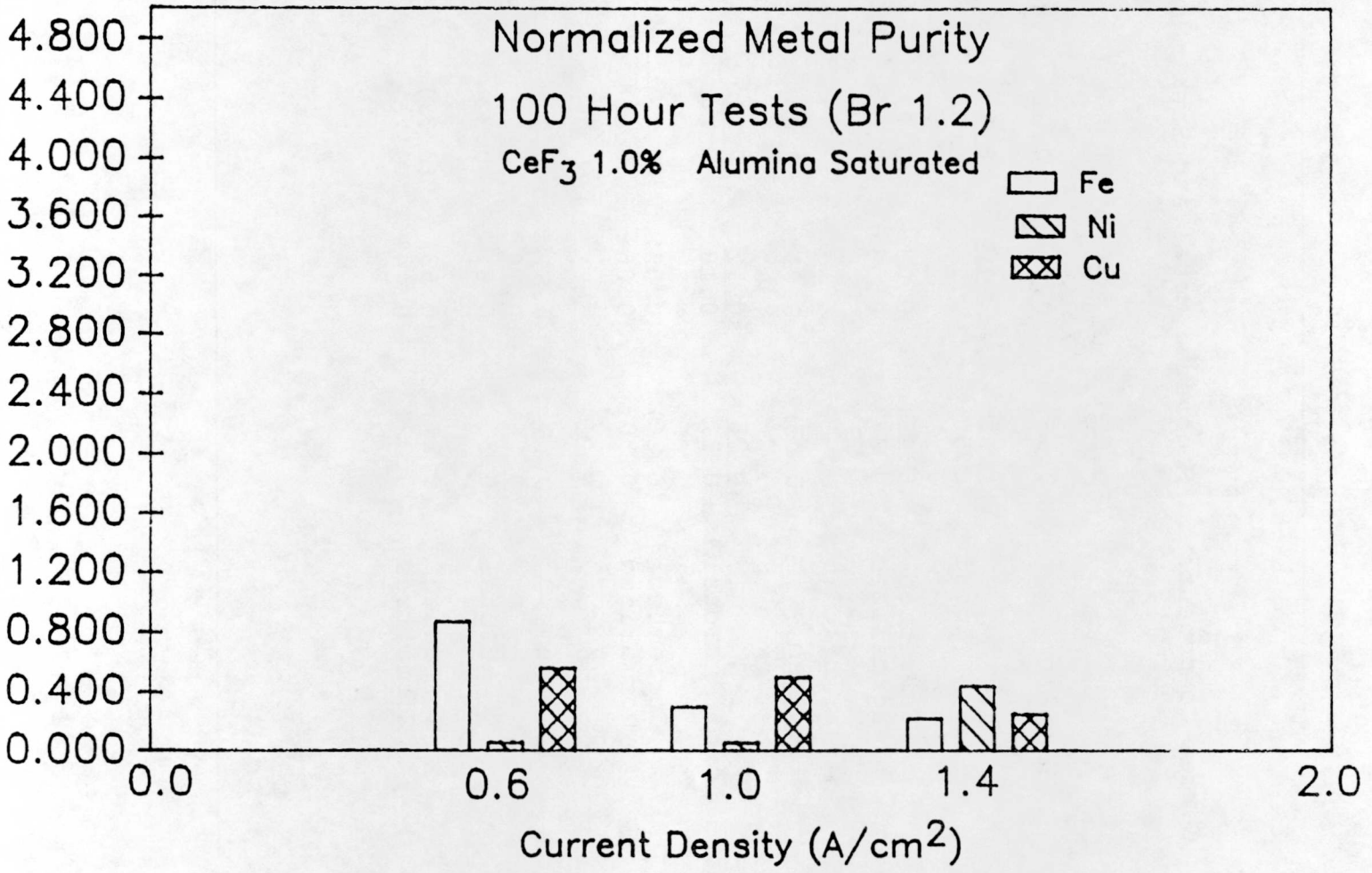
Normalized Metal Purity
100 Hour Tests (Br 1.2)
CeF_3 1.0% Alumina Saturated
Fe
Ni
Cu
% Cermet Components in Metal
(Normalized)
4.800
4.400
4.000
3.600
3.200
2.800
2.400
2.000
1.600
1.200
0.800
0.400
0.000
0.0
0.6
1.0
1.4
2.0
Current Density (A/cm^2)

FIGURE 50

Table 14. Tests (100 h)
1.0% CeF_3, BR 1.60

Cermet Components in Recovered Metal and Bath (Normalized)

	$Fe_{(gms)}$	$Ni_{(gms)}$	$Cu_{(gms)}$	
0.6 A/cm_2	0.37	0.04	0.10	Metal
	0.32	0.00	0.06	Bath
Total	0.69	0.04	0.16	
Corrected	(0.64)	(0.00)	(0.15)	
Normalized	1.23%	0.00%	0.29%	
1.0 A/cm_2	0.02	0.04	0.05	Metal
	0.25	0.21	0.27	Bath
Total	0.27	0.25	0.32	
Corrected	(0.22)	(0.17)	(0.31)	
Normalized	0.25%	0.19%	0.36%	
1.4 A/cm_2	0.01	0.02	0.05	Metal
	0.09	0.12	0.03	Bath
Total	0.10	0.14	0.08	
Corrected	(0.05)	(0.06)	(0.07)	
Normalized	0.04%	0.05%	0.06%	

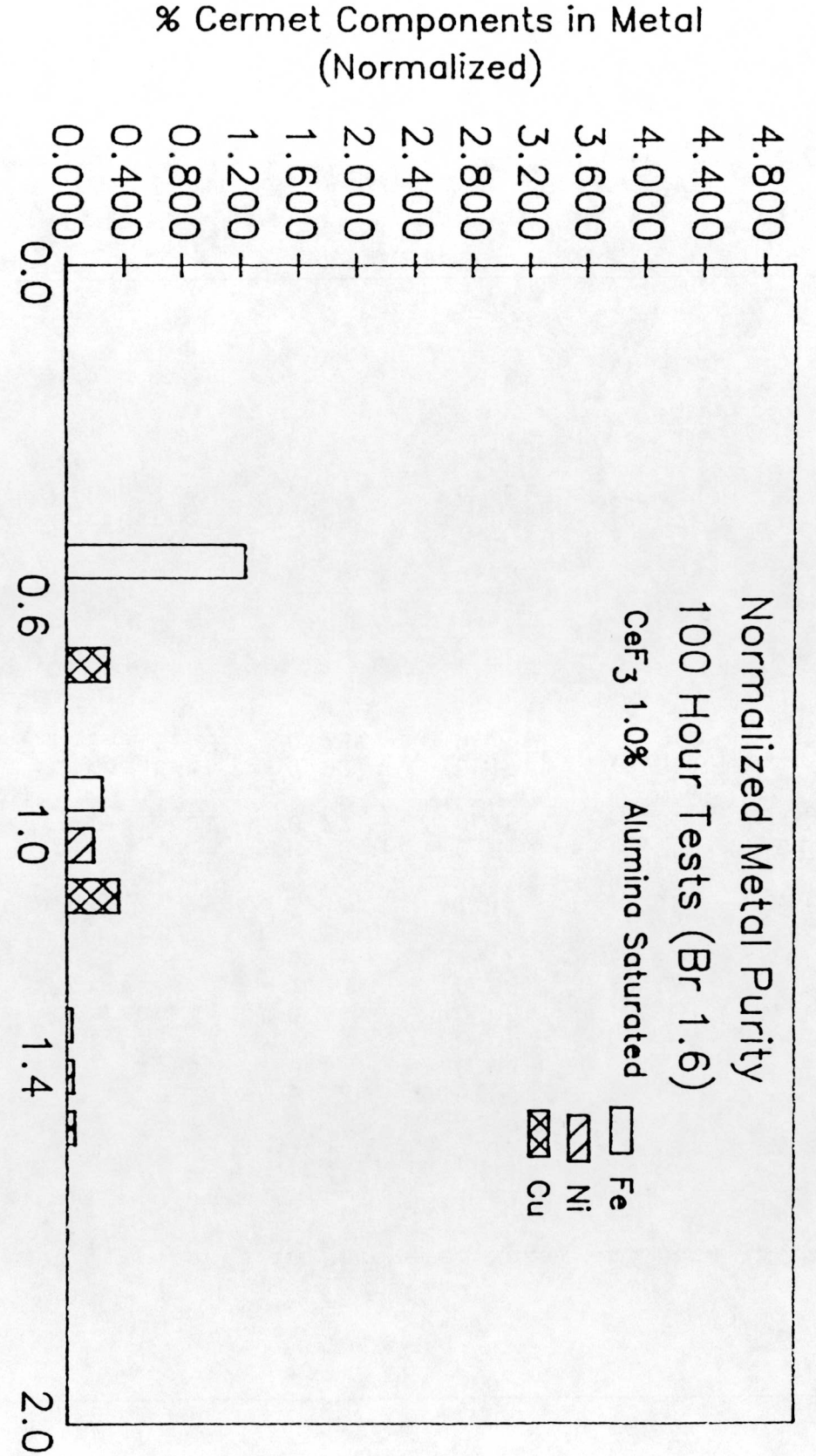
% Cermet Components in Metal
(Normalized)
4.800
4.400
4.000
3.600
3.200
2.800
2.400
2.000
1.600
1.200
0.800
0.400
0.000
0.0
0.6
1.0
1.4
2.0
Current Density (A/cm2)
Normalized Metal Purity
100 Hour Tests (Br 1.6)
CeF3 1.0% Alumina Saturated
Fe
Ni
Cu

FIGURE 51

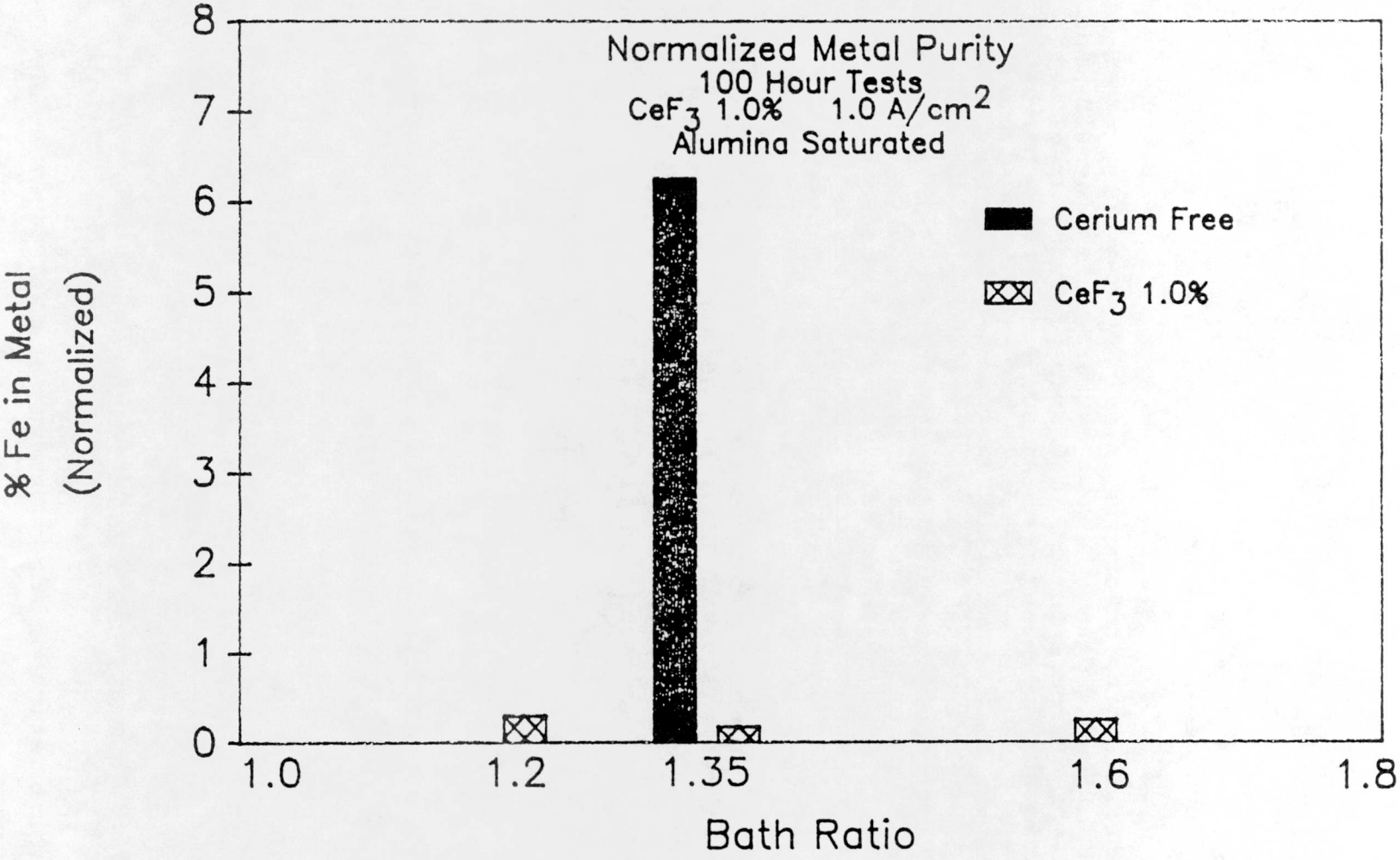
Normalized Metal Purity
100 Hour Tests
CeF3 1.0% 1.0 A/cm2
Alumina Saturated
Cerium Free
CeF3 1.0%
% Fe in Metal
(Normalized)
0
1
2
3
4
5
6
7
8
1.0
1.2
1.35
1.6
1.8
Bath Ratio

FIGURE 52

especially evident in the cerium-free test. The cells were operated with a large bath/Al metal ratio compared to industrial cells.

The Fe to Ni ratio of the recovered cermet components exceeds that in the cermet (0.88) in tests conducted at the low current densities (0.6 and 1.0 A/cm^2), indicating excessive Fe contamination. In the tests at 1.4 A/cm^2, the Ni is increased relative to the Fe and the ratio is lowered to ~0.4 to 0.48. This is true for most of the tests, both with and without cerium, and appears to be a function of the substrate.

General corrosion trends in all the tests is toward a decrease in Fe and Cu with higher current density and a slight increase in Ni. Corrosion results are lowest in the tests at BR 1.6 and highest at BR 1.35.

4.4.2.4 Wear rate calculations

If accurately measured, physical changes in the anode (i.e. anode weight loss and dimensional change) can be used to measure anode wear rates. However, because of the CEROX coating and cryolite crust formation on the anodes, the physical changes cannot accurately be measured. Therefore, anode wear rates were estimated from the cermet components found in the bath and metal. Anode wear rates were based on Fe corrosion and results are reported in cm/y based on the gravimetric equivalent of Fe, density, and geometry of the ELTECH produced cermet anodes.

The wear rate equation is

$$\text{Wear Rate (cm/y)} = \frac{\text{Fe (g/h)} \times 8760 \text{ (h/y)}}{\%\text{Fe}_{(\text{anode})} \times D_{(\text{anode})} \times A_{(\text{anode})}} \qquad (21)$$

$$\text{Fe (g/h)} = \frac{\text{Fe(g) (metal + bath)}}{\text{Total test hours}}$$

% Fe = Gravimetric ratio of Fe component in the anode = 0.30

D = Anode density = 5.76 g/cm^3

A = Anode surface area = 2.7 cm^2.

Calculated wear rates are shown in Figure 53. Wear rates generally decrease with current density. The lowest wear rate calculated was 0.75 cm/y for the anode operated at BR 1.6 and current density of 1.4 A/cm^2.

4.4.3 Summary and Conclusions

Corrosion data and microscopy show that there is deterioration of the substrate at the 0.6 A/cm^2 current

FIGURE 53

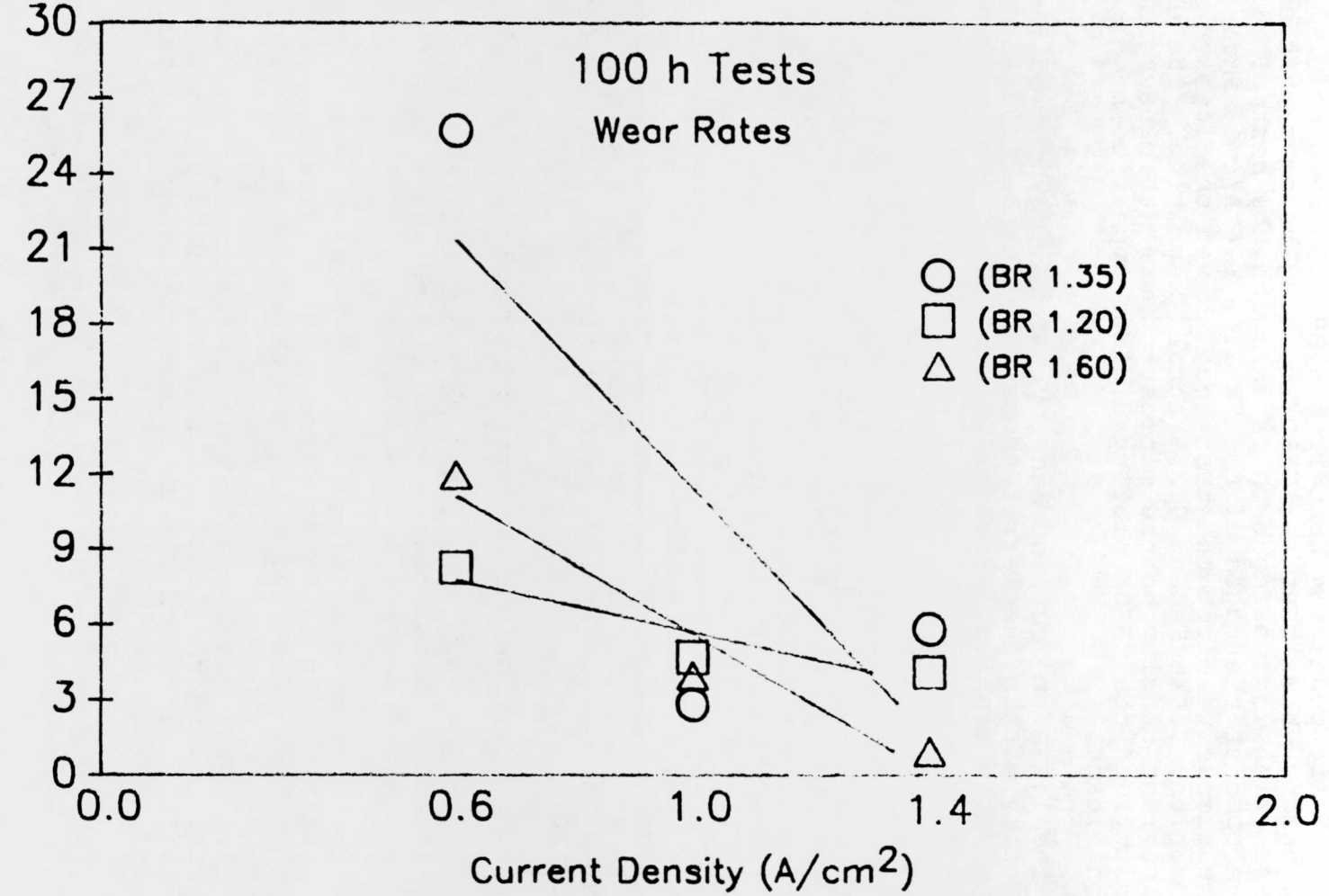
100 h Tests
Wear Rates
(BR 1.35)
(BR 1.20)
(BR 1.60)
Cm/Yr
30
27
24
21
18
15
12
9
6
3
0
0.0
0.6
1.0
1.4
2.0
Current Density (A/cm2)

density and that deterioration is reduced at higher current densities. In addition, corrosion data indicates that BR 1.2 and 1.6 are generally better than BR 1.35 samples. Microscopy shows that the CEROX coating becomes thicker and denser with increasing bath ratio, with the best coating developed on the edges of the BR 1.6, 1.4 A/cm^2 sample. This same sample was from the test that showed the lowest corrosion, 0.04% Fe and 0.15% total impurities. The effect of current density on the microstructure (thickness and density) of the CEROX coating did not appear to be significant.

At the 1.4 A/cm^2 current density, microscopy showed increased porosity within the ferrite substrate in the 1.35 and 1.6 bath ratio samples. However, there was no increase in contamination.

Cell voltage gives a rough indication of the voltage penalty of the CEROX coating. However, the voltage drop can also be attributed to O_2 bubbles, the bath, and the resistance of the anode, etc. so that if there is any change in one of these during a test or between different tests the cell voltage will also change. Cell voltage at BR 1.2 and 1.6 was very close to that of the Ce-free test with the exception of the BR 1.6, 1.4 A/cm^2 test. That test had a thick and dense CEROX coating on the edges, which may have led to the higher voltage. Because the coating was dense, it may be possible to reduce the thickness (and therefore the resistance) of the coating and still achieve good protection of the cermet substrate.

The major conclusions are summarized below:

1. Corrosion levels of 0.04% Fe and 0.15% total were present in the Al metal for an anode tested 100 h at a BR 1.6 and a current density of 1.4 A/cm^2.

2. Low current densities (0.6 A/cm^2) led to cermet-to-cermet delamination and high corrosion and therefore should be avoided. The reason for the delamination is not clear.

3. The CEROX coating increases in thickness and density with increasing bath ratio. Current density appears to have little effect on the structure (thickness and porosity) of the coating.

4. At 1.0 A/cm^2 and BR 1.35, the CEROX produced a 34 fold reduction in Fe compared to the Ce-free test.

5. Corrosion at 1.4 A/cm^2 current density is slightly less than at 1.0 A/cm^2 and both have much less corrosion than at the 0.6 A/cm^2. This disagrees with the Phase 1 program, in which low current densities were recommended.

6. Corrosion at BR 1.2 and 1.6 are generally less than at BR 1.35.

7. Cell voltage of BR 1.2 and 1.6 tests with the cerium were close to that of the cerium-free test (BR 1.35). The exception is the BR 1.6 test at 1.4 A/cm^2 that resulted in the highest cell voltage. This may be attributed to the thickness of the CEROX coating in that experiment.

8. A Cu metal depleted layer occurs on the exterior of the anode in the cerium-free and most of the cerium containing tests. The thickness of this layer roughly increases with increasing current density. The thickness in the samples with a CEROX coating is similar to that developed in the Ce-free sample.

9. An exterior layer containing large grains of Cu with increased Ni content was present in the BR 1.35 and 1.6 samples at the 0.6 A/cm^2 current density. This may be an indication of some melting of the Cu during heat-up or testing.

4.5 VERTICAL CATHODE EFFECTS

Four 50 h tests were planned using vertical TiB_2 cathodes with both the DOE Bath #3 (BR 1.15) and the Standard Bath (BR 1.35) to determine if flowing aluminum would change the cerium partition coefficients and metal impurities. Both electrolytes were evaluated in stirred and unstirred baths containing 1.0% CeF_3 at a current density of 1.0 A/cm^2 and saturated with alumina.

The first test with the Standard Bath and static conditions was operated with a porous TiB_2 cathode 1.2 X 0.6 X 6.2 cm long. The test failed after 36 h. Postmortem investigation revealed that the cathode was attacked at the meltline and severed, causing an open circuit in the cell.

The test was repeated with a theoretically dense TiB_2 bar 1.0 X 1.0 X 6.0 cm long. The cathode material was again attacked at the meltline but survived for the 50 hours. Below the meltline, the cathode had limited surface attack and maintained good dimensional stability. Figure 54 compares the tested cathode to an untested cathode.
The cathode was encased in a gray porous mass that held some encapsulated aluminum metal, which was not recoverable. No Al metal was found at the bottom of the cell. The anode was covered with a good CEROX coating and had good dimensional stability.

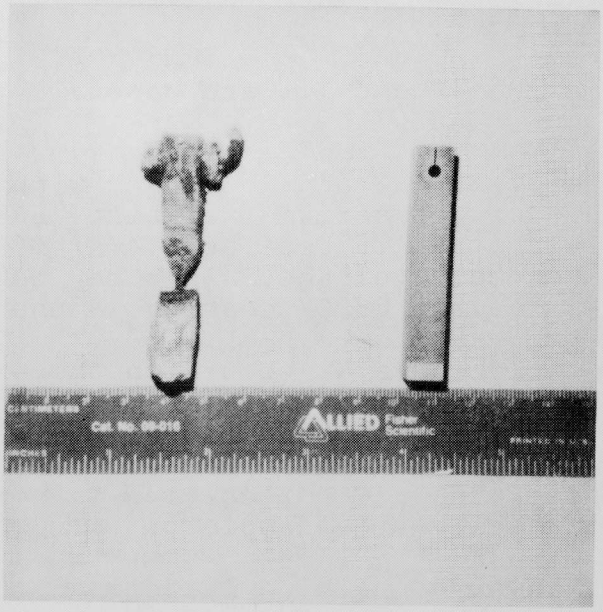

FIGURE 54
An untested TiB_2 cathode (right) is
compared to a tested cathode
with meltline corrosion

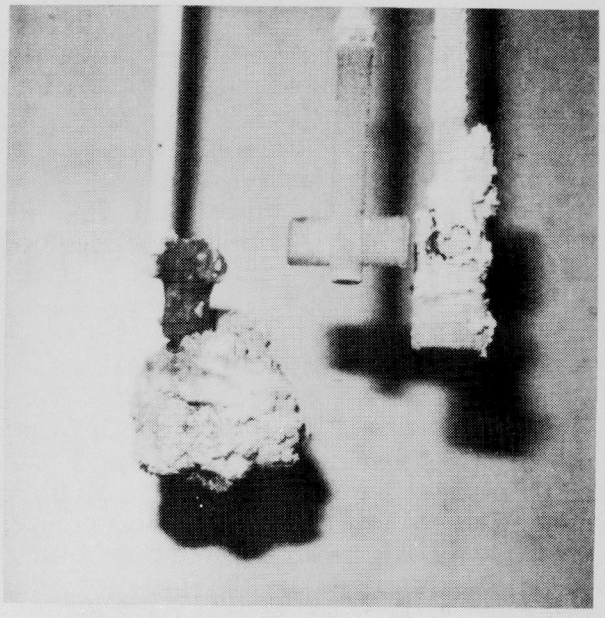

FIGURE 55
TiB_2 Cathode (left), Al_2O_3
Stirring Paddle (Center) and
Cerox coated Anode (right)
From a Stirred Experiment

The TiB_2 cathode at the meltline had the appearance of being burned by a high temperature torch; and may be indicative of localized aluminothermic reduction, which could take place by the following reactions:

Oxidation $TiB_2 + 5/2\ O_2 = TiO_2 + B_2O_3$ (22)

Aluminothermic Reduction $TiO_2 + B_2O_3 + 10/3\ Al = TiB_2 + 5/3\ Al_2O_3$. (23)

The second reaction is a thermite process that releases large amounts of heat locally that could account for the attack at the meltline.

A sample of the gray mass was analyzed by XRD for phase identification. The compounds identified were:

Compounds Identified	Compounds Possibly Present
Na_3AlF_6 (cryolite)	TiO_2 (rutile)
$Na_5Al_3F_{14}$ (chiolite)	Ti_3O_5 (anosovite)
$-Al_2O_3$ (corundum)	Ti_2B_5
CeB_6	

Because of the myriad of peaks in the pattern arising from the multiple phases present, it was not possible to confirm the presence of the listed titanium compounds while some peaks remained unidentified. The presence of titanium in the sample was confirmed by XRF. Although some of the by-products of a possible aluminothermic reduction were found, other competing reactions were taking place making it difficult to identify the reaction path. The presence of CeB_6, and the the limited TiB_2 corrosion below the meltline, indicates that the CeB_6 is formed after the oxidation reaction given above.

The second test, with the DOE Bath #3, had the same results as in the Standard Bath test. Again, the cathode was encased in a gray mass and had meltline corrosion while the anode had a good CEROX coating. No Al metal was recovered.

The tests were also operated with the Standard Bath and DOE Bath #3 in stirred experiments. A 60 rpm Servodyne motor with a graphite bushing rotated an Al_2O_3 stirring rod to which an Al_2O_3 paddle was connected. Both experiments had similar results to the unstirred experiment. A typical anode, the stirring paddle, and the encased cathode are shown in Figure 55.

Because of the corrosion of the TiB_2 cathodes at the meltline, and the lack of recoverable Al, an estimation of the partition coefficients and impurities was impossible from these experiments. A TiB_2 cathode immersed below the meltline (and away from O_2) should be used in future experiments of this type.

5. UTILIZATION AND RECOVERY OF CERIUM

Long term testing of in-situ deposited CEROX coatings on nickel ferrite/Cu cermets demonstrated favorable protection of the cermet from cryolite corrosion. With the anticipated use of this technology with a suitable inert anode substrate, DOE requested an economic analysis of the recovery of cerium from aluminum metal produced in cells equipped with the in-situ CEROX coated anodes. The economic analysis is a paper study based on a literature search of patents and standard sources of survey information of aluminum production and plant capacities for the aluminum smelting process.

The analysis provides:

1. Estimated quantity of cerium in the system expressed as a function of plant capacity. This includes inventories at various stages of production, i.e., in the pots, in the Al product, and as recycle.

2. Estimated losses of Ce as a function of produced Al.

3. Estimated costs of each step in utilizing and recycling of cerium as a function of produced Al.

5.1 CONCEPTUAL PLANT DESIGN FOR CERIUM RECOVERY

A study was made of the literature with particular attention given to U.S. Patent 4,668,351[32] as well as several descriptive articles pertaining to proven commercial processes for the removal of metallic impurities from aluminum. These sources[33,34,35,36] were used to develop a conceptual design of plant operations suitable for the recovery of cerium from the aluminum and the recycle of cerium to the pots. Once the concpetual design was formulated, the design and process assumptions were reviewed with consultants from the aluminum industry. They confirmed the systems as designed were viable and the assumptions made about in-plant operation would be suitable for use in aluminum plants of variable sizes and capacities.

From the study it was concluded that a viable design would include the following:

1. An operation in which the major portion of the cerium would be removed from the aluminum by the injection of AlF_3 into intensely agitated molten aluminum. In terms of guidelines provided by the above patent a 45-minute period of agitation is assumed. CeF_3 obtained by reaction, as well as excess AlF_3, would be skimmed off the molten aluminum and returned as recycle to electrolytic pots. This is written

$$AlF_3 + Ce = CeF_3 + Al. \qquad (24)$$

2. A clean-up operation in which the aluminum could be brought to specification grade by the injection of a Cl_2-N_2 gas mixture into a highly agitated bath of molten aluminum. Skimming of the $CeCl_3$ obtained by reaction would provide added recovery of cerium and is written

$$2Ce + 3Cl_2 = 2CeCl_3. \quad (25)$$

3. An operation in which $CeCl_3$ would be dissolved in cold water and reacted with soda ash to form insoluble $Ce_2(CO_3)_3$. Filtration and drying followed by pelletizing would provide a material suitable for recycle to the electrolytic pots and this becomes

$$2CeCl_3 + 3Na_2CO_3 = Ce_2(CO_3)_3 + 6NaCl. \quad (26)$$

The use of AlF_3 as a halogenation agent results in acceptable quantities of by-products of CeF_3, $Ce_2(CO_3)_3$, and unreacted AlF_3 and generated aluminum being formed. All of these by-products with the exception of the generated aluminum can be recycled to the cells.

All of the foregoing is illustrated in block diagram form in Figure 56. Included are material flow quantities for a 506 tonnes (558 tons) per stream day capacity plant. This medium sized plant, assumed to have 402 cells of 170 kA capacity is considered to be a typical operation. It will be noted that the basis for the flow calculations, including references to key articles, are shown in tabular form in Figure 56.

5.2 ESTIMATED QUANTITY OF CERIUM RETAINED IN THE SYSTEM

The estimated quantity of cerium retained in the system, as well as that retained in the individual sections of the plant as a function of plant capacity, is shown in Figure 57. Basis for the inventory calculations, as well as formulas developed in terms of these basis are included. Cerium distribution in the cell is based on the long term testing in Phase II of the DOE Anode Program. Long term testing established a partition coefficient for cerium distribution in the cell for the preferred conditions with an in-situ CEROX coating 1.0 mm thick, a BR 1.35, and a current density of 1.0 A/cm^2 as

$$\text{Partition Coefficient} = 2\%\ \text{Ce-Al} / 0.3\%\ \text{Ce-bath}. \quad (27)$$

Because of its overbearing effect upon the inventory calculations, the assumptions made with regards to the hold-up of molten Al in the cell requires special comment. Tapping of cells is performed once a day. Although practices vary somewhat from plant to plant, it appears that the general practice is to drain the cell pots to the halfway

FIGURE 56

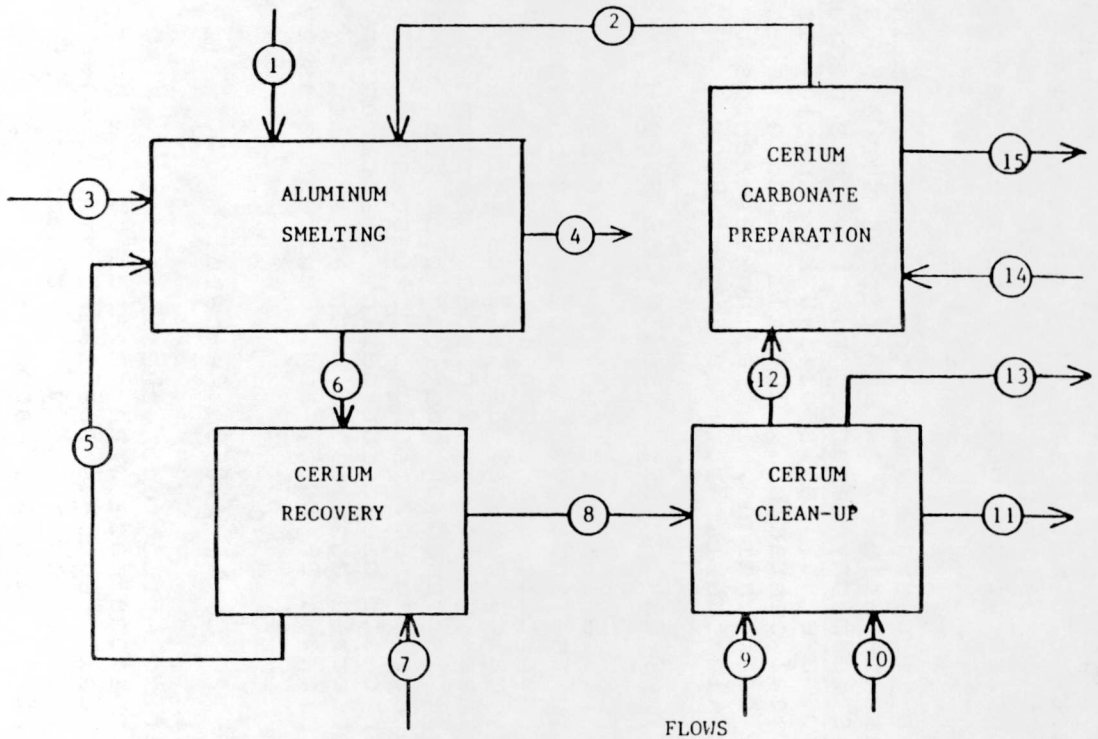

BASES FOR MATERIAL FLOW CALCULATIONS

1. 402 cells of 170 KA capacity at 92% current efficiency.
2. Cerium content of aluminum - % by wt.
   a) cell effluent - 2.0
   b) cerium recovery effluent - 0.2
   c) cerium cleanup effluent - 0.02
3. Stream 4 losses from cell of 140 lb/day estimated using as guidelines the LiF_3 cell losses listed in article by Peterson and Taberaux, Table III, P. 652, Light Metals, 1988.
4. Stream 7 AlF_3 feed is 125% of stoichiometry. This value with assumed 0.02% effluent, and 45 minute stirring time all lie within the preferred conditions specified in U.S. Patent 4,668,351.
5. In calculating line 5 flow allowance made for 99.9% recovery of CeF_3 & AlF_3 & additional 0.1% recycling loss.
6. Line 3 value calculated by fluorine balance on basis that cell feed requirement is 35.0 lb/tonne. This figure is in turn based on 27 kg/day value for a "high amperage cell" as specified in article by Desclaux, p. 309 Light Metals, 1987.
7. Cl_2 efficiency of 90% assumed for cerium clean-up as suggested by 95+% efficiency obtained in aluminum demagging article by Miller, p. 499, Light Metals, 1978. Excess Cl_2 assumed to form $AlCl_3$. Assumed that Cl2 will be in form of 10% mixture with nitrogen.
8. Line 12 calculation assumes 99.9% recovery of $CeCl_3$. Line 13 calculation assumes 95% recovery.
9. Line 2 calculation assumes process and recycle losses of $Ce_2(CO_3)_3$ at 5%.
10. Line 1 calculated by cerium balance assuming 0.1% loss in handling make-up CeF_3.
11. Assumed 5% in excess of stoichiometry for Line 14.

FLOWS

Aluminum - tonnes per day Other Materials - pounds per day

	(1)	(2)	(3)	(4)	(5)	(6)	(7)	(8)	(9)	(10)	(11)	(12)	(13)	(14)	(15)	◯
Aluminum						506.0		506.0			506.0					
Cerium						22,315		2,231			223					
AlF_3			1,028		4,671		16,719									
CeF_3				140	28,197											
Cl_2									1,693							
N_2										6,022						
$CeCl_3$												3,528				
$AlCl_3$													201			
Na_2CO_3														2,390	114	
$Ce_2(CO_3)_3$		3,129														
NaCl															2,510	
CeO_2	572															

UTILIZATION AND RECOVERY
OF CERIUM IN
ALUMINUM SMELTER OPERATION
506 Tonnes per Stream Day

JJL 3/1/89

FIGURE 57

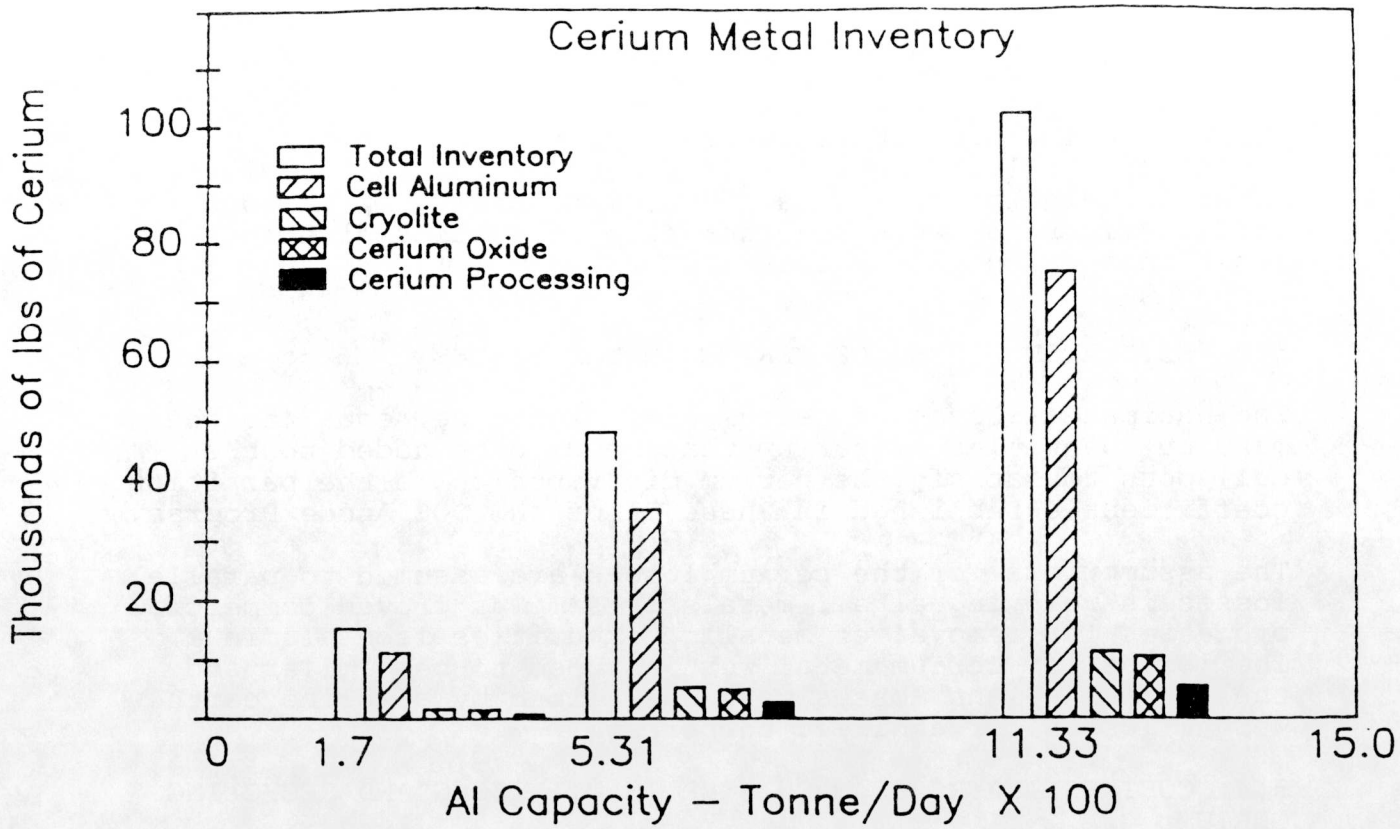

Bases for Inventory Calculations	Formula Lb/Day of Cerium
1. Pots drained halfway once per day. Therefore average holdup of Al=1.5 daily Al capacity with Ce at 2.0%.	66.150 x tonnes/day of Al
2. Weight of cryolite equal to average holdup of Al with Ce at 0.3%.	9.923 x t/d
3. Average size of tapping crucible = 4.6 tonnes. C cibles full one half the time with Ce at 2.0%.	101.43 x pot lines
4. Two holding furnaces to provide surge capacity of of 2.3 tonnes for each pot line. Ce at 2.0% in one & at 0.2% in other.	111.57 x pot lines
5. 45 minute holdup of Al production in Ce removal process at 2.0% Ce.	1.378 x t/d
6. 45 minute holdup of Al production in Ce clean-up process at 0.2% Ce.	0.138 x t/d
7. $Ce_2(CO_3)_3$ preparation unit holdup with holdup of Ce from 6. reduced to 0.18% Ce.	0.124 x t/d
8. Holdup of $Ce_2(CO_3)_3$ in feed bins equal to 1/2 day production - see Exhibit I.	1.883 x t/d
9. Holdup of CeO_2 equal to 10 day supply of makeup requirement - see Exhibit I.	9.202 x t/d
Total Inventory =	88.798 x t/d + 213.00 x P.L.
Inventory in Ce Processing (3 through 8) =	3.523 x t/d + 213.00 x P.L.

point. In terms of these two assumptions the average inventory of Al in the cells is 1.5 times the daily cell capacity. The high, low, and medium capcacity operations used in Figure 57 were selected from tabulation of plants shown in a recent DOE Report (DOE /RL-88-25).

UC-313

5.3 ESTIMATED LOSSES OF CERIUM IN THE SYSTEM

The estimated losses of cerium are, of course, equal to the make up quantities of cerium that need to be added to the cell pots to satisfy the cerium distribution in the partition coefficient established in Phase II of the DOE Anode Program.

The assumptions for the cerium losses are assumed to parallel losses in removing alkali metals by similar proven commercial processes for removal of metallic impurities from aluminum. The losses for cerium metal were assumed to be similar and thus cerium weight losses were normalized by alkaline earth weight losses for a direct comparison.

5.4 COST ESTIMATES OF EACH STEP IN UTILIZING AND RECYCLING CERIUM

The costs of each step in utilizing and recycling of cerium as a function of produced Al was calculated and is shown in Figures 58 and 59 for various sized plants. To prepare these figures, it was first necessary to develop investment figures and manufacturing costs for the cerium recovery, cerium clean-up, and the cerium carbonate preparation sections of the cerium processing plant. A summary of all of these estimates is shown in Figure 59 for the typical 506 tonnes/day plant (558 ton/d). Included in the figure are the sources of information as well as the assumptions made in preparing the estimates. The cost figures that have been developed are to be recognized as manufacturing costs. A profitability analysis, which would include a return on both the depreciable investment as well as that on the working capital tie-up in the cerium inventory, is considered beyond the scope of this study.

For the typical 506 tonnes/day plant the costs of removing the cerium from the Al are as follows:

	$/tonne[a]	$/ton
Cerium Recovery Step	3.32	3.01
Cerium Clean-up	2.71	2.46
Cerium Carbonate Preparation	2.59	2.35
TOTAL	8.62	7.82

a. 2205 pounds = 1 metric tonne

FIGURE 58

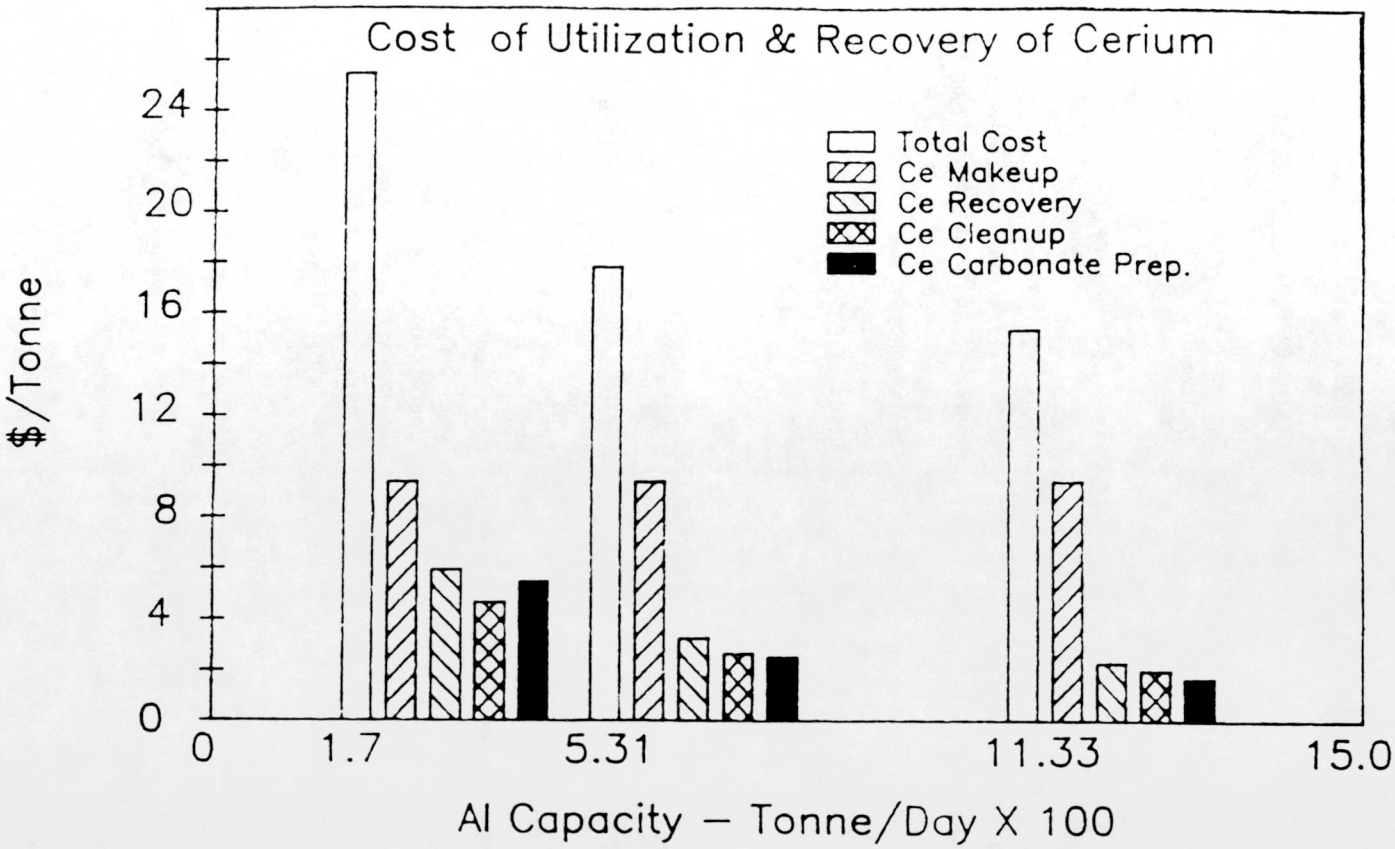

Notes

1. The cerium makeup, as determined from Exhibit I, amounts to 572 lbs. of CeO_2 for every 506 tonnes of Aluminum or 1.1304 lb. of CeO_2 per tonne of Al. This requirement is essentially independent of Al capacity. The quoted price for 99.5% CeO_2 is $20.25/kg with a likely reduction for large tonnage shipments. Assuming a 10% reduction the price = $8.31/lb. of CeO_2.

2. Costs for the three cerium processing sections were calculated in terms of the investment and cost information tabulated in Exhibit IV. Labor was assumed to remain constant. Raw material and utility costs were assumed to be proportional to Al capacity. Investments, and accordingly the investment related costs, were assumed to vary as the 0.6 power at the Al capacity.

ESTIMATED INVESTMENTS - M OF $ FOR 506 TONNES/DAY PLANT

CERIUM RECOVERY

5 Rotor Stirrer Station -	$525[A]
Molten Aluminum Holding Tank -	595[B]
Building	82[C]
Total	$1200

[A] Based on $280M for 3 Rotor System reported for 1984 Operation (pp. 913-915 Light Metals, 1986) +25% Contingency.

[B] Private communication figure + 25% contingency.

[C] 25% of 5000 ft^2 building.

CERIUM CLEAN-UP

3 Stage Chlorinator	$400[D]
Molten Al Holding Tank	595[B]
Building	82[C]
	$1080

[D] Based on average from budgetary quote and private communication figure + 25% contingency.

CERIUM CARBONATE PREPARATION

Reactor, Filters & Calciner	$646[E]
Building	164[F]
	$810

[E] Sum of $15M agitator vessel, $57M filters, $61M Calciner, $17M conveying equipment ratioed up by average Lange factor of 3.7 + 12-1/2% contingency + $22M Fork Lift.

[F] 50% of 5000 $ft.^2$ building.

ESTIMATED MANUFACTURING COSTS - M OF $ - 90% ONSTREAM 506 TONNES/DAY

CERIUM RECOVERY

Raw Materials [G]	- 0 -
Utilities [L]	35.0
Oper. Labor, 1/2 man/shift[H]	88.2
Oper.Supplies at 6% of Labor	5.3
Supervision	10.0
Repairs: Stirrer Station[I]	200.0
Holding Tank + Bldg.at 5%	33.9
Factory Expense at 5% of Invest.	60.0
Depreciation at 10% Str. Line	120.0
Total	552.4($3.32/tonne)

[G] Zero since process uses AlF_3 normally fed to pots.

[H] At $42M/yr. is essentially equal to $15/hr. + 35% IPC.

[I] Based on $76M repairs + $37M for rotors for 3 rotor system (p. 914 Light Metals, 1986)

CERIUM CLEAN-UP

Raw Materials [J]	95.2
Utilities [K]	35.0
Oper. Labor, 1/2 man/shift	88.2
Oper.Supplies, 6% of Labor	5.3
Supervision	10.0
Repairs at 5% of Invest.	54.0
Factory Expense at 5% of Invest	54.0
Depreciation at 10% Str.Line	108.0
	449.7($2.71/tonne)

[J] Exhibit I usages at $0.10/lb for Cl_2 and $0.02/lb for N_2

[K] Based on comparison with requirements of similar unit available commercially.

[L] Heating & stirring considered to essentially the same as in [K].

CERIUM CARBONATE PREPARATION

Raw Materials [M]	51.0
Utilities	10.0
Oper.Labor, 1 man/shift	176.4
Oper. Supplies at 6% of Labor	10.6
Supervision	10.0
Repairs at 5% of Invest.	40.5
Factory Expense at 5% of Invest.	40.5
Depreciation at 10% Str. Line	81.0
Waste Disposal	12.0
	432.0($2.59/tonne)

[M] Exhibit I usage at $130/ton

FIGURE 59

As shown in Figure 58, the cost of these three steps decreases with the size of the plant. The cost of the Ce makeup, which is the amount of new cerium that must be added back into the cell to balance losses, is constant regardless of cell size and must be added to the other three costs for the total cost of utilizing and recovering the cerium.

6. REFERENCES

1. Grjotheim, K.; Krohn, C.; Mali[illegible]vsky, M.; Matiasovsky, K. and Thonstad, J.; "Aluminum Electrolysis Fundamentals of the Hall-Herault Process," 2nd Edition, Aluminum-Verlag, Dusseldorf (1982).

2. Billehaug, K. and Cye, H.A.; "Inert Anodes for Aluminum Electrolysis in Hall-Herault Cells," Aluminum 57 (2), 146-150 (1980).

3. Billehaug, K. and Cye, H.A.; "Inert Anodes for Aluminum Electrolysis in Hall-Herault Cells," Aluminum 57 (3), 228-231 (1980).

4. Horinouchi, K.; Tachikawa, N. and Yamada, K., "DSA in Aluminum Reduction Cells," Proceedings of the First International Symposium on Molten Salt Chemistry and Technology, Kyoto, Japan, (April 22-23, 1983).

5. Weyand, J.D.; Ray, S.P.; Baker, F.W.; DeYoung, D.H., and Tarcy, G. P.; "Inert Anodes for Aluminum Smelting," Final Report Feb. 1986; DOE/CS/40158-20.

6. Duruz, J.J. and De Nora, V.; "The Dynamic Equilibrium of a Self-Forming Anode," presented at the Meeting of the Electrochemical Society.

7. A Survey of Potential Processes for the Manufacture of Aluminum, Arthur D. Little, Inc., ANL-OEPM-79-4.

8. Baker, F. W. and Rolf, R.L., "Hall Cell Operation with Inert Anodes" in Light Metals 1986, R. E. Miller (ed.) The Metallurgical Soc., Warrendale, PA (1986).

9. McLeod, A. D., Lihrmann, J. M., Haggerty, J. S., and Sadoway, D. R., "Selection and Testing of Inert Anode Materials for Hall Cells" in Light Metals 1987, R. E. Miller (ed) The Metallurgical Soc., Warrendale, PA (1987)

10. Belyaev, A.I. and Studentsov, Y.E., Legkie Metally 5 (3), 15 (1936).

11. Belyaev, A.I. and Studentsov, Y.E., Legkie Metally 6 (3), 17 (1937).

12. Kronenberg, M.L.; J. Electrochem Soc. 116, 1160 (1969).

13. Gadeau, R.; Bull. Soc. Fr. Electrician 7, 540 (1974).

14. Stender, V.V. and Trofimenko, [illegible].V.; Khim. Tekhnol 12, 42, (1969).

15. Belyaev, A.I., Legkie Metally 7 (1), 7 (1938).

16. Alder, H.P., US Patent 4,057,480, Nov. 8, 1977.

17. Thonstad, J., Can. J. Chem. 43, 3429 (1965).

18. Yoshida, K. and Dewing, E.W., Met. Trans. 3, 683 (1972).

19. Alder, H.P., US Patent 3,960,678 - June 1, 1976.

20. Alder, H.P., US Patent 3,974,046 - Aug. 10, 1976.

21. Ray, S.P., US Patent 4,374,050 - Feb. 15, 1983.

22. Tarcy, G.P., "Corrosion and Passivation of Cermet Anodes in Cryolite-Type Electrolytes" in Light Metals 1986, R. E. Miller (ed.) The Metallurgical Soc., Warrendale, PA (1986).

23. Ray, S.P., US Patent 4,374,761.

24. Ray, S.P., "Inert Anodes for Hall Cells" in Light Metals 1986, R. E. Miller (ed.), The Metallurgical Soc., Warrendale, PA (1986).

25. Duruz, J.J. and Derivaz, J.P., US Patent 4,397,729.

26. DeNora, V., Spaziante, P.M., and Nidola, A., US Patent 4,098,669.

27. Duruz, J.J., Derivaz, J.P., Debely, P., and Adorian, J., EP-A-0114085.

28. Piontelli, R., Mazza B., and Pederferri, P., Electrochem. Acta. 10 - 1117 (1965).

29. Burgman, J.W., Laistra, J.A., and Sides, P.J., J. Electrochem. Socs. 133, (3), 496 (1986).

30. McLeod, A.D., Haggerty, J.S., and Sadoway, D.R., "Inert Anode Materials for Hall Cells" in Light Metals 1986, R.E. Miller (ed.). The Metallurgical Society Inc., Warrendale, PA (1986).

31. Walker, J.K., "Cerium Oxide Coated Anodes For Aluminum Electrowinning", Final Report, June, 1987; Phase 1 of DE-AC07-86ID12655.

32. Dewing, E.W., Reesor, D.N. US Patent 4,668,351-May 26, 1987.

33. Garepy, B., Dube, G., Simoneau, C., Leblanc, G. "The TAC Process: A Proven Technology", in Light Metals 1984, J.P. McGeer (Ed) The Metallurgical Soc., Warrendale, PA (1984).

34. Derham, L.J., Derham, M.G. US Patent 3,650,730-March 21, 1972.

35. Buno, M.J., Jarrett, N., Slaugenhaupt, B.L., Graziano, R.E. US Patent 3,839,019-Oct. 1, 1974.

36. Miller, R.E. Blayden, L.C., Bruno, M.J., Brooks, C.E., "In-line Fumeless Metal Treatment" in Light Metals 1978, J. Miller (Ed) The Metallurgical Soc., Warrendale, PA (1978).

APPENDIX 1

Normalization Example

Ce-free anode operated at 1 A/cm^2, 1.35 BR.

Amount of Al metal recovered from test= 50.9 g
Amount of cryolite recovered from test= 551.0 g

1. ICP analysis

	%Fe	%Ni	%Cu
Metal	0.53	0.23	0.16
Bath	0.94	0.11	0.085

Calculate g of Fe, Ni or Cu.

$$\text{g in Al metal} = \text{g of Al metal} \times \frac{\%\ \text{Fe, Ni, or Cu}}{100}$$

$$\text{g in cryolite} = \text{g of cryolite} \times \frac{\%\ \text{Fe, Ni, or Cu}}{100}$$

$$50.9\ \text{g of Al} \times \frac{0.53\%\text{Fe}}{100} = 0.27\ \text{g Fe in Al}$$

$$551\ \text{g of bath} \times \frac{0.94\%\text{Fe}}{100} = 5.18\ \text{g Fe in bath}$$

$$50.9\ \text{g of Al} \times \frac{0.23\%\text{Ni}}{100} = 0.12\ \text{g of Ni in Al}$$

$$551\ \text{g of bath} \times \frac{0.11\%\text{Ni}}{100} = 0.61\ \text{g of Ni in bath}$$

$$50.9\ \text{g of Al} \times \frac{0.16\%\text{Cu}}{100} = 0.08\ \text{g of Cu in Al}$$

$$551\ \text{g of bath} \times \frac{0.085\%\text{Cu}}{100} = 0.47\ \text{g of Cu in bath}$$

2. Add the contamination of bath and metal to determine total contamination in grams.

	g Fe	g Ni	g Cu
Metal	0.27	0.12	0.08
Bath	+5.18	+0.61	+0.47
Total	5.45	0.73	0.55
3. Subtract Background Corrosion (g)	-0.05	-0.08	-0.004
	5.40	0.65	0.54

4. Normalize for industrial Al production. Calculate the theoretical amount of Al produced at 1 A/cm^2 (2.7 A) for 100 hours, assuming 95% current efficiency.

$$\text{Theoretical g of Al} = \frac{2.7\ A \times 60s \times 60min. \times 100h \times 27g/mol\ Al \times 0.95}{3\ \text{electrons} \times 96{,}500}$$

Theoretical Al at 1 A/cm^2, 100 hours = 86.12 g
Theoretical Al at 0.6 A/cm^2, 100 hours = 51.67 g
Theoretical Al at 1.4 A/cm^2, 100 hours = 120.56 g

$$\frac{5.4\ g\ Fe}{86.12\ g\ Al} \times 100 = 6.27\ \%\ Fe$$

$$\frac{0.65\ g\ Ni}{86.12\ g\ Al} \times 100 = 0.75\ \%\ Ni$$

$$\frac{0.54\ g\ Cu}{86.12\ g\ Al} \times 100 = 0.63\ \%\ Cu$$